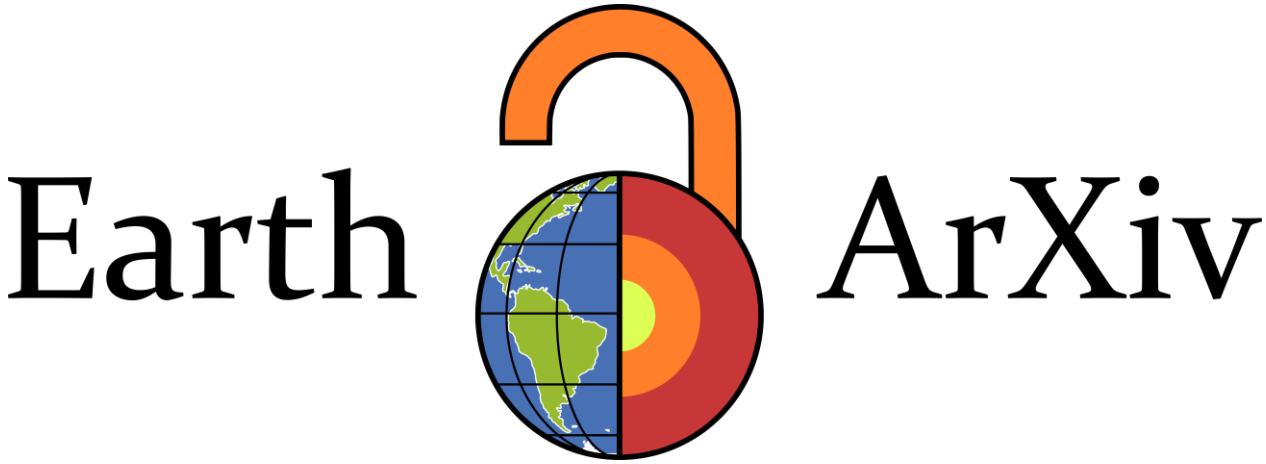

Formation and fluxes of natural hydrogen in the crust and upper mantle

Kevin Wong[1,2,3,*], Martina Cascone[4], Donato Giovannelli[4,5,6,7,8], and Alberto Vitale Brovarone[1,9,10,†]

[1] Dipartimento di Scienze Biologiche, Geologiche e Ambientali (BiGeA), Alma Mater Studiorum Università di Bologna, Piazza di Porta San Donato 1, 40126 Bologna, Italy

[2] Department of Earth Sciences, University of Cambridge, Downing Street, Cambridge, CB2 3EQ, United Kingdom

[3] Now at Earth and Planets Laboratory, Carnegie Institution for Science, 5241 Broad Branch Road NW, Washington, DC 20015, United States of America

[4] Dipartimento di Biologia, Università degli Studi di Napoli Federico II, Via Cinthia, 80126 Naples, Italy

[5] Istituto per le Risorse Biologiche e le Biotecnologie Marine, Consiglio Nazionale delle Ricerche, Largo Fiera della Pesca 2, 60125 Ancona, Italy

[6] Department of Marine and Coastal Science, Rutgers University, 71 Dudley Road, New Brunswick, New Jersey 08901, United States of America

[7] Marine Chemistry & Geochemistry, Woods Hole Oceanographic Institution, 266 Woods Hole Road, Falmouth, Massachusetts 02541-1050, United States of America

[8] Earth-Life Science Institute (ELSI), Tokyo Institute of Technology, 2-12-1 Ookayama, Meguro-ku, Tokyo 152-8550, Japan

[9] Sorbonne Université, Muséum National D'Histoire Naturelle, UMR CNRS 7590, IRD, Institut de, Minéralogie, de Physique des Matériaux et de Cosmochimie, IMPMC, 4 Place Jussieu, 75005 Paris, France

[10] Instituto di Geoscienze e Georisorse, Consiglio Nazionale delle Ricerche, Via Giuseppe Moruzzi 1, 56124 Pisa, Italy

*Corresponding author: kwong@carnegiescience.edu

[†]Corresponding author: alberto.vitaleb@unibo.it

Abstract

Molecular hydrogen (H_2) is a fundamental component of planetary evolution and an important energy source for microbial life. It is now understood that natural mechanisms, spanning geological and biological processes, can produce high concentrations of hydrogen in natural fluids. Quantifying the processes that modulate natural hydrogen concentrations is necessary not only for conceptualising the distribution of life on Earth and elsewhere in the universe, but also for identifying settings where natural hydrogen may potentially accumulate to complement industrial hydrogen production. However, uncertainties persist in assessing these natural fluxes. In this review, we explore the biological and geological processes that can generate natural hydrogen. Compared to previous summary efforts, we include in our updated inventory H_2 fluxes from biological processes, metamorphic degassing, and subduction zones. By integrating recent advances in quantifying hydrogen generation and transportation in geological environments, we demonstrate that significant concentrations and fluxes of hydrogen can arise in a plethora of settings worldwide, contributing towards a total abiotic production rate of 39 to 63< Mt H_2 yr^{-1}, which is twice as high as previous estimates and equivalent to 18–57< % of annual water subduction. We also highlight that geological environments characterised by high hydrogen production may be associated with high microbial hydrogen consumption (e.g., oceanic sediments). However, large uncertainties regarding the residence time of hydrogen within geological settings remain, and future research endeavours should aim to ascertain the long-term behaviour of hydrogen stored in the deep Earth to assess the viability of natural hydrogen as a renewable energy source.

Research highlights

- We review the production of natural hydrogen by biological and geological processes.
- Fluxes of natural hydrogen are assessed at a range of geological settings.
- Total natural hydrogen production is estimated to be 39 to 63< Mt H_2 yr^{-1}.

Keywords

hydrogen, natural hydrogen, natural energy, serpentinisation, radiolysis, deep volatile cycles, energy transition

1. Introduction

Hydrogen is the most abundant element in the solar system (Palme et al., 2014). Of this hydrogen, 99.99% is the isotope ^{1}H, and the majority of the remaining 0.01% is deuterium (^{2}H or D). In reduced environments, hydrogen takes the form of the diatomic hydrogen molecule (dihydrogen, molecular hydrogen, or H_2). H_2 is present at a concentration of ~0.5 ppmv in Earth's highly oxidised atmosphere (Novelli et al., 1999), with a short residence time of ~2 years (Ehhalt & Rohrer, 2009).

Although initially considered to be absent as a free phase in nature (e.g., Thomas, 1988), the presence of natural H_2 has now been recognised in a variety of settings at high concentrations (e.g., N. J. P. Smith et al., 2005; Truche et al., 2024), which may be considered paradoxical given that free H_2 is rapidly oxidised in the surface environments of present-day Earth. In spite of this 'H_2 paradox', subsequent studies over the two decades following Smith et al. (2005) have since highlighted the potential for substantial geological H_2 generation on Earth (e.g., Aiuppa & Moussallam, 2024; Hirose et al., 2011; Sauvage et al., 2021; Sherwood Lollar et al., 2014; Worman et al., 2020). The distribution and abundance of natural H_2 have important implications for Earth's geological and biological evolution (e.g., Cascone et al., 2025). Firstly, H_2 is a key source of energy for hydrogenotrophic microbial life, which thrives at mid-ocean ridge black/white smoker sites (e.g., Holden et al., 2012), in geothermal areas (Fullerton et al., 2021; Rogers et al., 2023), and within biospheres deep in the Earth's crust (Adhikari et al., 2016; Freund et al., 2002; Gold, 1992; Ménez, 2020; Plümper et al., 2017; Russell et al., 2010; Russell & Ponce, 2020; Templeton & Caro, 2023). Microorganisms in these ecosystems are believed to use metabolic pathways similar to those utilised by the earliest life on Earth (e.g., Martin & Müller, 1998; Ménez, 2020), and the biological consumption of abiotic H_2 (i.e., H_2 generated without any biological involvement or influence) is therefore a vital component in hypotheses regarding the evolutionary history of life on Earth (e.g., McCollom & Seewald, 2013; Preiner et al., 2018; Russell et al., 2010; Schut et al., 2014) and the potential for extraterrestrial life (e.g., Dzaugis et al., 2018; McMahon et al., 2016).

In addition, H_2 modulates and regulates the oxidation states of planetary surfaces. Atmospheric H_2 acts as an electron donor, thereby reducing oxidised species on the Earth's surface and restricting the concentrations of atmospheric O_2 (e.g., Canfield et al., 2006; Holland, 2002; Stolper et al., 2021). H_2 therefore plays an important role in conducting planetary greenhouse effects, and is hence a key factor in controlling the capacity of planetary atmospheres to become and remain

habitable (e.g., Hao et al., 2019; Liggins et al., 2020; Ramirez & Kaltenegger, 2017; Tian et al., 2005). Characterising the geological processes that can generate H_2 is vital if we wish to determine how life first arose amidst highly reduced and anoxic conditions on Earth (Canfield et al., 2006; Russell et al., 2010), and therefore how life may exist elsewhere in the universe (Glein & Zolotov, 2020; Liggins et al., 2020; Michalski et al., 2013).

Because of this H_2 paradox, the occurrence and generation of natural H_2 has not been investigated in detail until recently, and thus remains far from extensive. For example, H_2 generation by serpentinisation (Section 5.1.1) and radiolysis (Section 5.3) have been known for decades (Curtis & Gancarz, 1983; Moody, 1974, 1976; Thayer, 1966), yet only recently have their fluxes been quantified. Previous review work has explored the natural occurrences of H_2 on Earth at specific tectonic settings (e.g., Worman et al., 2020), within geographical regions (e.g., Boreham, Edwards, et al., 2021), and at a global scale from geological (Klein et al., 2020; Milkov, 2022; Zgonnik, 2020), biological (Gregory et al., 2019), and economic perspectives (e.g., Ellis & Gelman, 2024; Lévy et al., 2023). However, a central aspect of natural H_2 research—for both economic and fundamental science perspectives—are production fluxes of natural H_2. For example, the reviews by Worman et al. (2020) and Zgonnik (2020) provide estimates of 12 Mt H_2 yr^{-1} from mid-ocean ridges (where 1 Mt is equivalent to 10^{12} g) and 23 ± 8 Mt H_2 yr^{-1} from global geological (i.e., non-biological) sources respectively, while Ellis & Gelman (2024) hypothesise that as much as 25 to 25,000 Mt H_2 yr^{-1} may be generated naturally on Earth.

In 2024, the International Energy Agency (IEA) included natural H_2 among current and future energy sources for the first time, paving the ground for new, further decades of vigorous research activity (IEA, 2024). H_2 is utilised in a variety of industrial sectors, with increasing functions as a chemical ingredient (e.g., for ammonia production, food processing and hydrogenation), reducing agent, and an alternative to fossil fuels. In this latter case, H_2 is a cornerstone of the energy transition; its combustion provides nearly three times the energy of petrol (gasoline) per unit mass, yet generates only water as a product and therefore does not contribute to greenhouse gas emissions or air pollutants. Global hydrogen use reached 97 Mt in 2023, with industrial demand expected to rise to ~150 Mt in 2030 (IEA, 2024); however, at present H_2 is expensive and inefficient to produce, and is principally generated via fossil fuels (either through electrolysis or steam-methane reforming). As a consequence H_2 is considered an energy carrier in industry, and not an energy source in its own right (IEA, 2024). With increasing utility as a 'clean' source of energy, the natural generation, transport, storage, and extraction of H_2 generated within Earth

remains a subject of intense study (e.g., Blay-Roger et al., 2024; Gaucher, 2020; Gluyas et al., 2025; I. Moretti, Brouilly, et al., 2021; Osselin et al., 2022; Prinzhofer & Cacas-Stentz, 2023), with estimates of potential natural subsurface H_2 resources ranging substantially from 10^3 to 10^{10} Mt (Ellis & Gelman, 2024).

Our collective understanding of geological H_2 generation has vastly expanded in recent times (Figures 1 and 2; Table 1), and necessitates a re-evaluation of the known natural fluxes of H_2. In particular, we highlight the growing wealth of knowledge regarding H_2 generation and migration at subduction settings (e.g., Merdith et al., 2023; Suzuki et al., 2024; Vitale Brovarone et al., 2020), within subseafloor environments (e.g., Sauvage et al., 2021), during volcanic degassing (e.g., Aiuppa & Moussallam, 2024; Stolper et al., 2021), and within ophiolites (e.g., Baciu & Etiope, 2024; Carrillo Ramirez et al., 2023; Truche et al., 2024). Moreover, the literature often assumes that natural H_2 is essentially abiotically generated geological H_2. It is now understood that biology also plays a key role in orchestrating the natural abundances of H_2. Biotically sourced H_2 can be generated from sedimentary organic matter, either through its degradation by H_2-producing bacteria (e.g., Gregory et al., 2019), or through thermogenic maturation at high temperature (e.g., Li et al., 2015). Coupled with these new, exciting fields of development are evergrowing uncertainties in the H_2 fluxes and concentrations generated by each process, which may scale orders of magnitude. Hydrogen exploration, both for research and industrial advancements, must be driven forward considering these new environments, their H_2 fluxes, and any uncertainties in these fluxes.

In this manuscript we review and summarise the current understanding of the quantities of natural H_2 produced at geological settings (i.e., 'geological' H_2). Within this context, we will differentiate between 'biotic' processes that generate H_2 from microbial metabolisms and organic materials, and 'abiotic' mechanisms that do not involve any biological input. Geological H_2 is often the product of several processes that generate and consume H_2 during transport from its source to the Earth's surface. Disentangling the contributions that each individual process provides to an observed H_2 flux in a geological setting is key if we want to determine where on Earth we may locate and extract high quantities of natural H_2.

Our manuscript is presented as two complementary parts. In the first part (Sections 2–5), we provide an updated review of the key identifiers and processes of H_2 within geological settings, and discuss the limitations of methods used to assess and estimate H_2 fluxes from these

processes. We start with the origins and possible reservoirs of primordial H_2 on Earth (Section 2), before then discussing the biological processes that generate H_2 at or near Earth's surface (Section 3). Subsequently entering the deep Earth, we follow with the formation of H_2 through the thermal decomposition of organic matter (Section 4). We conclude this first part by providing an overview of the abiotic processes that can generate H_2 in the absence of biology (Section 5).

In the second part, we summarise and quantify the fluxes of H_2 at geological settings that arise from the processes discussed in Sections 2–5, with emphasis on highlighting the uncertainties and knowledge gaps in our current understanding of H_2 generation (Section 6) and migration (Section 7). In this part, and more generally throughout the manuscript, the term 'flux' is used interchangeably with 'production rate' or 'generation rate' to mean 'mass of H_2 produced per unit time', although some authors (e.g., Sherwood Lollar et al., 2014) note the difference between 'production rate' (concerning production from H_2-generating reactions only) and 'flux' (concerning reaction production rates combined with rates of subsequent migration out of the H_2 source environment). Wherever possible, we present flux values in their original units of measurement, and their equivalent in megatonnes (Mt) of H_2 generated per year. To conclude our manuscript, we utilise our perspectives on natural H_2 generation to discuss its implications for Precambrian life (Section 8), and combine our flux estimates to quantify a present-day global geological flux of H_2 to Earth's exosphere (Section 9).

1.1. Note on hydrogen isotopic fractionation

In geological and meteorological applications, a commonly used means of identifying the provenance of H_2 is the isotopic characterisation of hydrogen atoms comprising the diatomic H_2 molecule. The ratio between D and H can be used as a tracer of kinetic processes in H_2-producing/-transporting systems that may result in hydrogen mass fractionation, and is commonly expressed as delta notation (δ; Equation 1):

(Eqn. 1) $$\delta D = \left(\left[\frac{(D/H)_{sample}}{(D/H)_{reference}}\right] - 1\right) \cdot 1000$$

Where δD is reported in permille (‰) and typically referenced to Vienna Standard Mean Ocean Water (VSMOW). Geological H_2 possesses δD values ranging from -1000 to -100‰ (Etiope, 2023; Milkov, 2022); in particular, biological processes may result in a strong light isotope signature, i.e., very negative δD (Section 3) (e.g., Suzuki et al., 2017).

While hydrogen isotopic fractionation is often used to distinguish between known sources of H_2, we note that isotopic signatures cannot be solely used to differentiate between abiotic and biotic processes. Certain characteristics of isotopic equilibration in H_2, such as the kinetic isotope effect relative to other fluid species, remain uncertain and difficult to quantify in geological systems and at geological pressures and temperatures (Ni et al., 2011; Turner et al., 2021). In fact, certain abiotic H_2-generating processes do not appear to affect hydrogen isotopic fractionation in H_2 at all (e.g., Kawagucci et al., 2010; L.-H. Lin, Slater, et al., 2005). In addition, isotopic equilibrium of hydrogen between H_2 and H_2O is rapidly achieved at high temperatures (Horibe & Craig, 1995; Pester et al., 2018; Proskurowski et al., 2006; Ricci et al., 2022), and may be catalysed by hydrogenotrophic methanogens at low temperature (B. J. Campbell et al., 2009; Kawagucci et al., 2010). Finally, we note the potential for the mobilisation of light hydrogen within organic material by a number of abiotic processes, thereby generating geological H_2 with an apparent 'biological' isotope signature. The sources and processes generating H_2 in geological settings must therefore be principally inferred through geological context, with H_2 isotopic information only to be used in combination with other geochemical evidence.

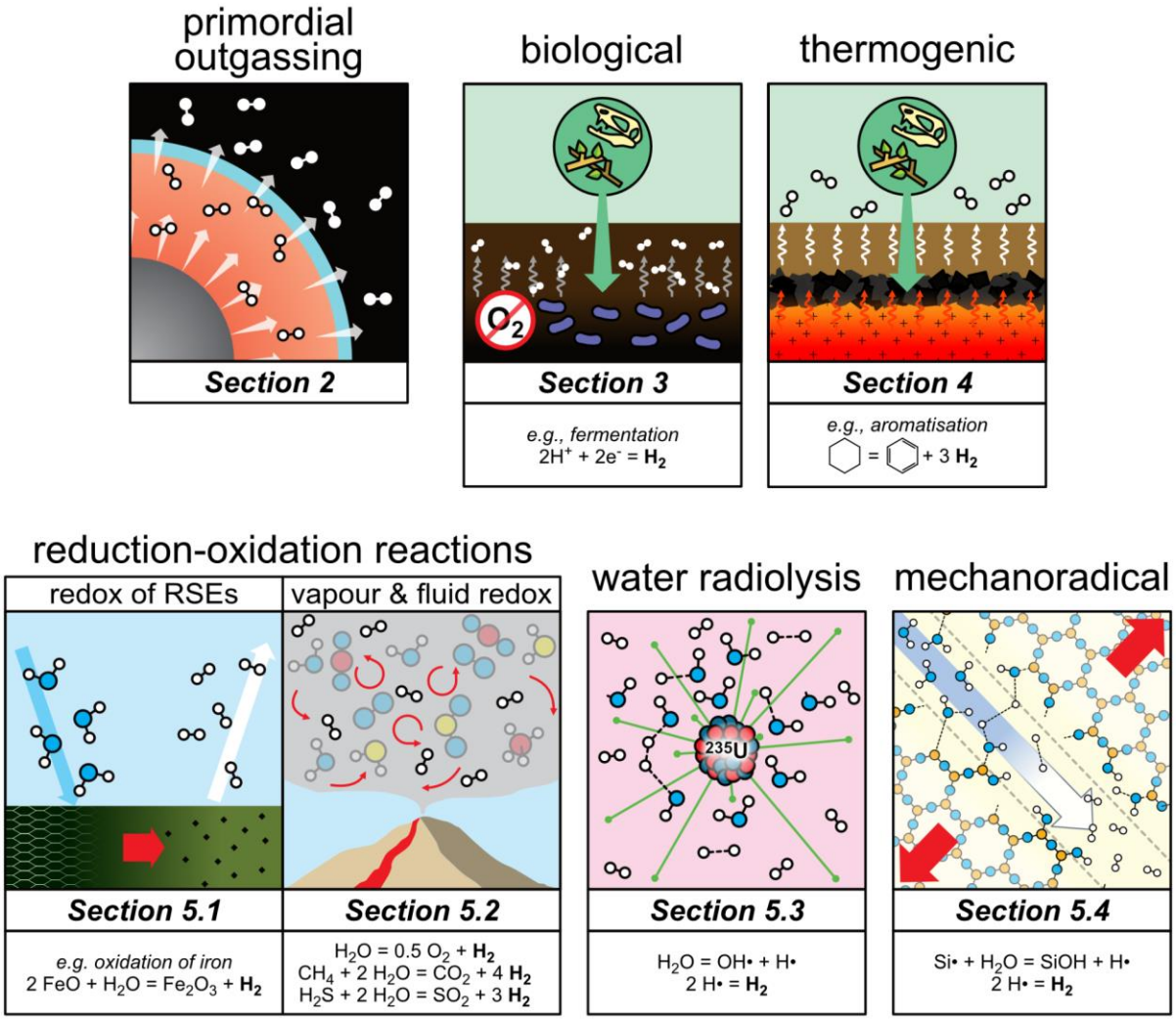

Figure 1. Cartoon summary of the principal geological processes that can result in the liberation and production of natural H_2, the sections in which we discuss each process, and the key reactions that underlie them. The example used for the redox of redox-sensitive elements (RSEs) is ferrous iron (Fe^{2+}) oxidation, which encompasses a number of secondary processes (e.g., serpentinisation, basalt auto-oxidation, etc.). Although iron oxidation has attracted great attention, we note that the oxidation of other RSEs may contribute towards H_2 generation in geological settings, such as carbon (including graphite-saturated C-O-H fluids), sulphur, manganese, chromium, etc. Similarly, processes such as demethylisation, polycondensation, and graphitisation will contribute to thermogenic H_2 generation in addition to the example of aromatisation shown above.

Process	**Factors promoting H_2 production or liberation**	**Natural settings**
primordial	deep mantle plume activity?	tectonically active settings? intraplate plume volcanoes? ubiquitous?
biological	anoxic environments, high organic carbon	anoxic environments (e.g., marine sediments, wetlands and bogs, organic-rich sedimentary basins)
thermogenic	diagenesis and metamorphism (highest production rates at 700–800 °C), open systems, low pressures(?), low sulphur(?)	subduction zones, organic-rich sedimentary basins, organic-rich sediments near magmatic intrusions
mineral redox	high source rock Fe^{2+}, low silica activity, fracture formation, 50–600 °C (maximum at 200–315 °C for serpentinisation), high pH and high salinity (serpentinisation), open systems (Fe-brucite oxidation), reduced conditions (C-O-H fluid speciation)	mid-ocean ridges (especially ultraslow) and transform faults, oceanic crust and lithosphere, subduction zone outer rises, subducting slabs, mantle wedges, ophiolites, greenstone belts, banded iron formations, Fe-rich granites, etc.
gas/vapour redox	reduced source magmas, high temperatures (maximum recorded in gases >900 °C), rapid transit through volcanic-hydrothermal system to avoid fluid-rock interactions	volcanic-hydrothermal settings
radiolysis	radioactivity sources (radiation proportional to ^{235}U, ^{232}Th, ^{40}K concentrations in igneous, metamorphic	oceanic crust and sediments, continental crust (especially Precambrian crust)

	and sedimentary settings), long water residence times, small pore spaces/fracture widths (e.g., by small grain sizes), high salinity	
mechanoradical	high frictional work and fracture surface area, high water availability, high silica exposed on fracture surface	tectonically active settings, subglacial environments

Table 1: Summary of the factors affecting H_2 generation and availability by the processes illustrated in Figure 1, and the natural settings where each process is active (Figure 2).

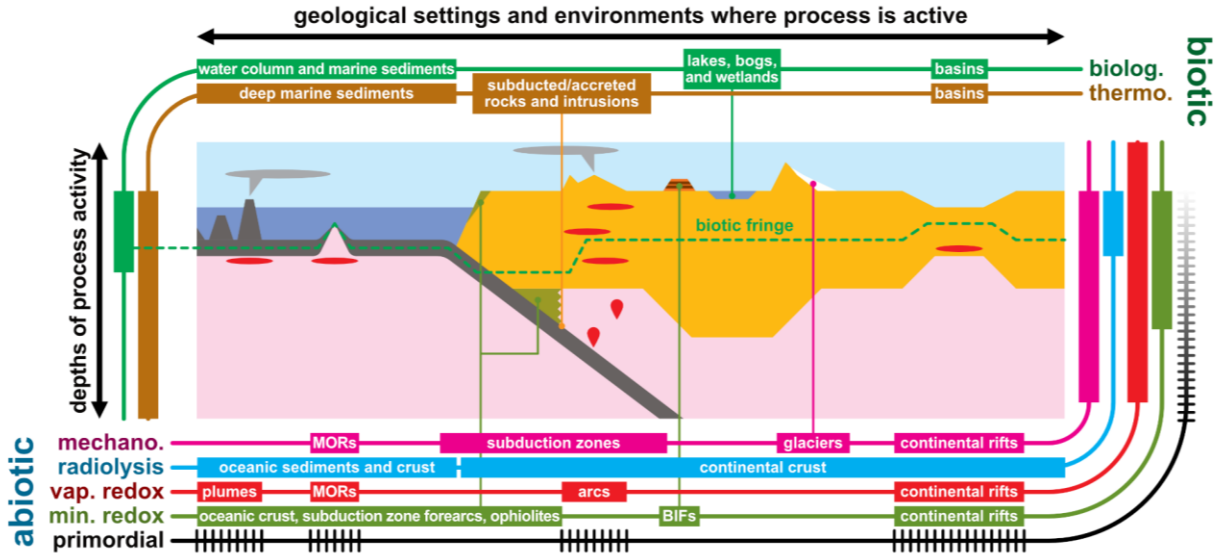

Figure 2. Schematic figure summarising geological environments where different H_2-producing or H_2-liberating processes may be active. Each line wrapping around the central schematic diagram represents a biotic (left and top) or abiotic (right and bottom) process as discussed in this manuscript. The horizontal and vertical bars respectively mark geological settings and depths in the schematic diagram where a specific process is active. The green dashed line marks the biotic fringe, representing the limit of deep life. The possible degassing of primordial H_2 (Section 2) remains unquantified, but may coincide with volcanically active settings.

2. Primordial H_2 degassing

Hydrogen was delivered to Earth alongside other volatile elements during planetary accretion (Broadley et al., 2022; R. W. Carlson et al., 2014; Marty et al., 2016). On the basis of hydrogen isotope ratios in the water molecule, hydrogen on Earth is believed to derive from the accretion of enstatite chondrite material (Piani et al., 2020) with possible additional contributions from carbonaceous chondrites (Alexander et al., 2012; Marty, 2012; Robert, 2003). Late veneer material, delivered post-accretion, did not contribute substantially to Earth's hydrogen budget (<5% mass; Wang et al., 2023). During planetary differentiation, a substantial portion of hydrogen partitioned into the core, where, alongside other light elements (including silicon, sulphur, carbon, and oxygen), it contributes towards a ~10% non-iron-nickel fraction in the present-day core (Tagawa et al., 2021; W. Wang et al., 2021). Hydrogen dissolved within the core may constitute as much as 80 ocean masses (Ikuta et al., 2019; Y. Li et al., 2020). Within the silicate Earth, hydrogen is present predominantly as water within hydrous and nominally anhydrous minerals in the crust and mantle (e.g., Novella et al., 2024). In contrast, H_2 may comprise only a few ppm in nominally anhydrous mantle minerals (Moine et al., 2020; X. Yang et al., 2016).

The reduced conditions on early Earth (e.g., Rubie et al., 2011; Yang et al., 2014) would have promoted the speciation of hydrogen into H_2 (e.g., Young et al., 2023). Primordial H_2, transferring between Earth's early atmosphere, silicate magma ocean, and metallic core, may have provided an important vector for the formation of liquid water on Earth (e.g., Gaillard et al., 2022; Genda & Ikoma, 2008; Young et al., 2023). In early planetary atmospheres, H_2 contributes towards the greenhouse effect, expanding the habitable zone around stars within which liquid water is stable (e.g., Ramirez & Kaltenegger, 2017). However, atmospheric H_2 is easily lost to space owing to its low molecular mass (e.g., Pierrehumbert & Gaidos, 2011). Although atmospheric H_2 may be replenished through geological processes such as volcanism (Liggins et al., 2020), retaining large quantities of H_2 in planetary atmospheres is challenging over geological timescales (>100 million years) (Wordsworth, 2012). The loss of primordial H_2 from the early Earth could have therefore driven its oxidation (Catling et al., 2001; Sharp et al., 2013).

Whether primordial H_2 reservoirs within Earth persist to the present day remains an open question. It is not unreasonable to suggest that primordial molecular H_2 derived from the capture of volatile-rich bodies may still be preserved within Earth, for example, as H_2 within nominally anhydrous mantle minerals (Gu et al., 2022; Moine et al., 2020; X. Yang et al., 2016). However, free H_2 is highly reactive, and is likely instead to be dissolved in carbon-oxygen-hydrogen (C-O-

H) fluids (see Section 5.1.2) and small-fraction volatile-rich melts, and possibly as mineralic fluid inclusions (E. M. Smith et al., 2016, 2018; Q. Williams & Hemley, 2001). Experiments demonstrate that the present-day mantle is metal-saturated at depths greater than ~250 km and permits the stability of deep H_2-bearing fluids (Rohrbach et al., 2007, 2011), an observation supported by metal and fluid inclusions preserved in diamonds (E. M. Smith et al., 2016, 2018). Such melts and fluids, in a static environment, would effectively have an infinite residence time (Q. Williams & Hemley, 2001). In practice however, their long-term preservation is unlikely owing to mantle convective flow, which will modulate mantle pressure-temperature-redox conditions and therefore the stability of these H_2-bearing fluids and small-fraction melts over geological timescales.

The capacity of these primordial H_2 reservoirs to degas is another open question. Hydrogen isotopes, measured from H_2O in ocean island basalt melt inclusions, record a strongly negative δD (up to -218‰), suggesting contributions from a protosolar component in Earth's mantle that persists to the present-day (δD = -870‰; Hallis et al., 2015). Similarly, noble gas isotopes demonstrate the presence of undegassed primordial material in Earth's deep mantle (e.g., Mukhopadhyay & Parai, 2019), which could operate as a deep reservoir of H_2. Primordial H_2 may therefore exist in the deep mantle and contribute to deep Earth hydrogen degassing—a factor that several studies hypothesise may be related to a range of natural phenomena (e.g., Gilat & Vol, 2005, 2012; N. Larin et al., 2015; V. N. Larin, 1993; Toulhoat & Zgonnik, 2022).

Complicating matters further is the absence of diagnostic signatures for identifying primordial H_2. While the hydrogen isotope signatures of the protosolar nebula and carbonaceous chondrites have been established (Robert, 2003), the hydrogen isotopic composition of Earth remains elusive (see Section 1.1; Q. Williams & Hemley, 2001). Isotopic fractionation of hydrogen between H_2 and water is strongly temperature-dependent and the exchange process at high temperatures (>200 °C) may be as rapid as a few hours (e.g., Proskurowski et al., 2006). At lower temperatures, isotopic exchange may be catalysed by hydrogenotrophic methanogens and other hydrogen-oxidising microorganisms (e.g., Campbell et al., 2009), erasing any isotopic evidence for primordial H_2 that would otherwise be preserved. As such, while deep, primitive hydrogen reservoirs may contribute towards global H_2 degassing, this review follows previous work (e.g., Zgonnik, 2020) in disregarding possible fluxes of primordial H_2 from Earth's interior.

We clarify here that our use of the term 'primordial' hydrogen is chosen to differentiate from 'deep-seated' hydrogen, which is defined by Zgonnik (2020) as "hydrogen originating from the Earth's

mantle or core, but not from crustal processes". 'Deep-seated' H_2, by Zgonnik's definition, could arise from a number of generative processes during subduction and magmatism as discussed below in addition to primordial H_2 degassing. By using the term 'primordial', we specify that this H_2 was captured as such during planetary accretion, and which has remained unaltered since its entrapment within Earth. Primordial H_2 could therefore contribute towards subsequent reactions in the solid Earth, possibly concluding in the production of H_2 by another means. Processes that generate and sequester hydrogen in the lower mantle and core are beyond the scope of this review.

3. Biological production of H_2

H_2 is used and produced by a large number of diverse microorganisms in all Earth environments. Microorganisms are capable of using H_2 as an electron donor in energy-conserving redox reactions (Hay Mele et al., 2023), coupling it to a broad selection of terminal electron acceptors such as oxygen, nitrate, sulphate, Fe^{3+} and carbon dioxide. H_2 is also produced by microorganisms either as a by-product of certain metabolisms or directly to balance cellular reducing equivalents during the anaerobic degradation of organic matter in the absence of electron acceptors—a process known as fermentation (e.g., Hackmann, 2024). H_2 can be produced through various metabolic processes in addition to fermentation, including nitrogen fixation, carboxydotrophy (anaerobic carbon monoxide oxidation), and phosphite oxidation; among these processes however, fermentation is by far the most prominent and widespread contributor to biological H_2 production (e.g., Gregory et al., 2019).

The enzymes involved in the production or consumption of H_2 are known as hydrogenases, and are characterised by the presence of a metal-containing catalytic centre responsible for the reversible reaction between H_2 and its constituent protons and electrons (Reaction 1; Cascone et al., 2025):

(Rxn. 1) $2H^+ + 2e^- = H_2$

Hydrogenases are classified into three main types based on their metal cofactors: [FeFe], [NiFe], and [Fe]. [FeFe]-hydrogenases, typically associated with H_2 production, are found in anaerobic bacteria, some archaea and some eukaryotes. [NiFe]-hydrogenases, found in cyanobacteria, archaea, and many bacteria, are involved in H_2 uptake and biological oxidation (i.e., use of H_2 as an electron donor). [Fe]-hydrogenases are found only in archaea and are responsible for H_2

production. Additional enzymes are used by microorganisms to sense and react to H_2 concentrations and gradients in the environment (Cascone et al., 2025).

Microbial handling of H_2 can induce strong kinetic isotope effects, with large isotopic fractionations induced by both the biological production and consumption of H_2. Experiments and theoretical works show that biologically produced H_2 has extremely negative values, with reported fractionations of up to -758‰ (Walter et al., 2012; H. Yang et al., 2016). The extent of fractionation between the H_2 undergoing biological oxidation and the final products are highly dependent on the electron acceptor of the redox reactions and the specific enzymes involved. When coupled to oxygen, nitrate, and sulphate as electron acceptors, reported fractionation rates between the biomass and environmental water are large ($\Delta_{biomass\text{-}water}$ between -130 and -247‰; Osburn et al., 2016). Fractionation effects during methanogenesis can vary from δD_{CH4} = -170‰ (vs. VSMOW) when biological H_2 oxidation is coupled to CO_2 reduction (Whiticar, 1999), to δD_{CH4} ~ -550‰ from the methanogenesis of methylated compounds (Whiticar, 1999). Direct measurements of the effect of biological H_2 oxidation on the isotopic composition of the local hydrogen budget are scarce, although field experiments suggest that microbial activity might induce rapid changes in the isotopic composition of H_2. Within the context of geological H_2 storage, experiments have shown that a fast (28 days) change in the isotopic composition of injected H_2 can be achieved in a porous reservoir (from -161‰ to -711‰), which was attributed to microbial hydrogenase activity (Löffler et al., 2022). Such extreme deuterium depletion suggests that biological H_2 might be an important contributor to the atmospheric hydrogen isotope budget, even if the mass contribution of biological H_2 to global cycles is considered small (around 10% of global annual H_2 production; Pieterse et al., 2011).

During fermentation, microorganisms oxidise organic carbon in the absence of an inorganic electron acceptor (e.g., Hackmann, 2024). Reducing equivalents (i.e., electrons) accumulated during these metabolisms cannot be discarded on high-potential electron acceptors (e.g., oxygen, nitrate, sulphate) that are absent in environments where fermentation occurs. To achieve redox balance, microorganisms release excess electrons as H_2. Several microorganisms are capable of switching to fermentation in the absence of suitable electron acceptors, and a large number of microorganisms are obligate fermenters; this mode of organic carbon degradation is their sole metabolic strategy. Fermentation is expected to be important in anoxic environments with a significant load of organic carbon. As such, fermentation is widespread in the deeper layers of marine sediments, in peatland, bogs and wetlands, in organic-rich sedimentary basins, and in all

other anoxic environments where conditions are reducing and a significant fraction of organic carbon is present.

Other lesser-characterised metabolic pathways that generate H_2 include nitrogen fixation, a process performed by nitrogenase enzymes which consume nitrogen gas to generate ammonia (NH_3; Reaction 2):

(Rxn. 2) $N_2 + 8H^+ + 8e^- = 2NH_3 + H_2$

Nitrogenases are present in a wide variety of anaerobes in subsurface environments (Gregory et al., 2019), although the diversity and distribution of genes that perform nitrogen fixation continues to remain a subject of study (Gaby & Buckley, 2011). Other known metabolic pathways that can generate H_2 include carboxydotrophy (Reaction 3; Sipma et al., 2006) and phosphite oxidation (Reaction 4; Yang & Metcalf, 2004), although both are considered minor contributors to microbial metabolisms:

(Rxn. 3) $CO + H_2O = CO_2 + H_2$

(Rxn. 4) $H_3PO_3 + H_2O = H_3PO_4 + H_2$

The H_2 produced through fermentation and these other pathways is generally expected to be consumed rapidly by the rest of the microbial community within the same ecosystem or surrounding ecosystems (e.g., in shallower sediment layers) in metabolic reactions such as sulphate reduction or methanogenesis (Section 6.6; Lupton et al., 1984). Data from subsurface marine sediments show that H_2 utilisation by the microbial community is very high while concentrations of free H_2 in pore waters are low (nM range), betraying a fast biological H_2 cycle that does not permit the accumulation and migration of H_2. Thus, while the biological production rate of H_2 might be very high as evidenced by molecular data (Conrad, 1996), the measured fluxes of H_2 are considered generally low.

4. Thermogenic production of H_2

During diagenesis and metamorphism, the thermal maturation (pyrolysis) of organic material in coals and carbonaceous shales over a wide temperature range (70–1200 °C) can result in the thermogenic generation of H_2 (J. Campbell, 1978; Froidl et al., 2021; X. Li et al., 2015; Mahlstedt et al., 2022). The breaking of C–H bonds during pyrolysis will free hydrogen atoms from

hydrocarbon structures, which can subsequently form H_2. Processes that break C–H bonds in hydrocarbons, such as aromatisation, polycondensation, and graphitisation, are therefore regarded as primary pathways for dehydrogenation and H_2 generation, with the amount of generated H_2 primarily correlated with the susceptibility of the hydrocarbon to undergo these reactions (X. Li et al., 2015). Furthermore, hydrogen dissociation from organic materials may result in the generation of exceptionally light H_2 (i.e., highly negative δD), as the dissociation energy of the C–D bond is greater than that of C–H (Suzuki et al., 2017).

Several factors, resolved through experimental pyrolysis, control the amount of H_2 that may result from the thermal maturation of organic materials. Firstly, the composition of the organic source controls H_2 generation. High yields of thermogenic H_2 are generated from source rocks with high total organic content and low thermal maturity; i.e., rocks with high hydrocarbon generation potential (X. Li et al., 2015; I. Moretti et al., 2024). In addition, H_2 production is a function of temperature; H_2 generation rates may fluctuate between multiple peaks at different temperatures depending on organic material composition (e.g., Li et al., 2015). At low temperatures (70–155 °C), thermogenic H_2 generation in seafloor sediments can be catalysed by prokaryotic activity, even beyond the prokaryotic temperature limit of 122 °C (Parkes et al., 2007, 2011). Thermogenic H_2 production then generally increases with pyrolysis temperature. From ~300 °C, thermal cracking and demethylisation of long-chain hydrocarbons (Espitalié et al., 1984; Lorant & Behar, 2002), and the breaking of non-C–H hydrocarbon heterobonds (Tissot et al., 1971) may liberate H_2, although specific mechanisms remain speculative for the latter process. Maximum thermogenic H_2 generation rates are achieved at ~700–800 °C from aromatisation and polycondensation, although H_2 production can continue to temperatures as high as 1200 °C (X. Li et al., 2015; Mahlstedt et al., 2022). In addition to temperature, other factors affecting H_2 generation include high total sedimentary sulphur, which may limit the production of H_2 in favour of H_2S at temperatures below 450 °C (X. Li et al., 2017, 2018). Furthermore, high pressures may slow the thermal maturation of organic materials at temperatures up to 400 °C (Dalla Torre et al., 1997; Le Bayon et al., 2011), but as a whole the effect of pressure on thermogenic H_2 generation remains highly uncertain (X. Li et al., 2015). High heating rates will accelerate the generation of H_2, although overall yields of H_2 are independent of heating rate (Horsfield et al., 2022).

H_2 produced from pyrolysis in open systems can immediately escape its source (e.g., Reynolds et al., 1991). However, H_2 cannot escape in closed systems and will contribute towards secondary reactions that consume H_2, such as unsaturated hydrocarbon hydrogenation (X. Li et al., 2017).

This is reflected in experiments with variable sample masses and corresponding void space volumes: lower void volumes will result in higher H_2 partial pressures, increasing the probability that newly generated H_2 may be consumed by secondary reactions (X. Li et al., 2017). Finally, H_2 liberated from hydrocarbons, regardless of open- or closed-system pyrolysis, are subsequently subject to a variety of other gas phase reactions, such as water-gas shift or reaction with CO (Horsfield et al., 2022; Mahlstedt et al., 2022).

Thermogenic H_2 can therefore be generated in geological environments where organic-rich sediments, sedimentary, and metasedimentary rocks are exposed to high temperatures, including hydrocarbon-bearing basins and coal deposits (Boreham et al., 2023; Horsfield et al., 2022; I. Moretti et al., 2024), thermal aureoles (Iacono-Marziano, Gaillard, et al., 2012), and accretionary prisms and subduction zones (Suzuki et al., 2017, 2024). With progressive subduction, organic matter undergoes progressive thermal maturation, chemical purification, and graphitisation (e.g., Beyssac et al., 2002; Buseck & Beyssac, 2014). During these processes, H_2 is certainly produced, but likely in smaller amounts compared to thermogenic decomposition of hydrocarbons. H_2 generation can therefore extend to high temperatures well above the limits of oil and gas exploration (Boutier, Martinez, Sissmann, et al., 2024), although the literature on the metamorphism of subducted organic-rich sediments at these pressure-temperature conditions generally neglects these high-temperature processes.

5. Abiotic processes liberating and generating geological H_2

The underlying abiotic processes that generate geological H_2 (Figure 1) are commonly observed in a multitude of different geological and tectonic environments (Figure 2; Table 1). In this section, we summarise these key processes and the factors that control the quantity of geological H_2 that may be generated through them.

5.1. Mineral redox reactions

Redox conditions control the physico-chemical nature of reactions within and between different reservoirs on Earth (B. R. Frost, 1991). Materials within the Earth's interior are reduced (i.e., lower oxidation state) relative to the surface environment. In the upper mantle, oxygen fugacity straddles the fayalite-magnetite-quartz (FMQ) buffer, with natural variation of ±2 log units relative to FMQ (e.g., D. J. Frost & McCammon, 2008; Lee et al., 2005; Li & Lee, 2004; McCammon, 2005). Redox-sensitive elements (e.g., Fe, C, and S) are primarily present in their reduced forms (e.g., Fe^0 and Fe^{2+}, C^0, S^0 and S^{2-}) in deep-Earth minerals, whereas they are more oxidised (e.g., Fe^{3+},

475 C^{4+}, S^{4+} and S^{6+}) in shallower environments. When materials derived from the mantle are exposed
476 to the Earth's surface, they are oxidised through reaction with H_2O, CO_2, O_2, and other electron
477 acceptors.
478
479 Iron is a key redox-sensitive element in geological materials, and occurs as ferrous (Fe^{2+}) and
480 ferric (Fe^{3+}) phases. On and within Earth, the oxidation of ferrous iron to ferric iron in the absence
481 of free oxygen is principally performed through reaction with H_2O, which itself is reduced to form
482 H_2. This is represented by the generalised reaction (Reaction 5):
483
484 (Rxn. 5) $2\ Fe^{2+}O + H_2O = {Fe^{3+}}_2O_3 + H_2$
485
486 A key metric for quantifying the amount of H_2 generated by such redox reactions is the ratio of
487 Fe^{2+} to Fe^{3+} in a rock that has undergone oxidation (e.g., Bach & Edwards, 2003). For example,
488 in the process of serpentinisation (see following section), Fe^{2+} is oxidised to Fe^{3+}, with most of
489 this Fe^{3+} incorporated within the by-product mineral magnetite ($Fe^{2+}{Fe^{3+}}_2O_4$). Bulk magnetite
490 content has therefore often been used to derive the cumulative H_2 flux throughout the
491 serpentinisation process (Bach et al., 2006; Sleep & Bird, 2007). However, this assumption may
492 not be appropriate if other Fe^{3+}-bearing minerals form during the serpentinisation reaction, as
493 these reactions will compete for the elemental components required to generate magnetite (Ely
494 et al., 2023; Klein et al., 2014). Furthermore, some reactions that may be attributed purely to
495 water-rock interactions may be catalysed through biological activity (Bryce et al., 2018), including
496 iron oxidation (Bach & Edwards, 2003).
497
498 **5.1.1. Serpentinisation**
499 In geological settings on or near Earth's surface, an important redox reaction resulting in the
500 generation of H_2 in high concentrations is serpentinisation (e.g., Klein et al., 2009, 2013;
501 McCollom et al., 2016, 2020; McCollom & Bach, 2009). Ultramafic rocks, which are the
502 predominant lithology in the mantle, are also present at crustal depths and exposed at the Earth's
503 surface in a variety of settings, including the oceanic lithosphere, large stratified intrusions, and
504 palaeo- and present-day convergent plate margins. These ultramafic lithologies contain a high
505 proportion of iron-magnesium minerals including olivine ($[Fe^{2+},Mg]SiO_4$) and pyroxene
506 ($[Fe^{2+},Mg]SiO_3$), and under a wide range of pressure and temperature conditions, the reaction of
507 these rocks with water will produce the hydrous mineral serpentine (e.g., antigorite,
508 $[Fe^{2+},Mg]_3Si_2O_5(OH)_4$) commonly with the iron oxide mineral magnetite ($Fe^{2+}{Fe^{3+}}_2O_4$) alongside

other iron-magnesium by-product minerals such as brucite ($[Fe^{2+},Mg](OH)_2$) (e.g., Thayer, 1966). During aqueous alteration, the Fe^{2+} in ultramafic and mafic minerals is oxidised to Fe^{3+} in minerals such as magnetite, haematite, serpentine, and andradite (Andreani et al., 2013; Klein et al., 2014). Coupled to this oxidation reaction is the reduction of H_2O to H_2. Serpentinisation can be generalised as the following expression (Reaction 6; e.g., McCollom et al., 2022):

(Rxn. 6) $[Fe^{2+},Mg]SiO_4$ [olivine] ± $[Fe^{2+},Mg]SiO_3$ [pyroxene] + H_2O = $[Fe^{2+},Fe^{3+},Mg]_3Si_2O_5(OH)_2$ [antigorite serpentine] ± $[Fe^{2+},Mg](OH)_2$ [brucite] ± $Fe^{2+}Fe^{3+}{}_2O_4$ [magnetite] + H_2

Understanding the mechanics and limits of this reaction is therefore paramount to determining where serpentinisation may occur on Earth, and therefore the fluxes of H_2 that may be released into the exosphere via this reaction. To this end, experimental studies have now extensively explored the range of conditions within which the serpentinisation reaction can occur, and how much by-product H_2 is generated as a result (e.g., McCollom, 2013). It is clear that both pressure and temperature are strong controls on the kinetics of the serpentinisation reaction and the quantity of H_2 and mineral products that may be generated (Barbier et al., 2020; Huang et al., 2020; Lazar, 2020; McCollom et al., 2016). H_2 production is maximised at temperatures of 200–315 °C (McCollom & Bach, 2009), although there is substantial experimental evidence that serpentinisation and other H_2-generating fluid-peridotite reactions may occur at temperatures as low as 25–100 °C (e.g., Mayhew et al., 2013; Neubeck et al., 2011; Okland et al., 2014). Low-temperature conditions will limit rates of reaction or result in the partitioning of Fe^{2+} into brucite, and hence restrict H_2 generation (McCollom & Donaldson, 2016). However, serpentinisation at low temperatures may be catalysed, for example through the presence of the Ni^{2+} cation (Song et al., 2021) or spinel-group phases such as magnetite (Mayhew et al., 2013; Neubeck et al., 2011). At higher temperatures (>390 °C), serpentinisation is faster, although thermodynamic equilibrium can be attained between olivine and fluid, therefore limiting reactions and H_2 generation (McCollom & Bach, 2009). Serpentine may also be replaced with talc as a high-temperature alteration product, restricting the Fe^{3+} that can be incorporated into product minerals (McCollom & Bach, 2009). At even higher temperatures—up to and potentially exceeding ~550 °C—H_2 production through serpentinisation may be hampered by the precipitation of Fe^{2+}-rich olivine as a reaction product (Evans, 2010). Nevertheless, natural rocks and thermodynamic models suggest that serpentinisation can produce H_2 at these high-temperature conditions (Boutier et al., 2021; Siron et al., 2024; Vitale Brovarone et al., 2020)

The range of the serpentinisation reaction is limited by the stability of the serpentine minerals (Evans, 2004; Evans et al., 2013; Schwartz et al., 2013; Ulmer & Trommsdorff, 1995). At low temperatures (<300–400 °C), the phases lizardite and chrysotile are favoured; at higher temperatures (>300 °C), antigorite is preferred (Evans, 2004). Above ~600 °C and ~6 GPa, antigorite is no longer stable and will dehydrate to form ultramafic minerals and aqueous fluids (Padrón-Navarta et al., 2011; Schwartz et al., 2013; Ulmer & Trommsdorff, 1995). H_2 generation from serpentinisation is thereby restricted to the pressure-temperature range at which the serpentine minerals, in particular the high-pressure form antigorite, are stable. Models considering H_2 generation from serpentinisation must therefore account for this 'serpentinisation window', usually by considering a maximum temperature limit to serpentinisation consistent with mid-ocean ridge conditions (typically 350–400 °C; e.g., (Rüpke & Hasenclever, 2017; Zwaan et al., 2025), although a serpentine stability field as a function of both pressure and temperature is more appropriate (e.g., Merdith et al., 2023; Siron et al., 2024).

In addition to pressure and temperature, the composition of the protolith, the composition of the fluid, and the fluid-rock ratio also have significant effects on the amount of H_2 produced during serpentinisation (Ely et al., 2023; Huang et al., 2017, 2021; Klein et al., 2013; McCollom et al., 2016; McCollom & Bach, 2009; Siron et al., 2024). H_2 generation is correlated to the degree of Fe^{2+} in ultramafic minerals that is oxidised to Fe^{3+} incorporated within product minerals (e.g., Marcaillou et al., 2011); for example, serpentinisation of high-Fe olivine generates more H_2 than high-Mg olivine, as more Fe^{3+} will partition into serpentine and magnetite (McCollom et al., 2022; Tutolo & Tosca, 2023). Faster serpentinisation rates may be promoted by raising the pH (Huang et al., 2019; McCollom, Klein, Solheid, et al., 2020) and the salinity (Huang et al., 2023) of the oxidising fluids. High aqueous SiO_2 concentrations also strongly limit H_2 generation during serpentinisation; at low temperatures (< 200 °C), high aqueous SiO_2 will form serpentine with elevated Si in its mineral structure, limiting Fe^{3+} uptake (Tutolo et al., 2020); at higher temperatures (>300 °C), high aqueous SiO_2 promotes talc as a product mineral in lieu of serpentine (Huang et al., 2024; Oyanagi et al., 2020; Syverson et al., 2017). Finally, petrological models show that H_2 generation at subduction interface conditions is decoupled from olivine serpentinisation, with the greatest production of H_2 achieved by the reaction of slab fluids with orthopyroxene-rich peridotites (Siron et al., 2024).

In natural systems, rates of serpentinisation tend to decrease with progressive reaction. Serpentine minerals have a greater molar volume than ultramafic minerals (e.g., Berman, 1988), and volume increase stresses from early serpentine growth will initially promote serpentinisation by increasing rock porosity by fracturing (Malvoisin et al., 2017; L. Zhang et al., 2019). However, these developing serpentine minerals will seal off fractures and passages of fluid flow as reaction progresses, thus decreasing permeability and limiting serpentinisation (Klein et al., 2015). Similarly, serpentinising surfaces will form a 'shielding' layer of serpentine minerals with progressive reaction, restricting the access of fluids to fresh ultramafic surfaces (Mayhew et al., 2013; Okland et al., 2014).

Because of these multiple compositional and mechanical controls on serpentinisation, predicting H_2 production through serpentinisation is not straightforward. As an example, the reactant and product mineral species in Reaction 5 are solid-solution series between Fe and Mg; much of the Fe^{2+} liberated from serpentinisation will remain as Fe^{2+} in serpentine and/or brucite solid solutions (e.g., McCollom & Bach, 2009). Natural serpentines from Hess Deep have Fe^{2+} contents lower than the olivines that form them (Früh-Green et al., 1996, 2004), showcasing the role of non-serpentine product minerals in partitioning unoxidised Fe^{2+} and limiting H_2 generation by serpentinisation (McCollom & Bach, 2009). Iron partitioning in serpentine minerals from various metamorphic terranes demonstrates that the Fe^{3+}/Fe^{2+} ratio in serpentine changes with pressure and temperature (Debret et al., 2014). Therefore, stoichiometric estimates of H_2 generation that a) assume no Fe-Mg solid solution and/or b) do not consider product minerals or product mineral solid solutions typically overestimate the H_2 that is produced in natural reactions.

Serpentinisation is commonly recognised in a plethora of geological environments, including mid-ocean ridges (see Section 6.1; e.g., Debret et al., 2024; Worman et al., 2020), subduction zones (see Section 6.2; e.g., Blakely et al., 2005; Deschamps et al., 2013; Peacock & Bostock, 2024), and ultramafic continental settings (see Section 6.4; e.g., Sherwood Lollar et al., 2014; Warr et al., 2019; Zgonnik et al., 2019). The ubiquity of serpentinisation is therefore a significant contributing factor towards the fluxes of H_2 generated at geological settings.

5.1.2. Other fluid-mineral redox reactions

Other H_2-generating non-serpentinisation mineral redox reactions may occur in the absence of ultramafic minerals, for example, in basaltic or granitic settings. However, rates of reaction relative

609 to serpentinisation may be lower, as these reactions tend to occur at comparatively lower
610 temperatures, higher silica activity, and lower Fe^{2+} budgets (Murray et al., 2020).
611
612 While serpentinisation is often the principal H_2-generating reaction in ultramafic settings, late-
613 stage hydrous alteration may contribute towards the overall H_2 liberated by fluid-rock reactions.
614 These alteration reactions are especially important within hydrothermal systems, which occur in
615 a range of volcano-tectonic systems flushed by aqueous fluids. For example, at mid-ocean ridges,
616 cold seawater percolating through the seafloor can be heated to ~400 °C at depth, subsequently
617 ascending as a hydrothermal plume as its density decreases. During this transit into and out of
618 the crust, this seawater will oxidise the surrounding basalt, liberating H_2 as an aqueous phase,
619 which is evident as high concentrations in hydrothermal fluids (Diehl & Bach, 2020; Humphris &
620 Klein, 2018). At high temperatures (300–400 °C), oxidation of ferrous silicate minerals by water
621 may be possible through the FMQ equilibrium reaction involving the oxidation of ferrous iron in
622 fayalite ($Fe^{2+}_2SiO_4$) (Reaction 7; Reed & Palandri, 2008):
623
624 (Rxn. 7) $3Fe^{2+}_2SiO_4 + 2H_2O = 3SiO_2 + 2Fe^{2+}Fe^{3+}_2O_4 + 2H_2$
625
626 whereas at lower temperatures (<250 °C), Reaction 5 and the following iron oxidation reactions
627 (Reactions 8–10) are possible (Bach & Edwards, 2003; Christie et al., 1986; Holloway & O'Day,
628 2000; Stevens & McKinley, 2000):
629
630 (Rxn. 8) $3Fe^{2+}O + H_2O = Fe^{2+}O{\cdot}Fe^{3+}_2O_3 + H_2$
631 (Rxn. 9) $2Fe^{2+}O + 4H_2O = 2Fe^{3+}(OH)_3 + H_2$
632 (Rxn. 10) $2Fe^{2+}O + 2H_2O = 2Fe^{3+}OOH + H_2$
633
634 These redox reactions can occur at temperatures as low as 55–100 °C, and may involve common
635 ferrous iron minerals such as olivine, pyroxene, spinel, and/or iron oxides including magnetite
636 (Geymond et al., 2022; Mayhew et al., 2013; Stevens & McKinley, 2000). For example, olivine
637 can alter to generate H_2 at exceptionally low temperatures (30–70 °C) in carbonate-rich
638 environments (Neubeck et al., 2011, 2014) and at pH ranging from 5 to 11 (Stevens & McKinley,
639 2000). The product minerals of serpentinisation are also Fe^{2+}-rich (Reaction 6), and are thus
640 susceptible to secondary oxidation and H_2 generation. For example, Fe^{2+}-bearing 'ferroan' brucite
641 ($Fe^{2+}(OH)_2$) has been identified as a mineral with the potential to generate H_2 at low temperatures
642 (<150 °C) at concentrations of µmol to mmol H_2 per kg of brucite (Carlin et al., 2024; Ellison et al.,

2021; Klein et al., 2014; Miller et al., 2017; Templeton & Ellison, 2020). Unlike serpentinisation, the oxidation of ferroan brucite is dependent on H_2 activity; progressive reaction of ferroan brucite necessitates the release of H_2 at a rate faster than it is produced, which is possible at sites of hydrothermal activity and fluid advection, such as the oceanic seafloor or within ophiolites (Carlin et al., 2024). As another example, magnetite can react with water to form maghemite (γ-$Fe^{3+}{}_2O_3$) at low temperatures (<200 °C), generating H_2 at concentrations of ~10 mmol H_2 per kg of magnetite (Geymond et al., 2023). Further oxidation of the Fe^{2+} partitioned into serpentine minerals themselves may also result in H_2 generation (Mayhew & Ellison, 2020).

Moreover, H_2 generation by redox processes is not limited to (ultra-)mafic environments, and can occur within silicic settings. Hydrocarbon-bearing fluid inclusions in peralkaline complexes have been attributed to the hydrous alteration of ferrous amphiboles (e.g., arfvedsonite) at high-temperature hydrothermal conditions (Potter et al., 2013; Salvi & Williams-Jones, 1997; Truche et al., 2021). Additionally, the Fe^{2+} of biotite-rich granites may be oxidised to generate H_2 (Murray et al., 2020). However, less H_2 is generated from alteration of silica-rich rocks relative to ultramafic lithologies, principally because silica-rich lithologies have a lower Fe^{2+} budget (Murray et al., 2020). Furthermore, the high silica activities of basalts and silicic lithologies promote the uptake of Fe^{2+} into silicate alteration minerals such as chlorite and amphibole rather than oxidation to Fe^{3+} (B. R. Frost & Beard, 2007).

Within iron formations, orogenic gold deposits, and metamorphic settings, the ferrous iron mineral siderite ($Fe^{2+}CO_3$) may be reduced by water to form H_2 (Reaction 11; Malvoisin & Brunet, 2023; McCollom, 2003; Milesi et al., 2015; Tao et al., 2018):

(Rxn. 11) $3Fe^{2+}CO_3 + H_2O = Fe^{3+}{}_2O_3 + 3CO_2 + H_2$

Finally, H_2 may be generated through redox reactions involving other fluid species than H_2O. The formation of metal sulphide phases can generate by-product H_2 through reaction with H_2S, for example, through the oxidation of pyrite or the reduction of iron oxides (Reactions 12–14; Arrouvel & Prinzhofer, 2021; Drobner et al., 1990; Rickard & Luther, 1997), or through reaction with metal cations in hydrothermal fluids (Reactions 15 and 16; Gallant & Von Damm, 2006; McDermott et al., 2018):

(Rxn. 12) $Fe^{2+}S^{2-} + H_2S^{2-} = Fe^{2+}S^{1-}{}_2 + H_2$

(Rxn. 13) $Fe^{3+}_2O_3 + 4H_2S^{2-} = 2Fe^{2+}S^{-}_2 + 3H_2O + H_2$

(Rxn. 14) $Fe^{2+}Fe^{3+}_2O_4 + 6H_2S^{2-} = 3Fe^{2+}S^{2-} + 4H_2O + 2H_2$

(Rxn. 15) $Fe^{2+} + 2H_2S^{2-} = Fe^{2+}S^{1-}_2 + 2H^{+} + H_2$

(Rxn. 16) $Cu^{+} + Fe^{2+} + 2H_2S^{2-} = CuFe^{2+}S^{1-}_2 + 3H^{+} + 0.5H_2$

The respeciation of C-O-H crustal fluids during fluid-rock interactions can also produce H_2. An example is provided by aqueous fluids in equilibrium with graphite (Boutier, Martinez, Daniel, et al., 2024; Connolly & Cesare, 1993; Holloway, 1984; Huizenga, 2001); in this graphite-saturated system, H_2 can be produced via the following equilibria (Reactions 17 and 18):

(Rxn. 17) $H_2O + C = H_2 + CO$

(Rxn. 18) $CH_4 = C + 2H_2$

Any aqueous fluid infiltrating and reequilibrating with graphite-bearing rocks will produce at least some H_2; however, considering the spatial distribution of graphite-bearing rocks in crustal rocks, the associated fluxes of H_2 may not be negligible at global scale (Section 6.2.6). The concentration of H_2 in these fluids is essentially dependent on the redox state of the system, pressure, and temperature (Figure 3). Figure 3 shows H_2 concentrations in graphite-saturated C-O-H fluids in the 0–4 GPa and 300–700 °C pressure-temperature field. Reduced conditions clearly promote higher H_2 concentrations in C-O-H fluids; at oxidized conditions (FMQ+1; Figure 3E), the highest H_2 concentrations are found at the lowest investigated pressure and temperature conditions. More reducing redox states increase not only H_2 concentrations, but also expand the pressure-temperature distribution of H_2 concentration maxima. At FMQ (Figure 3D), the pressure-temperature conditions producing the highest H_2 concentrations match the prograde paths of subducting slabs, especially for hotter thermal regimes. Redox states below FMQ (Figures 3B and 3C) further expand the domain of maximised H_2 concentrations and shift it towards higher temperatures, at conditions consistent with retrograde paths of exhuming subducted rocks or prograde conditions of regional metamorphism (e.g., Barrovian metamorphism) in accretionary complexes. Reduced high-temperature/low-pressure metamorphic conditions may yield the highest H_2 concentrations in these fluids, even though these conditions may not be commonly verified in natural systems. During migration, graphite-saturated C-O-H fluids may produce or consume H_2 as a result of respeciation across the pressure-temperature space, interactions with rocks, and mixing with other fluids. As an example, graphite precipitation from methane in C-O-H fluids may represent a common process producing H_2 in crustal fluids.

Reactions involving other redox-sensitive elements, such as manganese, titanium or chromium, may also generate H_2 (e.g., Kaim & Kaur-Ghumaan, 2019); however given that the concentrations of these transition metals are an order of magnitude lower than iron in bulk silicate Earth (McDonough & Sun, 1995), scientific focus has principally been on redox processes affecting iron. We also note that low-temperature (<200 °C) coal oxidation can also liberate appreciable quantities of H_2 (e.g., Nehemia et al., 1999; Wang et al., 2017) in a process distinct from thermal maturation (Section 4). A vast variety of geological environments therefore possess the potential to generate natural H_2, although, owing to this established ubiquity, the fluxes of H_2 from these redox reactions may not be well-constrained.

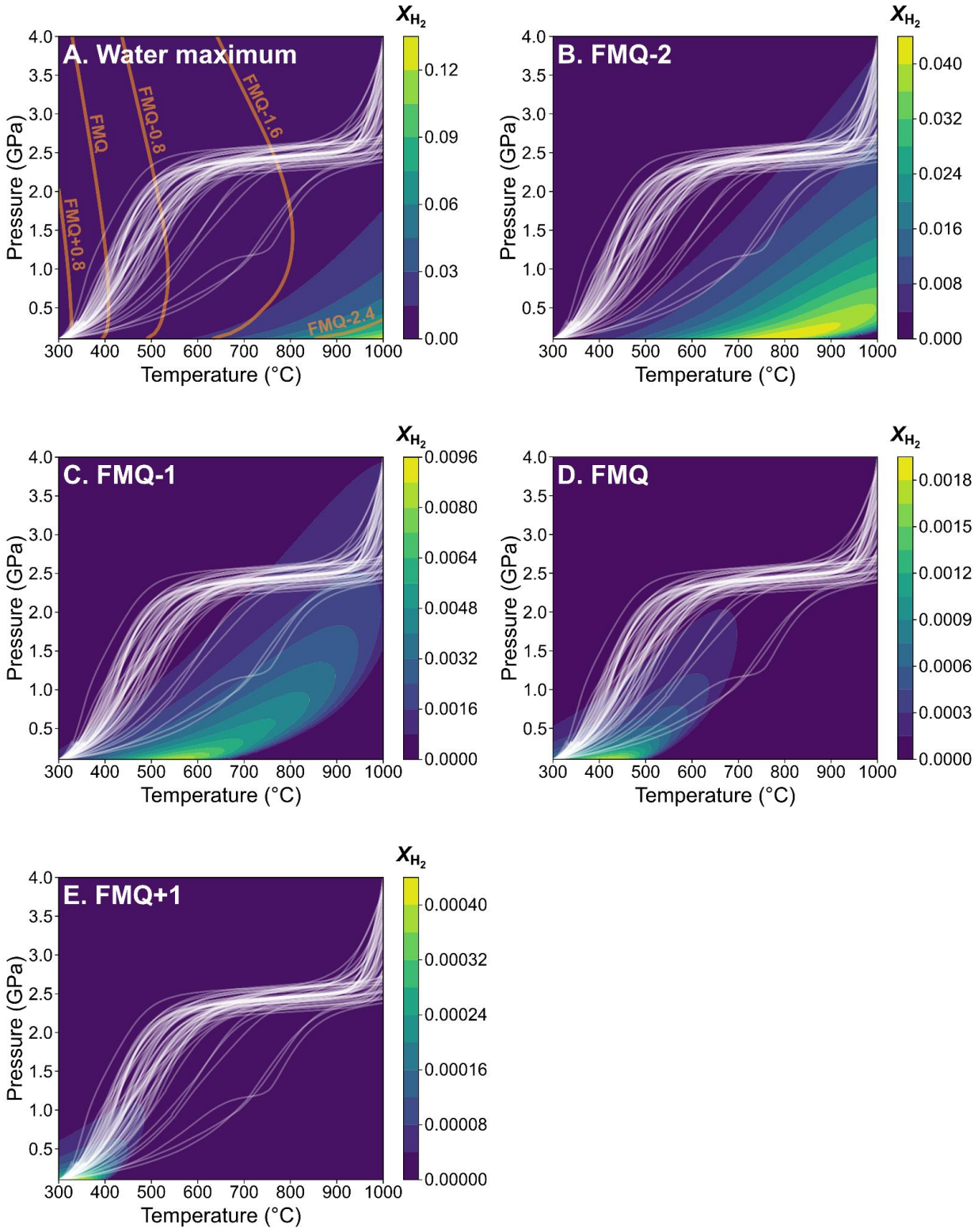

Figure 3: H_2 molar fractions of fluids in equilibrium with carbonate-free graphite-bearing rocks in the C-O-H system at water maximum conditions (A), which represents the conditions at which a graphite-saturated C-O-H fluid has its maximum amount of water and its minimum carbon

concentration, and at a range of different oxygen fugacities (B–E). The orange lines in panel A are contours for oxygen fugacity at the water maximum, calculated with the oxybarometer of Miozzi & Tumiati (2020). Contoured heatmaps of panel A are calculated with the Thermotopes-COH software (Boutier, Martinez, Daniel, et al., 2024). Slab pathways (white lines) are plotted from the updated D80 global subduction dataset (van Keken & Wilson, 2023). Note that the scale of the colormaps differ between each plot.

5.2. Gas and vapour redox

Gases and fluids in geological settings are defined by a variety of species and equilibrium reactions within a complex geochemical space, commonly simplified and expressed as carbon-oxygen-hydrogen-sulphur (C-O-H-S) systems (Fischer & Chiodini, 2015; Giggenbach, 1996). H_2 is a key component in the redox reactions that control the speciation of volcanic-hydrothermal gases in C-O-H-S space. Hydrogen partitions across several gas species, and water is commonly the most abundant species in volcanic gases (e.g., Giggenbach, 1996). The key control on the gas redox budget (i.e., the oxygen and hydrogen available for redox equilibria reactions; Henley & Fischer, 2021) is the dissociation of water (Reaction 19):

(Rxn. 19) $H_2O = 0.5O_2 + H_2$

Measuring H_2 in combination with H_2O can provide key information on the redox conditions of magmatic gases and their source magmas when considered together with other redox couples (e.g., H_2S/SO_2)(Moussallam et al., 2019, 2024; Symonds et al., 1994). Other H_2-forming gas-phase reactions include the following redox couples involving sulphur species (Reactions 20 and 21):

(Rxn. 20) $H_2S + 2H_2O = SO_2 + 3H_2$

(Rxn. 21) $S_2 + 4H_2O = 2SO_2 + 4H_2$

and Sabatier/Fischer-Tropsch-type reactions involving carbon (Reactions 22 and 23):

(Rxn. 22) $CH_4 + 2H_2O = CO_2 + 4H_2$

(Rxn. 23) $C_nH_{2n+2} + nH_2O = nCO + (2n+1)H_2$

In volcanic settings, the concentration and speciation of primary gases (i.e., gases exsolved directly from a magma) are controlled by gas redox state (Giggenbach, 1987, 1996), itself inherited from the oxidation state of the magma it exsolved from (e.g., Burgisser et al., 2015; Gerlach, 1993; Lee et al., 2005; Moretti & Papale, 2004). Controls on magmatic oxygen fugacity include the solubility of volatile phases in the melt during ascent (Burgisser & Scaillet, 2007), the crystallisation of ferrous iron-bearing minerals (e.g., Holloway & O'Day, 2000), and the loss of H_2 by reaction with conduit olivine and pyroxene during transit from the mantle (Tollan & Hermann, 2019). Oxidised magmas will therefore exsolve oxidised primary gases; the exsolution of reduced primary gases with high H_2 concentrations necessitates a reduced source magma.

While this link between primary gas and source magma oxidation state may suggest that volcanic gas redox observed at a degassing vent is directly correlated to magma redox, other factors will affect gas redox state after it has separated from the magma, including eruption style (Oppenheimer et al., 2018) and adiabatic cooling (Moussallam et al., 2019). Establishing the equilibrium state of emitted gases is key to unravelling their redox state. Rate constants of gas phase equilibrium reactions increase rapidly with increasing temperature; high-temperature volcanic gases (>900 °C) are therefore commonly assumed to be in redox equilibrium (Henley & Fischer, 2021; Symonds et al., 1994), and additionally in equilibrium with their source magmas (Aiuppa & Moussallam, 2024; Gerlach, 1993). At lower temperatures (<900 °C), reaction rates are lower, and the redox state of the gas is now principally controlled by the rates of redox exchanges between gas species (Giggenbach, 1987, 1996). Redox exchange with solid phases in contact with the gas is particularly important within lower temperature volcanic-hydrothermal gases (Henley & Fischer, 2021). Disequilibrium by 'gas scrubbing' is a significant possibility at lower temperatures, and will remove evidence of primary gas and source magma redox (Giggenbach, 1996; Symonds et al., 2001). Pressure also strongly controls speciation in volcanic gases; for example, at shallow pressure the molar difference between the reactions and products in Reaction 20 favours the right-hand side and H_2 generation (e.g., Gaillard et al., 2011).

These complex redox reactions involving a volcanic-hydrothermal gas can therefore be classified as either homogeneous, with speciation controlled solely by redox exchange of species in the gas phase (Giggenbach, 1987), or heterogeneous, and controlled by redox exchange between the gas and a silicate rock/melt (Henley & Fischer, 2021). The transition between predominantly homogeneous or heterogeneous redox reactions is believed to be controlled by the maturity of the volcanic-hydrothermal system, which governs the transit speed of vapour from its source to

the surface. However, both homogeneous and heterogeneous reactions are likely to operate concurrently within these systems, and differentiating these contributions towards the final redox of emitted gases remains a subject of ongoing study (Aiuppa & Moussallam, 2024). Nevertheless, there is now sufficient experimental characterisation of gas species equilibrium conditions in C-O-H-S space to predict volcanic-hydrothermal gas speciation at variable pressures, temperatures, and oxygen fugacity (e.g., Aiuppa & Moussallam, 2024; Burgisser et al., 2015; Giggenbach, 1987, 1996; Henley & Fischer, 2021), and therefore predict the H_2 that can result from these equilibria (Section 6.3).

5.3. Radiolysis

The decay of radionuclides common in Earth's crust (e.g., ^{40}K, ^{232}Th, and ^{235}U) will generate ionising radiation capable of breaking the O–H bonds of the water molecule, resulting in the formation of the two radical species H· and OH· (Reaction 24):

(Rxn. 24) $H_2O = H\cdot + OH\cdot$

The subsequent combination of two H· formed from H_2O radiolysis will form molecular H_2 (Reaction 25) among other hydrogen-oxygen chemical species (e.g., H_2O_2, H_3O^+, HO_2; Das, 2013):

(Rxn. 25) $2H\cdot = H_2$

The radiolytic production of H_2 is independent of pressure and temperature, and can affect water in solid, liquid, and vapour phases or bound within hydrous salts (e.g., Das, 2013; Smetannikov, 2011). Decomposition of water through radiolysis may therefore generate H_2 in a vast range of geological settings, with the principal controls being the availability of water and the quantity of ionising radiation generated from decaying radionuclides within water-containing lithologies (e.g., Lin, Hall, et al., 2005; Lin, Slater, et al., 2005). In addition, pore spaces and/or fracture widths will dictate the surface area for ionising radiation to interact with water (Dzaugis et al., 2016; L.-H. Lin, Slater, et al., 2005; W. Wang et al., 2018); in sedimentary rocks, large surface areas, and higher H_2 concentrations, can be achieved through small grain sizes (Blair et al., 2007; DeWitt et al., 2022). Radiolytic generation of H_2 is more substantial in brines relative to pure water because of the presence of Cl^-, which can react with oxidising radicals that would otherwise consume H· (Buck et al., 2012; LaVerne & Tandon, 2005). In contrast, strong electron-scavenging anions (e.g.,

827 SeO_4^{2-}, MoO_4^{2-}) may limit H_2 production if present (e.g., Pastina et al., 1999). H_2 may additionally
828 be generated by radiolysis of hydrocarbons (Boreham & Davies, 2020; Silva et al., 2019; W. Wang
829 et al., 2022), although this H_2 flux is geologically insignificant compared with that of water
830 radiolysis.
831
832 To estimate radiolytic H_2 production in geological settings, previous researchers have used the
833 ratio of H_2 to inert products of radioactivity in pore/inclusion fluids (e.g., ^4He, ^{40}Ar), which scale
834 with host lithology radioelement concentrations (e.g., Lin et al., 2005; Sherwood Lollar et al.,
835 2014). However, H_2 produced *in situ* by radiolysis may be consumed through microbial and/or
836 abiotic processes, which will result in H_2 underestimation (e.g., Kietäväinen & Purkamo, 2015;
837 Telling et al., 2018). Radiolytic H_2 may additionally be present alongside H_2 generated from other
838 processes such as hydration (Warr et al., 2019). Authors aiming to quantify H_2 produced by
839 radiolysis must therefore stoichiometrically account for a plethora of H_2-consuming reactions to
840 calculate natural radiolytic H_2 production rates (e.g., Warr et al., 2019). Models for predicting
841 radiolytic H_2 production are typically functions of the radiogenic dose rate, itself a function of the
842 type of radioactive element decay—which may be estimated from rock radionuclide
843 concentrations—and rock porosity (e.g., Karolytė et al., 2022; Lin et al., 2005). Estimating
844 radiolytic H_2 generation therefore strongly relies on the in-detail characterisation of the physical
845 and geochemical properties of the host rock.
846
847 Precambrian basements host significant radiolytic H_2, as they contain high concentrations of
848 radionuclides, and their ancient origins provide plentiful time to generate and accumulate large
849 amounts of H_2 (L.-H. Lin, Hall, et al., 2005; L.-H. Lin, Slater, et al., 2005; Parnell & Blamey, 2017a;
850 Sherwood Lollar et al., 2014; Warr et al., 2019). Fluid inclusions in detrital quartz from sedimentary
851 rocks derived from the erosion of Precambrian basements preserve higher H_2 concentrations
852 compared to Phanerozoic source rocks (Parnell & Blamey, 2017a). Radiolytic H_2 production is
853 also expected to be significant in younger felsic continental settings, where radionuclides
854 incompatible in Earth's melting mantle can be concentrated (L.-H. Lin, Hall, et al., 2005; L.-H. Lin,
855 Slater, et al., 2005), particularly within U-Th ores and deposits (Dubessy et al., 1988; Richard,
856 2017; Savary & Pagel, 1997). Finally, a substantial amount of H_2 is expected to be generated
857 from radiolysis in oceanic settings. Nearly 2% of global ocean seawater may be entrapped within
858 oceanic crust (Johnson & Pruis, 2003), potentially generating sufficient radiolytic H_2 to sustain life
859 in seafloor sediments (Blair et al., 2007; D'Hondt et al., 2009; Sauvage et al., 2021) and basaltic
860 oceanic crust (Dzaugis et al., 2016; Türke et al., 2015). Radiolytic H_2 generation is therefore near-

ubiquitous at the Earth's surface, and provides a convenient source of energy to hydrogenotrophic microorganisms in environments where photosynthesis is limited and organic matter is scarce (e.g., Lin et al., 2005), with important ramifications for the sustenance of extraterrestrial microbial life (Blair et al., 2007; Bouquet et al., 2017; Dzaugis et al., 2016, 2018; Onstott et al., 2006; Tarnas et al., 2018, 2021).

5.4. Mechanoradical H_2

Faulting and fracturing of rocks may accelerate H_2 production through the exposure of fresh surfaces to infiltrating fluids, thereby increasing the available surface area for redox reactions and radiolysis of water (e.g., Bayrakci et al., 2016; McCaig, 1988). H_2 can also be formed and released through the fracturing and breaking of the chemical bonds within rocks themselves. As an example, the fracturing of bonds in silica (SiO_2) can produce the Si· free radical, which in turn can interact with water to produce H· free radicals (Reaction 26; Kita et al., 1982; Saruwatari et al., 2004):

(Rxn. 26) $Si\cdot + H_2O = SiOH + H\cdot$

The subsequent combination of two H· free radicals will result in the formation of H_2 (Reaction 25). While silica is chosen as an example above, the fracturing of carbonate rocks in experiments has also been shown to generate H_2 (Hirose et al., 2011), although this has been questioned by subsequent experiments in which no H_2 is observed from carbonate fracturing (Telling et al., 2015).

The process described above, termed 'mechanoradical' or 'mechanochemical' H_2 generation, is believed to be a direct contributor to the large fluxes of H_2 observed at fault zones in the aftermath of earthquakes (e.g., Arai et al., 2001; Dogan et al., 2007; Li et al., 2013; Sato et al., 1984, 1986; Sugisaki et al., 1983; Ware et al., 1984). At fault zones, H_2 is measured directly through chromatography of soil gas samples (e.g., Wakita et al., 1980), or indirectly through the evaluation of fluid inclusions entrapped within fault rocks (e.g., McMahon et al., 2016). In the latter process, rocks of interest are crushed to liberate volatiles, which are subsequently passed through a mass spectrometer or measured through gas chromatography (Hirose et al., 2011; McMahon et al., 2016).

The controls on mechanoradical H_2 generation have been interrogated through experiments, which demonstrate that the fracturing of water-saturated rocks will generate more H_2 than dry rocks (Hirose et al., 2011; Liang et al., 2024). Pressure and temperature also affect H_2 generation, although their effects are largely unconstrained (Liang et al., 2024). Mechanoradical H_2 production is believed to scale with frictional work, and hence the seismic magnitude of earthquakes (see Section 6.5), which will govern secondary parameters such as the surface area of faults/fractures available for interaction with water (Telling et al., 2015). However, highly localised concentrations of ~1 mmol H_2 per kg of fluid may be achieved immediately after even low magnitude earthquakes, comparable to concentrations in hydrothermal fluids (Hirose et al., 2011, 2012). Further controls on mechanoradical H_2 generation may also include the availability of silica within the exposed rock surface (Damm & Peukert, 2009) and the composition of the silicate minerals that are being fractured (Kameda et al., 2004; Macdonald et al., 2018).

H_2 can therefore be formed in any environment where fracturing or grinding of silicate materials occur, and where sufficient fluid can flow into the region of abrasion to interact with silicate-derived radicals. Faults accommodate the majority of crustal deformation at tectonic settings, and mechanoradical H_2 generation at fault zones is therefore likely to be significant. Mechanoradical H_2 production is therefore believed to be a significant contributor of energy towards the subsurface biosphere in fault zones (Hirose et al., 2011). However, fluxes of H_2 recorded at fault zones are significantly difficult to quantify and allocate solely to mechanoradical generation. The formation of faults and fractures will introduce water to fresh rock surfaces through deep fluid circulation; H_2 measured from fractures is therefore likely to originate from a number of processes, and cannot be constrained solely to mechanoradical generation (Klein et al., 2020). The fault surface will be 'deactivated' shortly after H_2 formation as radicals are consumed and reaction products are generated and extracted, thereby limiting H_2 generation along the fault until a subsequent seismic event. Aseismic deformation may also generate significant H_2 prior to earthquakes (e.g., Ito et al., 1999). Additionally, in sub-glacial environments, ~100 nmol H_2 m^{-2} d^{-1} can result from the glacial abrasion of underlying bedrock to sustain microbial life (Macdonald et al., 2018; Telling et al., 2015). Mechanoradical H_2 has therefore been hypothesised as an energy source for life on early Earth (Hirose et al., 2011; Sleep & Zoback, 2007) and potentially on Mars (McMahon et al., 2016).

6. Fluxes of natural H_2 generation in geological settings

processes		oceanic	subduction	continental	total flux	references
		fluxes (**F**) in Mt H_2 yr^{-1} concentrations (**C**) in mmol unless otherwise stated				
biotic	fermentation	**F:** 21–108 **C:** ?	**F:** ? **C:** ?	**F:** ? **C:** ?	21–108	R+21
	nitrogen fixation	**F:** ? **C:** ?	**F:** ? **C:** ?	**F:** ? **C:** ?	2.4–9.0	CS80, GG22
	carboxydotrophy	**F:** ? **C:** ?	**F:** ? **C:** ?	**F:** ? **C:** ?	?	–
	methanogenesis	**F:** ? **C:** ?	**F:** ? **C:** ?	**F:** ? **C:** ?	?	–
	photosynthesis	**F:** ? **C:** ?	**F:** ? **C:** ?	**F:** ? **C:** ?	?	–
	Thermogenic, C-O-H fluids	**F:** ? **C:** ?	**F:** 8×10^{-4} ? **C:** ~1 cm^3 g^{-1} total organic carbon	**F:** ? **C:** <80 mol kg^{-1} organic-rich rock	8×10^{-4} ?	CC93, Ha08, Su+24, M+24
abiotic	primordial degassing	**F:** ? **C:** ?	**F:** ? **C:** ?	**F:** ? **C:** ?	?	–
	serpentinisation	**F:** ~6.0 **C:** 0–40	**F:** >0.8 ? **C:** 40 ?	**F:** ~0.72 **C:** <90 vol.%	>7.5	SL+14, RH17, Z+19, Wo+20, VB+20, DB20
	other RSE redox reactions	**F:** ~3.0 **C:** 0–40	**F:** ? **C:** ?	**F:** ~1×10^{-5} **C:** 30 mmol kg^{-1} rock	~3.0	Wo+20, DB20, Tr+21, MB23

	vapour redox	**F:** 1.4 **C:** ~30 vol.%	**F:** ? **C:** ?	**F:** 0.23 **C:** <2 mol.%	~1.6	H2+73, Wo+20, AM24
	radiolysis	**F:** ~23 **C:** <1	**F:** ? **C:** ?	**F:** <0.2 **C:** <0.6 vol.%	~23	SL+14, Wa+19, Dz+16, Wo+20, Sa+21
	mechanoradical	**F:** **C:** ~1	**F:** ? **C:** ~1	**F:** **C:** ~1	>1×10^{-4} ?	Hi+11, Te+15, Wo+20

Table 2: Summary of known and unknown fluxes (F) and concentrations (C) of H_2 generated by abiotic and biotic processes in geological settings. References are as follows: He+73: (Hekinian et al., 1973); CS80: (Conrad & Seiler, 1980); CC93: (Connolly & Cesare, 1993); Ha08: (Hacker, 2008); Hi+11: (Hirose et al., 2011); SL+14: (Sherwood Lollar et al., 2014); Te+15: (Telling et al., 2015); D+16: (Dzaugis et al., 2016); RH17: (Rüpke & Hasenclever, 2017); Z+19: (Zgonnik et al., 2019); Wa+19: (Warr et al., 2019); Wo+20: (Worman et al., 2020); VB+20: (Vitale Brovarone et al., 2020); DB20: (Diehl & Bach, 2020); Sa+21: (Sauvage et al., 2021); R+21: (Rosentreter et al., 2021); Tr+21: (Truche et al., 2021); GG22: (Greening & Grinter, 2022); MB23: (Malvoisin & Brunet, 2023); Su+24: (Suzuki et al., 2024); M+24: (I. Moretti et al., 2024); AM24: (Aiuppa & Moussallam, 2024).

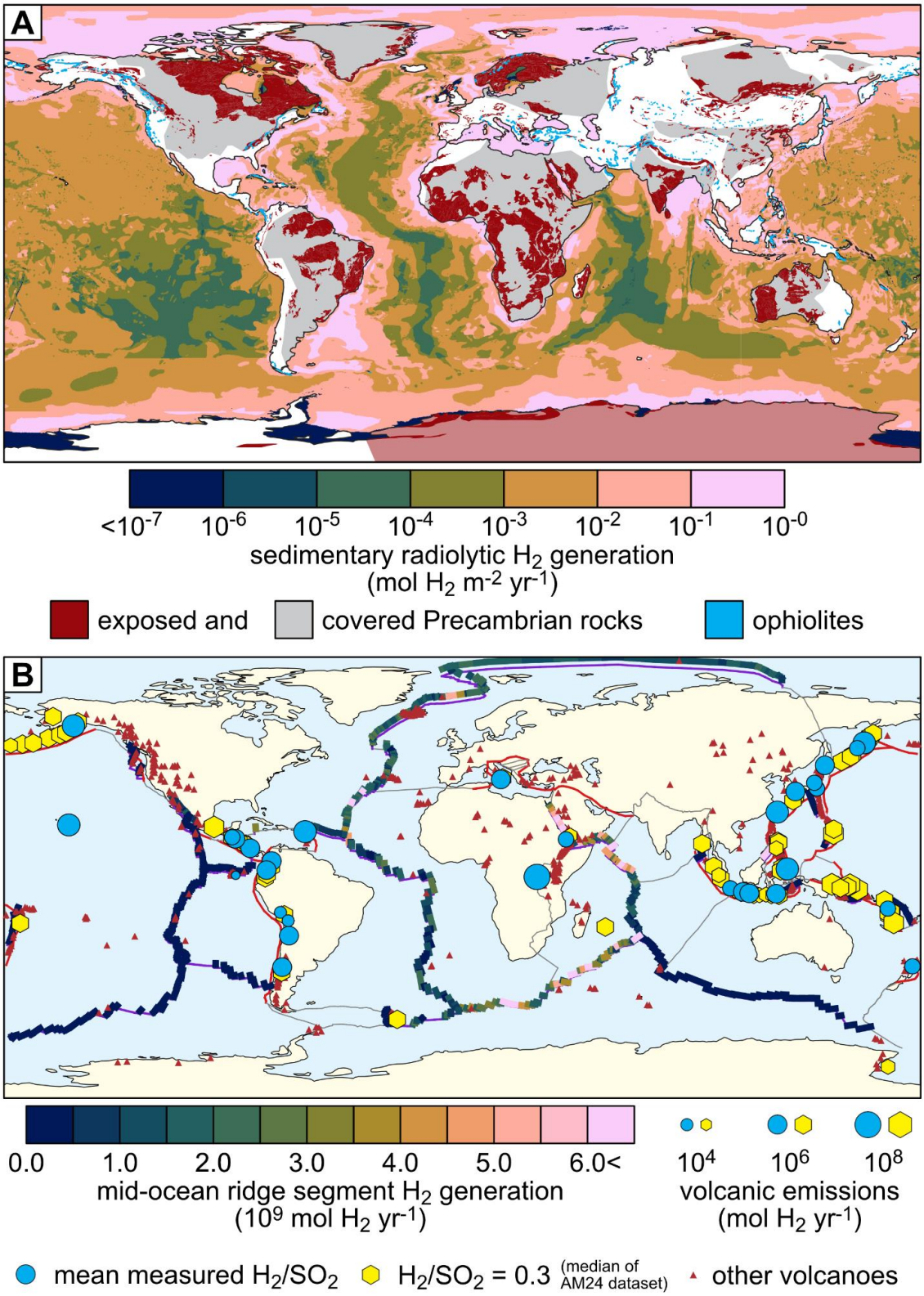

Figure 4. Maps illustrating some principal geological sites of H_2 generation. A. Areal H_2 fluxes from oceanic sedimentary radiolysis (Sauvage et al., 2021), and key sites of continental H_2

generation: continental ophiolites (S. Zahirovic, pers. comms., redrawn after Mann & Taira, 2004), and exposed (Chorlton, 2007) and covered Precambrian rocks (redrawn after Goodwin, 1996, following Sherwood Lollar et al., 2014). B. H_2 fluxes from mid-ocean ridge segments (Merdith et al., 2020), plotted alongside other tectonic boundaries (Matthews et al., 2016) and Holocene volcanoes (red triangles; Global Volcanism Program, 2024). Subduction zones are shown as bold red lines, and other tectonic boundaries and palaeoboundaries are thin grey lines. H_2 fluxes from individual volcanoes are determined by cross-referencing the SO_2 fluxes of the 91 strong emitter volcanoes of Carn et al. (2017) with their mean H_2/SO_2 if recorded by Aiuppa & Moussallam (2024) (blue circles), or the median H_2/SO_2 of Aiuppa & Moussallam (2024) otherwise (yellow hexagons; H_2/SO_2 = 0.3).

6.1. Mid-ocean ridge and oceanic fluxes

Hydrothermal waters at mid-ocean ridges host a significant concentration of aqueous H_2 relative to seawater (seawater H_2 concentration: ~10^{-6} mM; Klein et al., 2020). Sampled vent fluids typically contain ~0.1–1 mM H_2, although concentrations can range substantially from 0–40 mM H_2 (Diehl & Bach, 2020, 2023; Konn et al., 2015). Comparable H_2 concentrations are reported from geothermal fields in Iceland (0.022–20.5 mmol H_2, per kg of fluid), where total H_2 emissions are estimated at ~4.5 kt H_2 yr^{-1} (Combaudon et al., 2022). These high concentrations of H_2 contribute towards significant H_2 fluxes from hydrothermal systems at mid-ocean ridges, which are typically estimated to be on the order of 10^{10}–10^{12} mol H_2 yr^{-1} (~0.02–2 Mt H_2 yr^{-1}; Alt, 2003; Canfield et al., 2006; Diehl & Bach, 2020; Elderfield & Schultz, 1996; Welhan & Craig, 1979; Worman et al., 2020).

Previous literature has assumed that hydrothermal concentrations of H_2 are representative of the total H_2 generated by abiotic processes at mid-ocean ridges (e.g., Welhan & Craig, 1979). However, more recent studies have demonstrated that there are a range of processes, both biotic and abiotic, that will remove naturally generated H_2 from hydrothermal circulation (Worman et al., 2020), including hydrogenotrophic biological activity on or near the ridge axis (e.g., Edwards et al., 2011; McCollom & Seewald, 2013; Petersen et al., 2011; Wankel et al., 2011). Here, we summarise the principal processes that can contribute towards fluxes of H_2 in oceanic settings, both at mid-ocean ridges and in the oceanic lithosphere.

6.1.1. Mid-ocean ridge volcanism

At mid-ocean ridge settings, concentrations of H_2 in hydrothermal fluids have been directly correlated to volcanic activity (Lilley et al., 2003). Owing to the higher pressures of magmatic degassing at submarine settings, magmatic H_2O, and therefore magmatic H_2, is expected to be less prevalent in the vapour phase within erupted mid-ocean ridge basalts compared with subaerial volcanoes (see Section 6.3; Gaillard et al., 2011; Stolper et al., 2021). Some authors assume hydrothermal fluxes of H_2 to be representative of H_2 from mid-ocean ridge volcanism, regardless of other sources; for example, Canfield et al. (2006) suggest a ridge volcanic degassing value of 7–27×10^9 mol H_2 yr^{-1} (0.014–0.054 Mt H_2 yr^{-1}) based on H_2 concentrations and fluid fluxes recorded at hydrothermal vents. However, the best record of mid-ocean ridge H_2 derived from volcanism is obtained from undegassed basalts, also known as 'popping rocks' owing to their tendency to spontaneously explode while decompressing during sample collection. One such sample collected from the Mid-Atlantic ridge had a concentration of 26.7 vol.% H_2 in 0.881 cm^3 g^{-1} of total gas after exploding; comparison with a pillow lava fragment (34.7 vol.% H_2 in 0.734 cm^3 g^{-1} of gas) infers that the H_2 in the undegassed basalt was initially much higher, and contributed to the pre-analysis explosion alongside CO_2 (Hekinian et al., 1973). Considering these samples in combination with the rate of global mid-ocean ridge magma generation, Worman et al. (2020) suggest a mid-ocean ridge volcanic degassing flux of 7×10^{11} mol H_2 yr^{-1} (1.4 Mt H_2 yr^{-1}).

Measurements of Fe^{3+}/Fe^{2+} ratios in mid-ocean ridge basalts suggest that the oxidation state of mid-ocean ridge basalts increases as crystallisation progresses. This oxidation has been attributed to the progressive loss of H_2 from the melt, which is generated by the oxidation of Fe^{2+} to Fe^{3+} by water dissolved within magma (Christie et al., 1986; Holloway, 2004; Holloway & O'Day, 2000). H_2 generation through this auto-oxidation mechanism depends solely on the concentration of dissolved water in the melt, and the degree to which the melt crystallises; this is estimated to be ~300 moles H_2 per m^3 of crystallising basalt, or equivalently ~0.2 g H_2 per kg of basalt (Holloway & O'Day, 2000). Expanding this production rate for all basaltic crust, an estimate of 6.3×10^{12} mol H_2 yr^{-1} (12.7 Mt H_2 yr^{-1}) is suggested (Holloway & O'Day, 2000), although differing degrees of auto-oxidation noted in different mid-ocean ridge basalt samples may suggest a value closer to 3×10^{12} mol H_2 yr^{-1} (6.0 Mt H_2 yr^{-1}) (Worman et al., 2020). This is a highly uncertain estimate, as the composition of the oceanic crust and the processes that occur within it remain poorly characterised. In particular, the gabbroic lower oceanic crust is known to be

compositionally diverse (Gillis et al., 2014; Perk et al., 2007; D. S. Wilson et al., 2006), which will affect the rate of H_2 generation through this mechanism relative to erupted basalts.

Finally, the Fe^{2+} within freshly erupted mid-ocean ridge basalts can be oxidised via interaction with seawater at magmatic temperatures to generate H_2 (e.g., Soule et al., 2006). Through an approach considering the stoichiometry of the iron oxidation reaction (Reaction 2) and the annual surface area of basalt extruded onto the seafloor, Worman et al. (2020) predict that H_2 generation from lava oxidation may be ~1×10^{11} mol H_2 yr^{-1} (0.2 Mt H_2 yr^{-1}), although they acknowledge that this estimate may be low owing to erupted basalt morphologies, fracturing of cooling basalts, or other factors that can introduce seawater into the body of a lava flow and/or increase the surface area of a flow.

6.1.2. Alteration of basaltic oceanic crust

Further H_2 generation will result from the high-temperature alteration of mid-ocean ridge basalts by seawater after their eruption and emplacement (e.g., Lin et al., 2014; Reed & Palandri, 2008; Stevens & McKinley, 1995, 2000). The flux of H_2 by alteration is dependent on the degree to which seawater can infiltrate the upper crust. A conservative estimate of H_2 generation based on the FMQ equilibrium, derived from a 2 mM concentration of H_2 in hydrothermal vent fluids, suggests that high-temperature basalt alteration by seawater may result in the generation of 6×10^{10} mol H_2 yr^{-1} (0.12 Mt H_2 yr^{-1}; Sleep & Bird, 2007). Using a similar approach but a higher axial flux of hydrothermal fluid, Worman et al. (2020) suggest a production rate of ~1×10^{12} mol H_2 yr^{-1} (~2 Mt H_2 yr^{-1}). However, if the volume of unaltered basalt available for hydration is considered instead of H_2 concentrations in vent fluids, fluxes of H_2 from basalt alteration could be as high as 3.75×10^{12} mol H_2 yr^{-1} (7.56 Mt H_2 yr^{-1}; Sleep & Bird, 2007).

Basalt alteration may continue at lower temperatures along the ridge flanks as oceanic crust migrates away from the ridge, up to an age of ~10–20 Myr (Bach & Edwards, 2003). This alteration will affect the FeO in basalts (Bach & Edwards, 2003), or by-products of ultramafic mineral serpentinisation such as ferroan brucite (e.g., Carlin et al., 2024). The low-temperature partial oxidation of the uppermost crust may contribute ~$4.5 \pm 3.0\times10^{11}$ mol H_2 yr^{-1} (0.91 ± 0.60 Mt H_2 yr^{-1}) to mid-ocean ridge H_2 generation (Bach & Edwards, 2003), comparable to H_2 fluxes from high-temperature alteration. Widespread high- and low-temperature alteration may also affect the middle and lower crust, although further work is necessary to characterise the degree to which the lower crust is hydrated by hydrothermal activity (e.g., Jian et al., 2024).

H_2 can additionally be formed at mid-ocean ridges through the inorganic reduction of pyrite (Reactions 9–13; Bach & Edwards, 2003; Worman et al., 2020), although the distribution of sulphides around mid-ocean ridges suggests that the H_2 produced through these reactions is likely to be several orders of magnitude lower than other mechanisms (~9×10^5 mol H_2 yr^{-1}, or ~1.8 t H_2 yr^{-1}; Worman et al., 2020). As a result, pyrite formation at mid-ocean ridges is unlikely to be a significant contributor to global H_2 fluxes, but may be an important source of H_2 near hydrothermal vents.

6.1.3. Serpentinisation of abyssal peridotite at mid-ocean ridges

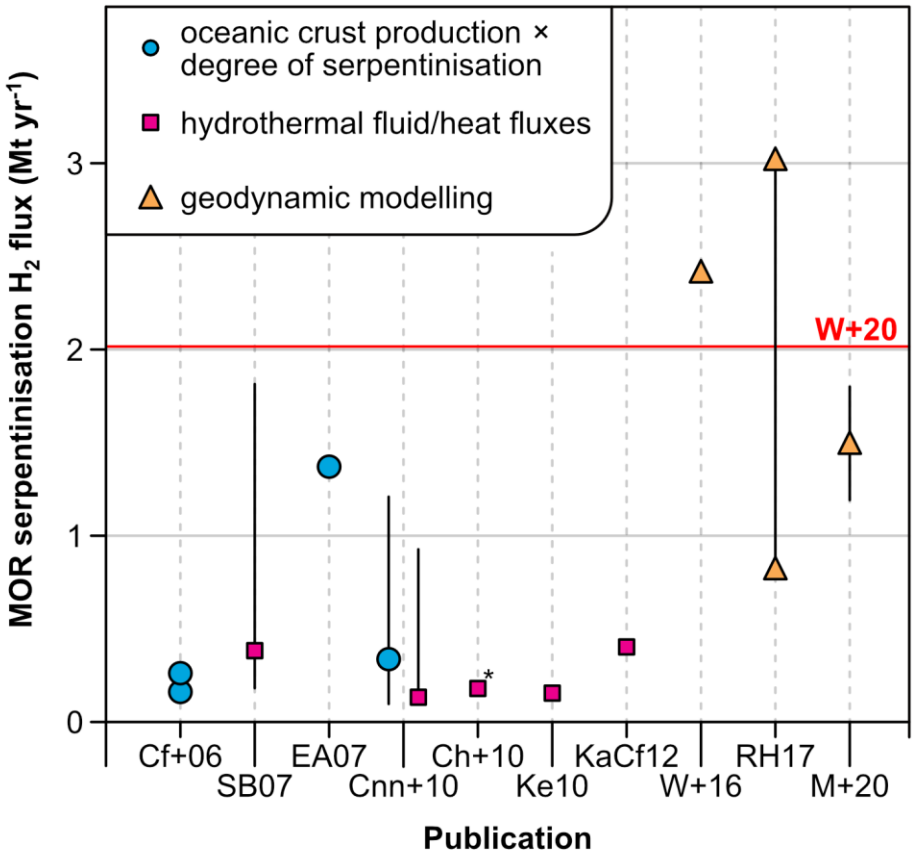

Figure 5. Compilation of recent H_2 flux estimates from global serpentinisation of abyssal peridotites at mid-ocean ridges. Estimates are categorised by the method used to calculate the H_2 flux. Where a range is provided (i.e., black line), markers highlight the minimum and maximum flux values, or a chosen value within that range. Publications are as follows: Cf+06: Canfield et al. (2006)`; SB07: Sleep & Bird (2007); EA07: Emmanuel & Ague (2007); Cnn+10: Cannat et al. (2010)—note that there are two estimates provided by the two approaches used; Ch+10: Charlou

et al. (2010)—the asterisk indicates that this estimate is considered for (ultra-)slow mid-ocean ridges only; Ke10: Keir (2010); KaCf12: Kasting & Canfield (2012); W+16: Worman et al. (2016); RH17: Rüpke & Hasenclever (2017); M+20: Merdith et al. (2020); horizontal red line and preferred H_2 flux, W+20: Worman et al. (2020).

At slow (20–40 mm yr^{-1}) and ultra-slow (<20 mm yr^{-1}) spreading centres, decompression melting near the Earth's surface is limited (e.g., Turcotte & Morgan, 1992), and the thickness of the basaltic oceanic crust is thin or absent (Dick et al., 2003). Detachment faults are formed to accommodate extension, exposing fresh ultramafic mantle rocks at the seafloor, where they are vulnerable to serpentinisation (Cannat et al., 2009; Escartín et al., 2008; Reston & McDermott, 2011). Exposure of abyssal peridotites at slow and ultra-slow spreading ridges can therefore result in substantial H_2 production by serpentinisation (Figure 4B; e.g., Canfield et al., 2006; Cannat et al., 2010; Merdith et al., 2020; Sleep & Bird, 2007; Worman et al., 2016).

Compared with other processes at mid-ocean ridges, there have been an extensive number of studies characterising fluxes of H_2 from serpentinisation of abyssal peridotites. This is principally due to the potential that peridotites have to generate H_2 per unit volume relative to other lithologies. Key to these studies is a means of linking the amount of peridotite that has been serpentinised with a volume of H_2 that is liberated as a result (Section 5.1.1). Estimates of abyssal peridotite serpentinisation across these studies are broadly consistent to the same order of magnitude despite diverse methodology, with typical estimates within the range ~0.1–3.0 Mt H_2 yr^{-1} (Figure 5).

Flux estimates in the literature are determined through three principal methods (Figure 5). a) The rate of peridotite exposed during oceanic crust production is assessed, and a representative H_2 flux from serpentinisation of this exposed peridotite is assigned (e.g., Canfield et al., 2006; Emmanuel & Ague, 2007). b) Hydrothermal fluxes of H_2 or heat are used as a proxy for the H_2 generated by serpentinisation at specific mid-ocean ridge sites, which is subsequently generalised for the global ridge system (e.g., Cannat et al., 2010; Sleep & Bird, 2007). However, the H_2 in hydrothermal fluids may additionally comprise a component of H_2 from other sources at mid-ocean ridges, such as H_2 generated through basalt redox reactions (e.g., Bach & Edwards, 2003), thereby exaggerating fluxes from serpentinisation only. c) More recently, different geodynamic approaches have been used to assess the controls on oceanic lithosphere serpentinisation (Merdith et al., 2020; Rüpke & Hasenclever, 2017; Worman et al., 2016). These

models often necessitate assumptions regarding the H_2 generated by serpentinisation, which are obtained from petrological observations or models (e.g., Andreani et al., 2013). Based on these estimates and approaches, Worman et al. (2020) select a flux value from serpentinisation of ~1×10^{12} mol H_2 yr^{-1} (~2 Mt H_2 yr^{-1}) for the present day (Figure 5).

At fast spreading ridges, local tectonic processes can generate deep faults into the oceanic lithosphere, exposing peridotite underlying oceanic crust to seawater. However, such exposures are scarce, and the high geothermal gradients at fast-spreading ridges may restrict the formation of serpentine minerals at the ridge axis; the extents of crustal and lithospheric mantle serpentinisation at fast spreading ridges therefore remain highly uncertain (Debret et al., 2024).

6.1.4. Transform faults

Oceanic transform faults permit the infiltration of fluid into the mantle (e.g., Boschi et al., 2013), thereby facilitating serpentinisation to depths of up to 13 km (Klein et al., 2024; Prigent et al., 2020). Unlike intermediate/fast-spreading oceanic ridges, the low magma supply at transform faults results in thin or non-existent oceanic crust. When coupled with local tectonic movements that can displace portions of the underlying mantle, the exposed seafloor at transform faults will be predominantly composed of mantle peridotite (Bonatti & Michael, 1989), whose exposure is independent of the spreading rates of the surrounding ridge segments.

As the total length of oceanic transform faults is comparable to the lengths of other tectonic settings (on the order of 10,000 km; Bird, 2003), it has been posited that H_2 fluxes from transform fault serpentinisation may be substantial, and comparable to fluxes from serpentinisation at slow-spreading mid-ocean ridges (Rüpke & Hasenclever, 2017). Geodynamic models of transform fault serpentinisation show that the principal controls on H_2 generation by serpentinisation at transform faults are fault length, which determines the degree to which water can reach cold oceanic mantle, and slip rate, which controls the volume of mantle transiting through the serpentinisation window. H_2 generation is therefore amplified at long transform faults with intermediate (50–80 mm yr^{-1}) slip rates; higher slip rates will result in mantle temperatures exceeding serpentine stability, whereas lower slip rates will limit the volume of mantle that can be serpentinised (Rüpke & Hasenclever, 2017). Rüpke & Hasenclever additionally highlight the role of hydrothermal circulation in cooling the lithosphere, thereby increasing the size of the serpentinisation window. Based on these models, global transform faults are estimated to produce 6.1–10.7×10^{11} mol H_2 yr^{-1} (1.2–2.2 Mt H_2 yr^{-1}).

An alternative value of ~1×10^{10} mol H_2 yr^{-1} (0.02 Mt H_2 yr^{-1}) is estimated from geodynamic models of plate reconstructions (Merdith et al., 2020). While this estimate is significantly lower than that of Rüpke & Hasenclever (2017), Merdith et al. note that the transform faults in their model are narrower and do not facilitate hydration of the lower oceanic lithosphere, which subsequently limits the overall volume of mantle that can be serpentinised.

6.1.5. Oceanic crust radiolysis

Based on radiolytic production rates of H_2 in basalts (Dzaugis et al., 2016), Worman et al. (2020) suggest that basalt radiolysis near mid-ocean ridges may generate ~$0.5–50\times10^{5}$ mol H_2 km^{-1}, which, when applied to the volume of extrusive basaltic crust generated at mid-ocean ridges (10^{7} km^3 yr^{-1}), translates to ~$0.5–50\times10^{12}$ mol H_2 yr^{-1} (1–100 Mt H_2 yr^{-1}) of which the lower value is favoured for conservatism. However, it is worth noting that this value is determined solely for young oceanic crust radiolysis (up to 10 Ma). Radiolysis may continue to progress in basaltic aquifers away from mid-ocean ridges, although the total H_2 flux from older crust remains unconstrained (Dzaugis et al., 2016).

6.1.6. Oceanic sediment radiolysis

In addition to the oceanic basement, substantial H_2 can be generated through sediment radiolysis (Blair et al., 2007; D'Hondt et al., 2009) with volumetric mean fluxes ranging from ~$0.1–1.0\times10^{-12}$ mol H_2 yr^{-1} cm^{-3} sediment (see Figure 6 and Table 3 of Blair et al., 2007) Integrating over the sediment column, radiolytic H_2 may generate areal fluxes of ~10^{-9} to 10^{-3} mol H_2 per cm^2 of seafloor, a highly variable range controlled primarily by sediment thickness and lithology (Blair et al., 2007; Sauvage et al., 2021). Using a radiolytic H_2 generation approach coupled with seafloor sediment surveys, Sauvage et al. (2021) estimate that global marine sediment-hosted radiolysis may generate 1.34×10^{13} mol H_2 yr^{-1} (27 Mt H_2 yr^{-1}; Figure 4A). Concentrations of H_2 within marine sediment cores are typically very low (<1 to ~200 nM) compared to model predictions of radiolytic H_2 concentration (1 μM to 1 mM), suggesting that the H_2 that is generated is rapidly consumed by microbial life, particularly within anoxic sediments and at greater depths in sediment columns where organic carbon oxidation is less prevalent than at shallower pressures (see Section 7.4.1; D'Hondt et al., 2009; Sauvage et al., 2021). Sedimentary H_2 is therefore a considerable source of energy for sub-seafloor biology (Section 7.5.1; Adhikari et al., 2016).

6.1.7. Ultramafic cumulates

Serpentinisation may affect gabbroic cumulates, both in the lower oceanic crust and more generally within magmatic settings. One such example is the partially serpentinised Duluth Complex, USA, which exposes magmatic intrusions related to the opening of the ~1.1 Ga Midcontinent Rift (e.g., Swanson-Hysell et al., 2021). Serpentinised tholeiitic cumulates from the Duluth Complex have been used as an compositional analogue for Martian crust owing to their similar FeO and MgO concentrations. The serpentinisation of Fe-rich olivine generates more H_2 than Mg-rich olivine (McCollom et al., 2022), and, based on the high bulk rock Fe^{3+} of these cumulates, it has been estimated that nearly 1 mol H_2 per kg of cumulate may be generated with the potential of sustaining a primitive Martian biosphere (Tutolo & Tosca, 2023). However, the degree to which the lower crust remains serpentinised is highly speculative. Samples from the gabbroic lower crust are limited, highly diverse in composition (Coogan, 2007), and may display variable degrees of alteration and serpentinisation (Jian et al., 2024). The H_2 that may be generated from fluid-rock reactions in ultramafic cumulates is therefore unconstrained.

6.2. Subduction zone fluxes

Subduction is the principal manner by which materials collected in Earth's exosphere are returned into Earth's interior. These materials, including volatile elements, are locked within hydrous mineral structures in sediment and oceanic lithosphere. During subduction, prograde metamorphism results in the formation of new minerals, liberating water and other fluids into the overlying accretionary wedge and mantle wedge. Subduction zones are therefore sites of significant deep H_2 generation, with the potential to supply energy to the deepest subsurface microbial life (Plümper et al., 2017; Rogers et al., 2023; Vitale Brovarone et al., 2020).

6.2.1. Serpentinisation at the outer rise

As oceanic plates approach the trench at subduction zones, they will begin to bend, resulting in the formation of trans-lithospheric extensional faults (Christensen & Ruff, 1988). These faults provide avenues for water infiltration, enhancing the volume of the oceanic plate that can be serpentinised (Faccenda, 2014; Grevemeyer et al., 2018; Lefeldt et al., 2012; Ranero et al., 2003). Outer rise serpentinisation is evident from lower seismic velocities measured in the mantle at a number of trenches worldwide (e.g., Grevemeyer et al., 2018; Hatakeyama et al., 2017; Shillington et al., 2015; van Avendonk et al., 2011), although the degree and extent of serpentinisation at outer rises remains uncertain.

Geodynamic models demonstrate that multiple parameters control how oceanic plate is faulted and serpentinised, including crustal age, crustal structure, plate velocity, slab dip angle, mantle temperature, and the degree of coupling between the subducting and overriding plate (Faccenda, 2014; Grevemeyer et al., 2018; Naliboff et al., 2013; Rüpke et al., 2004). Furthermore, the interconnection between faults along the outer rise will affect the degree of serpentinisation (e.g., Miller et al., 2021). Uncertainties regarding the ability of water to infiltrate into the deepest parts of outer rise faults (Korenaga, 2017) and the lateral extent of serpentinisation away from fault zones (Hatakeyama et al., 2017; N. C. Miller & Lizarralde, 2016) have introduced ambiguities into how widespread upper mantle hydration may be at outer rises. Based on seismic anisotropy, focused serpentinisation around discrete faults may significantly limit overall mantle hydration at the Middle American Trench (6.1–8.8% of the uppermost 10 km mantle; Miller et al., 2021). In comparison, the compilation of geophysical evidence tabulated by Faccenda (2014) suggests that 0–40% of the mantle may be serpentinised at outer rises at a number of trenches, with the depth of serpentinisation spanning 0–24 km. In particular, a maximum degree of serpentinisation of 30–40% is recorded for the uppermost mantle at Alaska (R. L. Carlson & Miller, 2003). As a result of these variable controls and uncertainties on serpentinisation, total H_2 generation at outer rises are largely unquantified. One broad estimate of ~2.7–5.3 Mt H_2 yr^{-1}, derived from global subduction modelling, is obtained by assuming 10% of subducting upper mantle mass is serpentinised at outer rises (Merdith et al., 2023).

6.2.2. Serpentinisation of the subducting slab

Devolatilising fluids from the subducting oceanic lithosphere can serpentinise ultramafic minerals in the uppermost portions of the downgoing slab itself. Given these circumstances, abyssal peridotite exhumed at slow-spreading ridges that has not been completely serpentinised on the ocean floor can undergo a secondary phase of serpentinisation during subduction (Boutier et al., 2021; Merdith et al., 2023; Vitale Brovarone et al., 2017, 2020). Evidence of ‘slab serpentinisation’ recorded within supra-subduction ophiolite complexes can be obscured by syn-subduction processes, which may alter any diagnostic signatures distinguishing slab serpentinisation from abyssal serpentinisation at mid-ocean ridges and/or mantle wedge serpentinisation (C. Martin et al., 2020). The principal evidence for serpentinisation of subducted slab peridotites is obtained from field observations and petrological studies. For example, ophiolites in the Alps have boron isotope signatures indicative of slab peridotite alteration unrelated to mid-ocean ridge processes (Scambelluri & Tonarini, 2012); as the Alps have previously experienced residual abyssal peridotite subduction (Boutier et al., 2021; Scambelluri & Tonarini, 2012; Vitale Brovarone et al.,

2017, 2020, 2021), these geochemical signatures are believed to result from serpentinisation of peridotite in the slab after subduction into the Earth.

The quantity of H_2 generated through slab serpentinisation remains speculative. As discussed in Section 5.1.1, the maximum extent to which slab serpentinisation can occur is assumed to be the serpentine-out reaction. Slab serpentinisation is therefore only possible at pressure-temperature conditions where serpentine is stable. Therefore, the key control on the production of H_2 is the amount of unserpentinised peridotite within the downgoing slab itself that can potentially transit through the serpentinisation window. This variable is controlled by tectonic parameters, which dictates a) how much abyssal peridotite is exposed on the seafloor at mid-ocean ridges (itself a function of mid-ocean ridge spreading rate; Section 6.1.3), b) how much abyssal peridotite is serpentinised at the mid-ocean ridge, and c) the convergence rate and subduction geometry, and therefore the pressure-temperature-time pathway of the subducting slab (Merdith et al., 2020, 2023). Based on serpentinisation reaction stoichiometry, and assuming that present-day peridotite exhumation rates at mid-ocean ridges are representative of equivalent peridotite subduction, Vitale Brovarone et al. (2017) suggest that slab serpentinisation may generate >0.8 Mt H_2 yr^{-1}. By estimating the mass of residual abyssal peridotite transiting through the serpentinisation window at subduction zones, Merdith et al. (2023) suggests from the serpentinisation stoichiometric relationship that ~6.8 Mt H_2 yr^{-1} can be generated from global slab serpentinisation. Alternatively, thermodynamic models suggest that 90–300 g of H_2 can be produced from 50% serpentinisation of 1 m^3 of reactant peridotite by an equivalent mass of fluid at slab conditions (Vitale Brovarone et al., 2020), which yields 0.042–0.24 Mt H_2 yr^{-1} when applied to geodynamic models (Merdith et al., 2023).

6.2.3. Mantle wedge serpentinisation

Fluids released from the subducting slab during devolatilisation at high pressure will enter the mantle wedge above it. This fluid influx will hydrate the ultramafic mantle at forearc pressures and temperatures prior to the onset of hydrous flux melting (Fryer, 2012; Vitale Brovarone et al., 2020). Serpentinisation of the mantle wedge is known from geophysical observations (see Peacock & Bostock, 2024 for a recent review) that highlight the low shear wave velocities of the mantle wedge nose (Bostock et al., 2002; DeShon & Schwartz, 2004; Hyndman & Peacock, 2003), seismicity related to the migration of fluids along the subduction interface (Halpaap et al., 2019) and the presence of large-scale magnetic anomalies (Blakely et al., 2005; Teknik et al., 2024; S. E. Williams & Gubbins, 2019). Additionally, buoyant low-density serpentinites can be exposed at the

seafloor overlying subduction forearcs, where the venting of fluids, originating from slab devolatilisation and mantle serpentinisation, can form serpentinite mud volcanoes that erupt representative xenoliths of the slab and wedge (Albers et al., 2019; Fryer et al., 2020; Mottl et al., 2003). Furthermore, ophiolites representative of the cold mantle wedge demonstrate evidence for serpentinisation and H_2 generation and migration at mantle conditions (Boutier et al., 2021; Dandar et al., 2019; Deschamps et al., 2013; C. Martin et al., 2020; Nozaka, 2018; Peverelli et al., 2024; Piccoli et al., 2021; Vitale Brovarone et al., 2017). A recent study of gas compositions measured in the Bolivian Altiplano may hint towards the migration of mantle-wedge-sourced H_2 to the Earth's surface, although the authors concede that this is highly speculative (I. Moretti et al., 2023). This geological production of H_2 in subduction settings may provide essential sources of energy to life deep within the Earth, greatly expanding the range of the biosphere to as deep as 10 km under the surface (Peverelli et al., 2024; Plümper et al., 2017).

Key to resolving the role of mantle wedge serpentinisation in sustaining a deep biosphere is an understanding of how ubiquitous this process is. Initial studies resolved forearc serpentinisation at a number of subduction systems worldwide (Hyndman & Peacock, 2003; Peacock & Hyndman, 1999). However, this viewpoint has been challenged from thermo-petrological modelling suggesting that slab dehydration does not release sufficient water to hydrate forearcs over subduction lifetimes (Abers et al., 2017). Several suggestions have been put forward to bridge the discrepancy between geophysical and petrological observations (Peacock & Bostock, 2024), including the co-evolution of slab and wedge thermal structure over geological time which can modulate the degree slab dehydration and wedge hydration (Epstein et al., 2024; Holt & Condit, 2021), the compositional structure of the downgoing slab which will affect the depth of fluid release (Wada et al., 2012), and the role of slab fluid migration into the cold forearc nose from the deeper parts of the slab (Halpaap et al., 2019; Kawano et al., 2011; Piccoli et al., 2021). Furthermore, the H_2 generated during wedge hydration is strongly controlled by fluid and mantle composition (Vitale Brovarone et al., 2020), and H_2 generation itself may be decoupled from the degree of serpentinisation at slab-wedge interface conditions (Siron et al., 2024). The ubiquity of mantle wedge serpentinisation therefore remains an open question, and the subject of extensive ongoing research.

By scaling thermodynamic models to the water released from downgoing slabs, Vitale Brovarone et al. (2020) estimate that mantle serpentinisation may generate a broad range of 0.009–0.3 Mt H_2 yr^{-1}. Following this methodology, Merdith et al. (2023) suggest from their modelling of slab

serpentinisation that 0.34–18 kt H_2 yr^{-1} may be generated from wedge serpentinisation. Estimates of H_2 fluxing from wedge serpentinisation therefore remain hugely uncertain, and subject to a myriad of observational and modelling assumptions.

6.2.4. Metamorphism of subducted altered oceanic crust

Metamorphism of altered oceanic crust during subduction can result in the generation of H_2. Carbon stored within the subducting slab can contribute towards the generation of methane during subduction; such methane is preserved within fluid inclusions in high-pressure metamorphic rocks in the Western Tianshan of China, where carbon is sourced from ankeritic dolomite or graphite in the slab (L. Zhang et al., 2023). While no H_2 is recorded in these fluid inclusions, it is probable that H_2 may be generated through the same redox reactions that generate CH_4. The presence of abiotically generated CH_4 may therefore act as an indicator of geological H_2. Further investigations will be necessary to constrain the volumes of reduced species that may be generated by redox-sensitive elements in the downgoing crust.

6.2.5. Thermogenic H_2 in subducted marine sediments

Isotopically light H_2 recorded from shales, gas manifestations, and mud volcanoes in Japanese subduction systems suggest that thermogenic H_2 constitutes a significant portion of subduction-related H_2, and contributes towards high H_2 and CH_4 concentrations measured from underthrust subducting sediments (Suzuki et al., 2017, 2024). Experimental results suggest that pyrolytic transformation of subducted organic matter produces higher H_2 concentrations with increasing temperature (see Section 4). The metamorphic evolution of subducted organic sediments may therefore generate H_2 which contributes towards the high volumetric fluxes of CH_4 observed at subduction zones such as the Nankai Trough ($3.5–27\times10^4$ m^3 CH_4 yr^{-1} per km of subduction zone; Suzuki et al., 2024).

6.2.6. Graphite-water equilibria

Besides generation of H_2 through thermogenic cracking of organic matter during metamorphism, aqueous metamorphic fluids equilibrating with or being released from subducting rocks may also contain H_2. At present, estimates of H_2 concentrations in fluids equilibrated with metamorphic rocks in the subducting slab are not available. However, first order estimates can be derived for carbonate-free, graphite-bearing rocks within the C-O-H system (Connolly & Cesare, 1993; Holloway, 1984). The H_2 concentrations in these slab fluids strongly depend upon the oxidation state of the system. Assuming prograde metamorphism of graphite-bearing rocks at water

maximum conditions (Figure 3A) (Connolly & Cesare, 1993) and redox conditions from FMQ-2 to FMQ+1 (Figures 3B–E), the molar fraction of H_2 (where $XH_2 = H_2 / [H_2O + CO_2 + CH_4 + H_2 + O_2]$) ranges from 10^{-5} to 10^{-2} (calculated with Thermotopes-COH software; Boutier et al., 2024). H_2 concentrations resulting from more-oxidised graphite-free or carbonate-bearing metasedimentary rocks are likely to be lower than their more-reduced graphite-bearing equivalents. Considering the fluxes of water generated from subducted pelagic sediments—typically containing organic carbon—in active subduction zones before 4 GPa (80 Mt H_2O yr^{-1}; Hacker, 2008), it can be estimated that at least 8×10^{-4} to 0.8 Mt H_2 yr^{-1} could be produced. These values can increase to at least 1.8×10^{-3} to 1.8 Mt H_2 yr^{-1} if the total fluid released by the whole subducting lithospheric section (180 Mt H_2O yr^{-1}; Hacker, 2008) equilibrates with graphite-bearing metasedimentary rocks at the slab top.

6.3. Subaerial volcanic fluxes

Volcanic magma and gas volatile compositions are dominated by CO_2 and the oxidised form of hydrogen, H_2O (Edmonds, 2008; Fischer & Chiodini, 2015; Giggenbach, 1996; S. Lee et al., 2018). H_2 is a trace gas in volcanic systems, typically comprising a molar proportion in the gas of the order of magnitude of <0.1–2 mol.% (Aiuppa & Moussallam, 2024; Fischer & Chiodini, 2015; Oppenheimer, 2003). However, H_2 plays a key role in volcanic gas redox reactions and speciation (Section 5.2). Significant efforts have therefore recently been made to improve the characterisation of H_2 concentrations from degassing volcanoes worldwide (Figure 4B; e.g., Aiuppa et al., 2017; Aiuppa & Moussallam, 2024).

H_2 within volcanic gases cannot be determined using remote sensing methods. Instead, it must be measured by electrochemical sensors incorporated within MultiGAS instruments (e.g., Aiuppa et al., 2011; Moussallam et al., 2012), or by direct sampling of the gases themselves at fumaroles and volcanic edifices (e.g., Symonds et al., 1994). Gas can also be directly sampled from fresh lavas, particularly after the development of well-developed fracture networks which provide clear routes for degassing (e.g., Pasquet et al., 2022). However, compared with the more voluminous CO_2, direct *in situ* flux measurements are rare in the literature, and typically localised to single volcanoes or volcanic-hydrothermal systems. To obtain total fluxes of volcanic H_2 into the atmosphere, a ratio is normally performed with a gas that is easier to quantify using remote methods, such as SO_2. By estimating the total SO_2 degassed from volcanoes (e.g., Carn et al., 2017; Halmer et al., 2002) and combining this flux with the H_2/SO_2 ratio measured in the volcanic plume, the corresponding total H_2 flux can be determined (e.g., Figure 4B). This method has been

utilised previously to estimate global subaerial volcanic fluxes of H_2 (Canfield et al., 2006); however, owing to vapour redox behavior during degassing, the range of H_2/SO_2 ratios vary significantly between different volcanoes (Aiuppa & Moussallam, 2024; Canfield et al., 2006) and even within different edifices and hydrothermal manifestations on a single volcano itself (Aiuppa & Moussallam, 2024).

Estimates of global volcanic H_2 fluxes are subject to large uncertainties, owing to the limited dataset recorded from degassing volcanoes (Aiuppa & Moussallam, 2024). Further uncertainties in quantifying volcanic H_2 arises from the degassing of magmas at depth, which can diffusely distribute volcanic gases over a broad fault zone as opposed to distinct fumaroles or volcanic edifices (e.g., Burton et al., 2013; Mörner & Etiope, 2002; Werner et al., 2019). However, broad trends controlling H_2 concentrations in volcanic gases are noted by Aiuppa & Moussallam, namely that anhydrous intraplate and continental rift settings yield comparatively high volcanic fluxes of H_2, and that H_2 concentrations are strongly correlated with temperature at arc volcanoes. These broad trends are a likely function of magma redox conditions (reduced at anhydrous settings vs. oxidised at arcs) and their effects on C-O-H-S gas partitioning (Section 5.2).

An early estimate of volcanic contributions of H_2 to the atmosphere combined carbon:water ratios in volcanic gases with gas equilibria at the FMQ buffer and volcanic carbon fluxes to obtain a broad estimate of $4.8 \pm 3.6 \times 10^{12}$ mol H_2 yr^{-1} (9.7 ± 7.3 Mt H_2 yr^{-1}; Holland, 2002). However, this estimate makes a highly simplified assumption that redox partitioning of H_2 in magmatic gases occurs at the FMQ buffer, and therefore fails to capture the broad thermal, oxidation, and compositional ranges of volcanic gases worldwide. As noted by the volcanic gas emission data collated in Table 5 of Canfield et al. (2006), the H_2/SO_2 molar ratio of volcanic gases ranges from 0.02–24, with a median value of 0.8. By assuming a representative range of H_2/SO_2 ratios based on this data (0.3–1.0), and combining this with a SO_2 global flux estimate (Halmer et al., 2002), Canfield et al. calculate a volcanic H_2 flux of $0.8–3.1 \times 10^{11}$ mol H_2 yr^{-1} (0.2–0.7 Mt H_2 yr^{-1}). While this early estimate is restricted by the size of the dataset and the assumptions made concerning global variability of H_2/SO_2 at the time of its publication, Canfield et al. demonstrate that volcanic H_2 emissions are on the same order of magnitude as oceanic serpentinisation (as discussed in previous sections).

More recently, Stolper et al. (2021) estimate volcanic H_2 by coupling volcanic gas H_2/H_2O ratios with measurements of volcanic gas emissions (Fischer et al., 2019). However, in contrast to

Canfield et al., (2006), Stolper et al. use thermodynamically derived H_2/H_2O ratios based on appropriate pressure-temperature-oxygen fugacities of present-day subaerial volcanoes and their typical gas compositions (via the software of Burgisser et al., 2015). By considering the minimum and maximum values in the H_2/H_2O ranges, and multiplying these ratios by global H_2O fluxes, their estimated volcanic H_2 flux is $0.05–0.20\times10^{12}$ mol H_2 yr^{-1} (0.11–0.45 Mt H_2 yr^{-1}). However, it is noted by Aiuppa & Moussallam (2024) that this estimate is strongly dependent on the assumption that surface gas emissions are in equilibrium with their source magma, which only holds true for gases emitted at magmatic temperatures (Section 5.2). Re-equilibration and concurrent oxidation of the gas during adiabatic cooling will generally remove H_2 from the volcanic gas (Henley & Fischer, 2021).

Aiuppa & Moussallam (2024) refine the approach of Stolper et al. (2021) by compiling an extensive database of volcanic H_2 emissions, which is categorised by how strongly degassing the volcanoes are. These categories are then assessed for H_2 fluxes by determining the total flux of SO_2 from their constituent volcanoes (or CO_2 in the case of quiescent 'hydrothermal' volcanoes). The total SO_2 (or CO_2) flux is then combined with median H_2/SO_2 (or H_2/CO_2) to obtain a total H_2 flux of 0.06–1.0 Mt H_2 yr^{-1}, with a chosen median value of 0.23 Mt H_2 yr^{-1}. The principal contributors to this value are the ‘strong emitter’ volcanoes, which degas high-temperature SO_2-rich gases (>0.14 Mt SO_2 yr^{-1}; Carn et al., 2017; Fischer et al., 2019) and account for nearly all the volcanic H_2 flux (Figure 4B). Weak emitters typically contribute lower temperature gases, which are prone to oxidation during adiabatic cooling and the removal of sulphur during gas-liquid interactions in hydrothermal systems, thereby limiting their H_2 fluxes (Aiuppa & Moussallam, 2024).

Although unquantified, we note that further processes can produce abiotic H_2 both during and after volcanic activity. Magmatic intrusion and emplacement into an organic carbon-rich crust will generate significant volumes of H_2 through thermal decomposition of organic material (Section 4) and/or reduction of the magma by the assimilation of reduced organic carbon (Iacono-Marziano, Gaillard, et al., 2012). H_2 generated in this manner may subsequently contribute towards the fluxes of H_2, CH_4 and H_2S from volcanoes, for example, as observed during large igneous province emplacement (e.g., (Capriolo et al., 2021; Iacono-Marziano, Marecal, et al., 2012; Svensen et al., 2004, 2023). Finally, Fe^{2+}-bearing minerals in lavas will oxidise as they degas H_2O and SO_2 during late-stage crystallisation, forming H_2 as a by-product (Section 5.1.2; e.g., Bach & Edwards, 2003; Holloway & O’Day, 2000). While such mechanisms will be active in magmatic

systems, their H_2 contributions likely pale in comparison to the significant proportions emitted from volcanic edifices through magmatic degassing.

6.4. Fluxes within continental settings

Although oceans provide an environment where water is abundant for redox reactions and radiolysis, the continents also host sites of significant H_2 generation. The possibility of serpentinisation and alteration of ultramafic rocks at temperatures below 100 °C allows for generation of H_2 within ultramafic domains within continental settings (e.g., Mayhew et al., 2013; McCollom & Donaldson, 2016; Neubeck et al., 2011; Okland et al., 2014; Stevens & McKinley, 2000). In the absence of ultramafic lithologies, the oxidation of Fe^{2+} minerals in silicic rocks (Murray et al., 2020), and the ubiquity of radiolysis (Sherwood Lollar et al., 2014) and rock fracturing (Hirose et al., 2011; Telling et al., 2015) can generate substantial H_2 within continental settings.

6.4.1. Precambrian shields

Although often not considered in earlier reviews of geological H_2 fluxes (e.g., Sleep & Bird, 2007), it has now been recognised that Precambrian shields, comprising ~72% of the present-day continents (Figure 4A; Goodwin, 1996), may be significant contributors of H_2. Precambrian shields provide environments in which ancient waters within fractures and inclusions can reside for millions to billions of years (G. Holland et al., 2013; Lippmann-Pipke et al., 2011; Parnell & Blamey, 2017a; Sherwood Lollar et al., 2024). Samples of crystalline basement gas and fracture water, collected from borehole collars, therefore provide the basis for compositional and isotopic analyses of crustal gas production by radiolysis and serpentinisation.

The radiolysis of water within Precambrian basement can generate significant amounts of H_2 over geological time (e.g., Lin et al., 2005). Radiolytic H_2 generation rates are typically of the order of 10^{-9}–10^{-8} mol H_2 yr^{-1} per m^3 of Precambrian crystalline basement (Warr et al., 2019), which is sufficient to sustain deep subsurface life (Sherwood Lollar et al., 2007; Telling et al., 2018). An early estimate determined, through steady-state diffusion of radiolytic H_2 from the Witwatersrand sedimentary basin, that global areal H_2 fluxes from radiolysis within continental settings would be 8 μmol H_2 m^2 s^{-1} (L.-H. Lin, Hall, et al., 2005). If this is extrapolated to the scale of continents, radiolytic production could be 9×10^8 mol H_2 yr^{-1} (0.002 Mt H_2 yr^{-1}), as determined by Sherwood Lollar et al. (2014), which is minor in comparison to other geological settings. However, subsequent authors note the limitations of extrapolating a single regional sedimentary basin for

global crystalline continental crust, and considering only H_2 in fissure fluids and ignoring H_2 within the rocks themselves (Sherwood Lollar et al., 2014). It has been recognised that old Precambrian basement typically carries elevated concentrations of H_2 within fluid inclusions relative to younger Cenozoic basement (up to 0.6 vol.% in gases released during crushing), thus acting as a significant reservoir of geological H_2 (Parnell & Blamey, 2017a, 2017b). Scaling of the continental crust ^{4}He production rate as a function of mean continental crust porosity yields a H_2 production estimate of 1.6–4.7×10^{10} mol H_2 yr^{-1} (0.03–0.09 Mt H_2 yr^{-1}), although radiolytic generation facilitated by high porosities in crystalline crust could yield as much as 1×10^{11} mol H_2 yr^{-1} (0.2 Mt H_2 yr^{-1}; Sherwood Lollar et al., 2014).

Combined with radiolytic H_2 fluxes are fluxes resulting from the hydration of mafic and ultramafic material within continental crust. Precambrian greenstone belts, characterised by ultramafic and mafic igneous domains that are several kilometres thick, account for ~30% of exposed continental surface area, thereby providing significant potential for H_2 generation through serpentinisation and related redox reactions (e.g., Hutchinson et al., 2024). By considering this exposed surface area, Sherwood Lollar et al. (2014) suggest that 0.2–1.8×10^{11} mol H_2 yr^{-1} (0.04–0.36 Mt H_2 yr^{-1}) may be generated from greenstone serpentinisation. When combined with estimates of radiolytic H_2 generation, total Precambrian crustal H_2 flux is 0.36–2.27×10^{11} mol H_2 yr^{-1} (0.07–0.45 Mt H_2 yr^{-1}). This flux is captured by a broad range of borehole H_2 concentrations (<0.01 to over 80 vol.%) and high H_2 concentrations in groundwaters (2.4–64 mM) (Sherwood Lollar et al., 2006, 2014).

More recent estimates by Warr et al., (2019), determined through the combination of an empirical model with H_2 ratios with the noble gas isotopes ^{4}He and ^{40}Ar, suggest that total Precambrian shield H_2 production is 0.4–5.4 ×10^{10} mol H_2 yr^{-1} (0.008–0.11 Mt H_2 yr^{-1}), towards which greenstone hydration contributes 0.1–4.8×10^{10} mol H_2 yr^{-1} (0.002–0.09 Mt H_2 yr^{-1}) and radiolysis 0.7–1.2×10^{10} mol H_2 yr^{-1} (0.01–0.02 Mt H_2 yr^{-1}). While Warr et al. acknowledge that they may overestimate H_2 production rates owing to their selection of radioelement concentrations and rock porosities, a later study by the same authors using a statistical approach suggest that their selections can be considered sensible (Warr et al., 2023).

6.4.2. Ophiolite complexes

Ophiolites are ultramafic oceanic material that has been emplaced onto continental crust through tectonic processes (Figure 4A). In comparison to Archean greenstone belts, Phanerozoic ophiolites lack the komatiites associated with Precambrian settings, and are mutually structurally

similar in their construction compared to greenstone belts (see Furnes & Dilek, 2022, for a review). Ophiolites have recently garnered significant interest as sites where large amounts of natural H_2 can be abiotically generated, trapped and accumulated in reservoirs, and feasibly extracted for use as an energy source (Bachaud et al., 2017; Etiope, 2024; N. J. P. Smith et al., 2005), and are therefore considered key targets for natural H_2 exploration.

Geological H_2 may be liberated from ophiolites either from serpentinisation, or by decrepitation of H_2-bearing fluid inclusions within which H_2 has formed from Fischer-Tropsch Type reactions at mantle conditions (Etiope, 2024; Grozeva et al., 2020; Leong et al., 2023). Reaction path modelling suggests that it is possible to generate ~0.3 mol H_2 per kg of ultramafic rock in ophiolitic settings (~0.6 g H_2 per kg of rock; Leong et al., 2023). Evidence for H_2 generation and accumulation takes the form of intense gas fluxes recorded in ophiolitic sites worldwide (e.g., Vacquand et al., 2018; Zgonnik, 2020). Measured H_2 fluxes at some ophiolites, comprising 10 to >80 vol.% of discharging gas (e.g., Sherwood Lollar et al., 2014; Truche et al., 2024; Zgonnik et al., 2019), are too high to sustain through slow natural generation alone (i.e., through the processes discussed above in Section 2–5); it has therefore been suggested that such high fluxes must be the result of accumulation of H_2 prior to gradual release (Truche et al., 2024). Accumulation also justifies how H_2 is commonly associated with other low-production-rate gases such as CH_4 and hydrocarbons. Gas fluxes measured in ophiolitic surface seeps indicate that pressure gradients in ophiolites resulting from gas accumulation can drive the advection of H_2 towards Earth's surface (Etiope, 2023). High geological H_2 fluxes resulting from prior entrapment and accumulation is therefore implicitly suggested at several ophiolites worldwide (Abrajano et al., 1988; Baciu & Etiope, 2024; D'Alessandro et al., 2018; Etiope, 2023; Truche et al., 2024).

Owing to their potential economic importance, significant efforts have been placed into resolving the fluxes of H_2 from ophiolites. One example is the Chimaera seep within the Tekirova Ophiolite of Turkey, which has been outgassing at a rate of ~4 t H_2 yr^{-1} for at least two millennia (Etiope, 2023). More recently, large volumes of H_2 have been identified trapped within a reservoir in the Bulqizë Jurassic ophiolite complex in Albania, resulting in the venting of >200 t H_2 yr^{-1} (Truche et al., 2024). Other recent studies performed within ophiolitic sites in Brazil (I. Moretti et al., 2021) and Oman (Zgonnik et al., 2019) yield H_2 fluxes of a similar magnitude to that of Bulqizë. Zgonnik et al. (2019) suggest that 70–150 m^3 H_2 km^{-2} d^{-1} may flow from the Semail ophiolite massif in Oman. If generalised for the total global surface area of ophiolites, 0.18–0.36 Mt H_2 yr^{-1} may be generated from the serpentinisation of ophiolites worldwide (Zgonnik, 2020). However, Leong et

al. (2023) note that only H_2 shallow drill holes and holes in altered lithologies are considered by Zgonnik et al., which may exaggerate this estimate of global ophiolitic H_2 generation. Furthermore, the recorded total outgassing of the Semail ophiolite is exceptionally high for ophiolites (see Table 1 of Etiope, 2023). This global H_2 flux estimate must therefore be considered an upper bound on ophiolitic degassing.

6.4.3. Continental rifts and passive margins

Hydrogen exploration of continental rifts remains an ongoing subject of research. Continental rift settings are known to release significant volumes of volatile elements such as CO_2, which are sourced primarily from the mantle during redox melting and decompression melting (e.g., Brune et al., 2017; Foley & Fischer, 2017; Lee et al., 2016). It would therefore be reasonable to suggest that large quantities of H_2 are also degassed during continental rift volcanism as a component of the overall budget of volatiles liberated from the mantle. However, at present there are no measured fluxes of H_2 from active continental rift settings beyond gas measurements from individual rift volcanoes in East Africa (de Moor et al., 2013; Deville et al., 2023; Pasquet et al., 2022). For example, at the carbonatite rift volcano Ol Doinyo Lengai, H_2 comprises ~1 mol.% of diffuse emissions at fumaroles (Koepenick et al., 1996). Similarly, measurable quantities of volcanic H_2 are recorded from degassing rift volcanoes, volcanic rift zones, and lava flows within the Afar Triple Junction (Darrah et al., 2013; de Moor et al., 2013; Deville et al., 2023; Pasquet et al., 2023).

Geodynamic models suggest that H_2 may be produced from the serpentinisation of exhumed mantle during continental breakup. The key controls on H_2 generation in this regard are the formation of large faults permitting the access of fluids into the exhuming mantle, and the thermal gradient within the rifting lithosphere which controls the intersection of the serpentinisation window with exhuming mantle (Zwaan et al., 2025). Fluid flow via active lithosphere-scale faults at continental rifts is key for increasing the susceptibility of lower crustal basement rocks and the upper mantle to serpentinisation; however the degree of serpentinisation will be dependent on the thermal gradients that restrict serpentine stability, and the growth of serpentine minerals that will limit fluid flow into the continental basement (Bayrakci et al., 2016). Serpentinisation through faulting and exhumation in this manner is believed to have affected the hyperextended Mauléon Basin in the Pyrenees (Lefeuvre et al., 2022; Saspiturry et al., 2024; Tichadou et al., 2021). The timescales of rifting and subsequent post-rift cooling also control whether serpentinisation may

affect exhumed mantle material in rifts. Rapid rifting will exhume a hot mantle, whereas slow rifting will allow the mantle to cool into the serpentinisation window (Zwaan et al., 2025).

Numerical geodynamic models suggest that serpentinisation of exhumed mantle during slow rifting could generate 1.5×10^{8} mol H_2 yr^{-1} per km of rift (0.3 kt H_2 yr^{-1} km^{-1}; Zwaan et al., 2025). Using the present-day length of continental rifts (14,500 km; Brune et al., 2017), and assuming that the entirety of this exhumed mantle is undergoing serpentinisation, the modern H_2 rift flux resulting from serpentinisation could be as high as 4.38 Mt H_2 yr^{-1}. However, we stress that this value should only be considered an extreme maximum: rift kinematics differ significantly worldwide and even within individual rifts themselves (e.g., Brune et al., 2023; Ebinger, 2005), and only a small fraction of rifts may be able to exhume sufficient mantle material into the serpentinisation window for H_2 to be generated.

Magma-poor passive margins demonstrate evidence for serpentinisation during and/or after rifting. Perhaps the best studied example is the Iberian Margin of the North Atlantic, within which ODP drill sites have revealed extensive serpentinite exposed within the seafloor (Schwarzenbach et al., 2013) which may extend to depths of 5–6 km (Minshull, 2009). In contrast to serpentinisation of mantle peridotite exposed at mid-ocean ridges, magma-poor rifted margin peridotite has a composition closer in compositional affinity to sub-continental lithospheric mantle than aluminous lherzolite (Albers et al., 2021). Sparse magnetite within these serpentinites suggest that serpentinisation occurred at low temperatures, with further, much slower H_2 generation occurring from the long-term post-serpentinisation oxidation of magnetite and serpentine exposed to seawater (Albers et al., 2021).

Thermo-geochemical models have demonstrated that magma-poor continent-ocean transitions are sites of rampant serpentinisation and significant H_2 generation. Assuming that the formation of continent-ocean transitions in the North Atlantic occurred over timescales of ~30 million years, Liu et al. (2023) derive a maximum flux rate of 1.4×10^{17} mol H_2 Myr^{-1}, or equivalently 0.028 Mt H_2 yr^{-1} for 'average' H_2 production at the Iberian margin, similar to an estimate by Klein et al. (2020) of $0.1–2.0\times10^{11}$ mol H_2 yr^{-1} (0.02–0.40 Mt H_2 yr^{-1}) following Skelton et al. (2005). However, as with other settings, serpentinisation is likely to be strongly concentrated around faults (Bayrakci et al., 2016), and may not be widespread throughout the margin as a whole.

The quiescence of active rifting will limit the H_2 that is generated (Bayrakci et al., 2016). Subsequent rift basin inversion—the tectonic switch from an extensional regime to a compressional one—can uplift significant volumes of already-exhumed mantle material into the serpentinisation window and result in formation of lithosphere-scale faults, thereby resulting in the formation of significant volumes of H_2 during orogenesis: as high as 3×10^{10} mol H_2 yr^{-1} per km of rift-inversion basin, or alternatively 0.06 Mt H_2 yr^{-1} km^{-1} (Zwaan et al., 2025). Uplifted lithospheric mantle found within regions of ongoing orogenesis, such as along the Alpine-Tethyan domain (Etiope, 2023; Lefeuvre et al., 2021, 2022; Truche et al., 2024) and south-western Brazil (Prinzhofer et al., 2024), are therefore potential sites of ongoing natural H_2 generation. In particular, natural H_2 reservoirs and seals may develop within rift-inversion orogens from the large volumes of permeable sediment and impermeable ultramafic domains that may be present during exhumation and uplift, thereby providing environments for H_2 accumulation (Zwaan et al., 2025).

6.4.4. Sedimentary basins

Structures in sedimentary basins can allow hydrocarbons to accumulate in quantities that are economically feasible and worthwhile to extract. Hydrocarbon source rocks can be overlain by porous reservoir rocks, which in turn underlie an impermeable trap to limit hydrocarbon escape. As the same principles apply to the accumulation of H_2, sedimentary basins have been considered sites for natural H_2 exploration (Hutchinson et al., 2024; Jackson et al., 2024).

In sedimentary basins, H_2 may be generated by a number of processes. Firstly, basins allow for the accumulation of siliciclastic material derived from the erosion of continental basement, which is a reservoir of radiolytic H_2 within fluid inclusions (Parnell & Blamey, 2017a). H_2 preserved in this manner may be liberated by decrepitation. Furthermore, the pore space fluids within sedimentary lithologies provide an additional vector for radiolytic H_2 generation so long as radionuclides continue to decay. Radiolysis is likely to be a key contributor to H_2 generation in basins where uranium deposits are located, such as the Athabasca Basin, Canada (Richard, 2017). In addition, the processes that can generate hydrocarbons may also produce H_2. The cracking and thermal maturation of hydrocarbons means that H_2 is frequently associated with natural gas generation. This is believed to be a principal means of generating high concentrations of H_2 in the Cooper Basin, Australia (Boreham et al., 2023) and from Colombian coals (I. Moretti et al., 2024). It has been estimated that 8–80 mol H_2 may be generated from thermogenic processes at 200–400 °C per kg of organic-rich rock (I. Moretti et al., 2024), which contributes

towards an estimated ~35 Gt of H_2 that may potentially be sourced from global organic matter (Mahlstedt et al., 2022).

Finally, the serpentinisation of exhumed mantle rock or rift volcanics under or within basins can yield high concentrations of H_2, as measured from natural gas in the Songliao Basin, China (Horsfield et al., 2022; Q. Liu et al., 2025) and soil gases in the North Perth Basin, Australia (Frery et al., 2021). Intracratonic basins with deep ultramafic/mafic lithologies or reduced sediments also show potential for substantial deep H_2 generation, such as the Paris Basin, France (Lefeuvre et al., 2024) and the Taoudeni Basin, Mali (Hutchinson et al., 2024; Maiga et al., 2023; Prinzhofer et al., 2018). Mafic sills in sedimentary basins may additionally provide impermeable barriers to the upwards migration of H_2-rich fluids (Prinzhofer et al., 2018) to facilitate H_2 accumulation. Therefore, although globally unquantified, H_2 sourced from sedimentary basins may constitute a substantial contribution towards continental fluxes.

6.4.5. Iron-bearing formations (BIFs; siderite)

H_2 may be generated through the reduction of Fe^{2+} minerals within iron-bearing lithologies, such as Precambrian banded iron formations (BIFs; Geymond et al., 2022, 2023; McCollom, 2003; Milesi et al., 2016) and ultramafic cratonic rocks (Boreham, Sohn, et al., 2021; Frery et al., 2021). However, the presence of minerals such as siderite ($FeCO_3$), magnetite (Fe_3O_4) and haematite (Fe_2O_3), which are more oxidised than pyrite or FeO, will buffer the redox capacity of such lithologies and make the environments less reducing as a result, thereby slowing H_2 generation relative to ultramafic lithologies (Jackson et al., 2024; Malvoisin & Brunet, 2023). As a result, it has been predicted—with considerable uncertainty—that the total potential H_2 that can be generated by ferrous iron oxidation in gold deposits, BIFs and other iron formations, and carbonatites worldwide is ~6×10^{14} mol H_2 (~1.2×10^{3} Mt H_2), which, if linearly oxidised over the age of continental crust (2 Gyr), produces a global mean flux of ~3×10^{5} mol H_2 yr^{-1} (~60 kg H_2 yr^{-1}; Malvoisin & Brunet, 2023). As a result, oxidation of orogenic gold deposits, iron ore formations and carbonatites can be considered negligible relative to the overall flux of H_2 generated by other abiotic processes.

6.4.6. Granites

In granites, the principal means of generating H_2 is through radiolysis, owing to high concentrations of lithophile radionuclides. Radiolytic H_2 generation rates are typically low, and on the order of 10^{-9}–10^{-8} mol H_2 yr^{-1} per m^3 of rock (Boreham, Edwards, et al., 2021). However,

continental granites rich in ferrous iron minerals such as Fe-biotite, Fe-amphibole, and magnetite can also generate substantial H_2 through water-rock reactions (Truche et al., 2021). A study of the Soultz-sous-Forêts granite field suggests that 1 km^3 of biotite-rich granite has the potential to yield 5.1×10^{10} mol H_2 (102 kt H_2) (Murray et al., 2020) Similarly, metasomatic fluid circulation within the Roxby Downs granite could produce 85 mol H_2 per m^3 granite from fluid-rock reactions, with a further radiolytic production rate of $7.1–9.9\times10^{-9}$ mol H_2 m^{-3} yr^{-1} (Bourdet et al., 2023).

6.4.7. Mechanoradical H_2 generation by sub-glacial abrasion

Glaciers comprise ~700,000 km^2 of the present-day Earth's surface (Pfeffer et al., 2014; RGI 7.0 Consortium, 2023). If a representative abrasive production rate of 100 nmol H_2 d^{-1} per m^2 of glacial catchment is applied to this area (Macdonald et al., 2018; Telling et al., 2015), the H_2 flux from glacial abrasion is ~50 t H_2 yr^{-1}. While this value is not significant relative to other settings, this H_2 is locally important as an energy source for sub-glacial microbial life (Telling et al., 2015). It is therefore evident that constraining mechanoradical H_2 remains a significant knowledge gap in understanding of H_2 fluxes.

6.5. Mechanoradical H_2 generation by seismicity

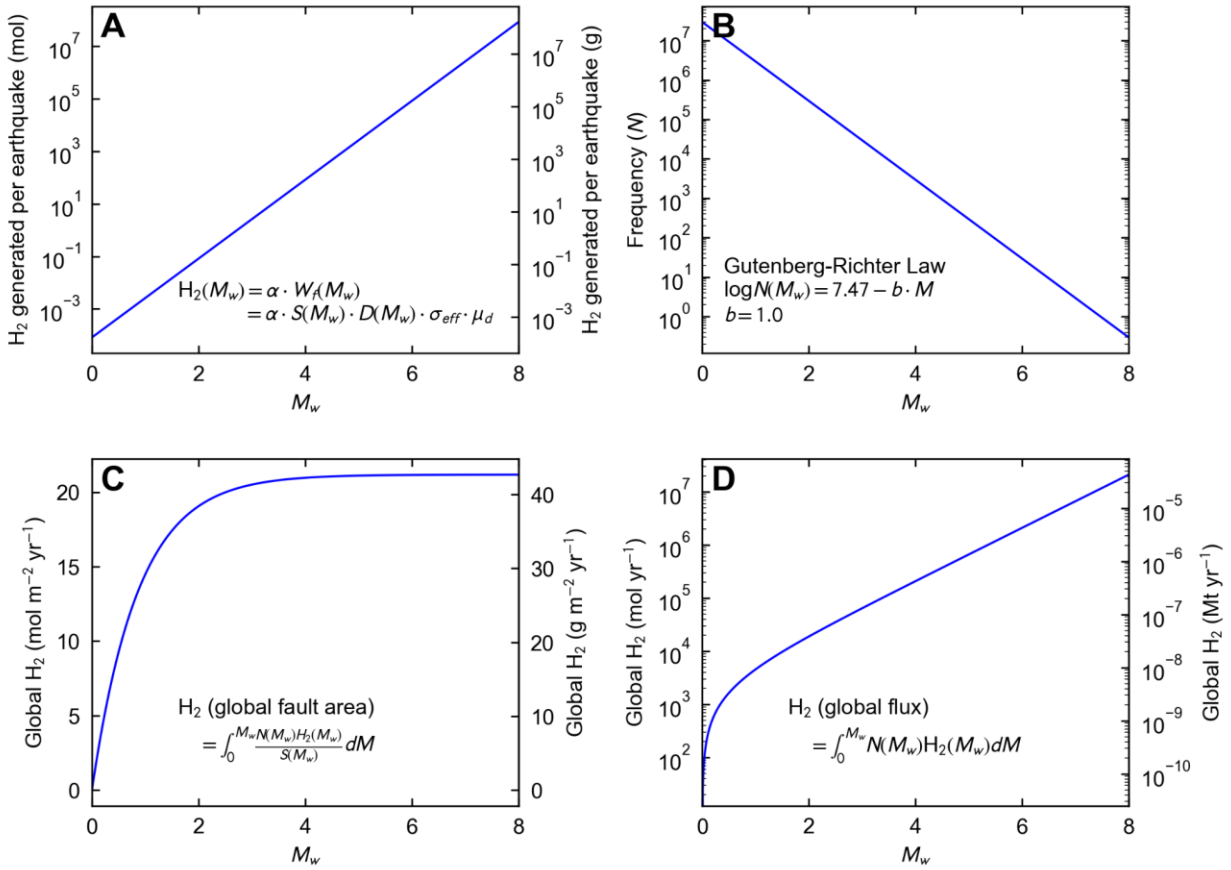

Figure 6: Plots illustrating mechanoradical H_2 generation as a function of earthquake moment magnitude (M_w). A. H_2 generated per single earthquake of a specified M_w, as described by Equation 2. B. Gutenberg-Richter Law (Equation 5) describing the frequency of earthquakes with M_w greater than or equal to the specified M_w, with coefficients chosen for annual global earthquakes following Hirose et al. (2011). C. H_2 generated annually per area of fault surface as described by Equation 3. D. H_2 generated annually by earthquakes following Equation 4.

The role that mechanoradical H_2 plays in H_2 fluxes in the oceans and continents remains hugely unconstrained. While identified at fault zones in the aftermath of large earthquakes (Arai et al., 2001; Dogan et al., 2007; Hirose et al., 2011; Y. Li et al., 2013; Sato et al., 1984, 1986; Sugisaki et al., 1983; Ware et al., 1984) and suggested as a possible source for H_2 accumulations in parts of the Paris Basin (Lefeuvre et al., 2024), mechanoradical H_2 generation as a result of low-magnitude earthquakes, aseismic deformation, fracturing, and abrasion is firstly difficult to measure—especially if microbial H_2 consumption in fault zones is rapid—and secondly difficult to quantify globally.

The key reference for modelling global mechanoradical H_2 generation is the study of Hirose et al. (2011, 2012). Through experimental investigation, Hirose et al. determine the moles of H_2 generated by the frictional work done (W_f) during faulting. These experiments are subsequently scaled to earthquake moment magnitudes (M_w) to yield the following parameterisations for H_2 fluxes (Equations 2 and 3):

(Eqn. 2) $H_2(M_w)$ (per individual earthquake) = $\alpha \cdot W_f(M_w) = \alpha \cdot S(M_w) \cdot D(M_w) \cdot \sigma_{eff} \cdot \mu_d$

(Eqn. 3) $H_2(M_w)$ (global flux per unit fault surface area) = $\int^{Mw}_0 [N(M_w) \cdot \alpha \cdot W_f(M_w) / S(M_w)] \, dM_w$

Worman et al. (2020) obtain Equation 4 for global mechanoradical flux by multiplying the integrand by $S(M_w)$:

(Eqn. 4) $H_2(M_w)$ (global flux) = $\int^{Mw} N(M_w) \cdot \alpha \cdot W_f(M_w) \, dM_w$

Where $S(M_w)$ is the empirically derived fault surface area of an earthquake with moment magnitude M_w ($\log S(M_w) = M_w + 2$, in m^2), $D(M_w)$ is the empirically derived fault displacement of an earthquake with moment magnitude M_w ($\log D(M_w) = 0.5 \cdot M_w - 3.1$, in m), σ_{eff} is the effective stress acting on the fault surface (16 MPa), μ_d is the average dynamic friction coefficient (0.25, dimensionless), α is the experimentally derived correlation between the moles of H_2 generated and the frictional work done along the faulting surface (0.26 μmol/kJ), and $N(M_w)$ is the frequency of earthquakes with moment magnitude of at least M_w as given by the Gutenberg-Richter Law (Equation 5):

(Eqn. 5) $\log_{10} N(M_w) = a - (b \cdot M_w)$

Where a and b are coefficients taken to be 7.47 and 1.0 respectively for annual global seismicity (Hirose et al., 2011). From Equations 2–4, it is clear that mechanoradical H_2 fluxes are strongly dependent on earthquake magnitude (Figures 6A, 6C, and 6D) and the frequency of these earthquakes (Figure 6B). As the upper bound of integration progresses to higher magnitude, the H_2 generated per unit fault surface area plateaus at 21 mol H_2 m^{-2} yr^{-1} (not 230 mol H_2 m^{-2} yr^{-1} as presented by Hirose et al.; Figure 6C), although H_2 fluxes as a whole will continue to increase exponentially because more earthquakes are being considered (Figure 6D).

Misunderstanding arises from this annual areal H_2 flux presented by Hirose et al. via Equation 3. In this equation, the integrand includes $S(M_w)$, the fault surface area, in the denominator; the areal H_2 flux returned by Equation 3 is therefore H_2 generated per unit area of fault surface, and not H_2 per unit area of Earth's surface, which is the unit by which values for H_2 generation by radiolysis and iron oxidation reactions within appropriate geological settings are commonly presented (e.g., Sleep & Zoback, 2007). Therefore, the flux obtained by Hirose et al. is applicable only to fault surfaces, and cannot be extrapolated to Earth's surface area as a whole. This confusion may have resulted in significant overestimation of mechanoradical H_2 generation; for example, colossal values of 3.4×10^{16} mol H_2 yr^{-1} (68,000 Mt H_2 yr^{-1}) (Parkes et al., 2019) and 235,000 Mt H_2 yr^{-1} (Zgonnik, 2020) are obtained by multiplying the reported areal flux of Hirose et al. (2011) (230 mol m^{-2} yr^{-1}) by the surface area of the continents (1.48×10^{14} m^2) and Earth (5.1×10^{14} m^2) respectively.

By resolving Equation 4 for earthquakes up to $M_w = 8$, we determine that H_2 generation by global seismicity up to $M_w = 8$ is 2×10^7 mol H_2 yr^{-1} (40 t H_2 yr^{-1}; Figure 6D). Our solution is three orders of magnitude lower than the mid-ocean ridge estimate returned by Worman et al. (2020) using the same expression and integration limits (~3×10^{10} mol H_2 yr^{-1}, or 0.06 Mt H_2 yr^{-1}). This is principally the consequence of a unit conversion error within Worman et al.'s calculations (S. Worman, pers. comms.); the minimum estimate for mechanoradical H_2 generation by global seismicity may therefore be significantly lower than previously determined. We highlight, however, that global mechanoradical H_2 fluxes, especially in comparison to other fluxes presented in this manuscript, are likely to be significantly uncertain. Our estimate, and those of prior studies, is highly dependent on Hirose et al.'s own experimental findings and their application of a global Gutenberg-Richter Law (Equation 5). Such a parameterisation will not account for H_2 generation by aseismic deformation (Ito et al., 1999). Furthermore, frictional work on faults may be lower, reducing overall H_2 generation (e.g., Copley, 2018). In spite of this, we note that H_2 concentrations in fault zones are independent of earthquake magnitude, as demonstrated by Equation 7 of Hirose et al. (2011), and are of the order of ~0.1 mM.

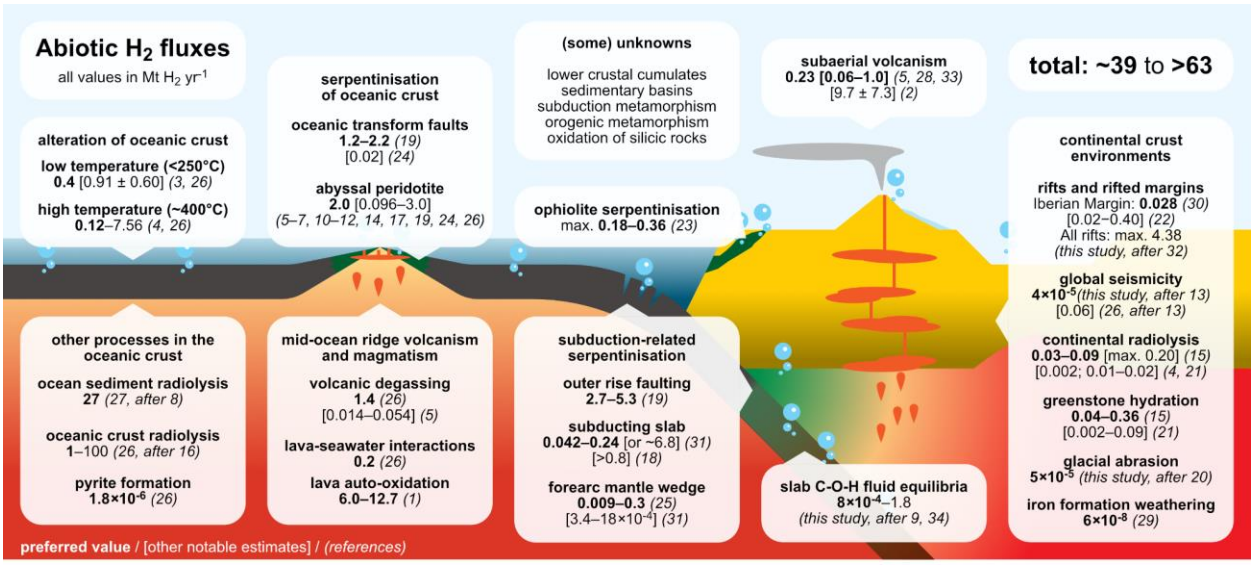

References

1. Holloway and O'Day, 2000, *Int. Geology Rev.*
2. Holland, 2002, *Geochim. Cosmochim. Acta*
3. Bach and Edwards, 2003, *Geochim. Cosmochim. Acta*
4. Lin et al., 2005, *Geochem. Geophys. Geosyst.*
5. Canfield et al., 2006, *Philos. Trans. R. Soc. B: Biol. Sci.*
6. Sleep and Bird, 2007, *Geobiology*
7. Emmanuel and Ague, 2007, *Geophys. Res. Lett.*
8. Blair et al., 2007, *Astrobiology*
9. Hacker, 2008, *Geochem. Geophys. Geosyst.*
10. Cannat et al., 2010, *Geophys. Monogr. Ser. 188*
11. Charlou et al., 2010, *Geophys. Monogr. Ser. 188*
12. Keir, 2010, *Geophys. Res. Lett.*
13. Hirose et al., 2011, *Geophys. Res. Lett.*
14. Kasting and Canfield, 2012, *Fundamentals of Geobiology*
15. Sherwood Lollar et al., 2014, *Nature*
16. Dzaugis et al., 2016, *Front. Microbiol.*
17. Worman et al., 2016, *Geophys. Res. Lett.*
18. Vitale Brovarone et al., 2017, *Nat. Commun.*
19. Rüpke and Hasenclever, 2017, *Geophys. Res. Lett.*
20. Macdonald et al., 2018, *Front. Earth. Sci.*
21. Warr et al., 2019, *Chem. Geol.*
22. Klein et al., 2020, *Elements*
23. Zgonnik, 2020, *Earth-Sci. Rev.*
24. Merdith et al. 2020, *Geochem. Geophys. Geosyst.*
25. Vitale Brovarone et al., 2020, *Nat. Commun.*
26. Worman et al., 2020, *Proceed. Natl. Acad. Sci.*
27. Sauvage et al., 2021, *Nat. Commun.*
28. Stolper et al., 2021, *Am. J. Sci.*
29. Malvoisin and Brunet, 2023, *Sci. Total Environ.*
30. Liu et al., 2023, *Geology*
31. Merdith et al., 2023, *Geochem. Geophys. Geosyst.*
32. Zwaan et al., 2023, *preprint*
33. Aiuppa and Moussallam, 2024, *C. R. Geosci.*
34. Boutier et al., 2024, *Comput. Geosci.*

Figure 7. Schematic figure summarising estimates of present-day geological fluxes within geological environments. All values given in Mt H_2 yr^{-1}. Where values are preferred, font weight is bold; other notable estimates are provided in the square brackets, with italicised numbers in curved brackets providing references.

6.6. Biological production rates of H_2

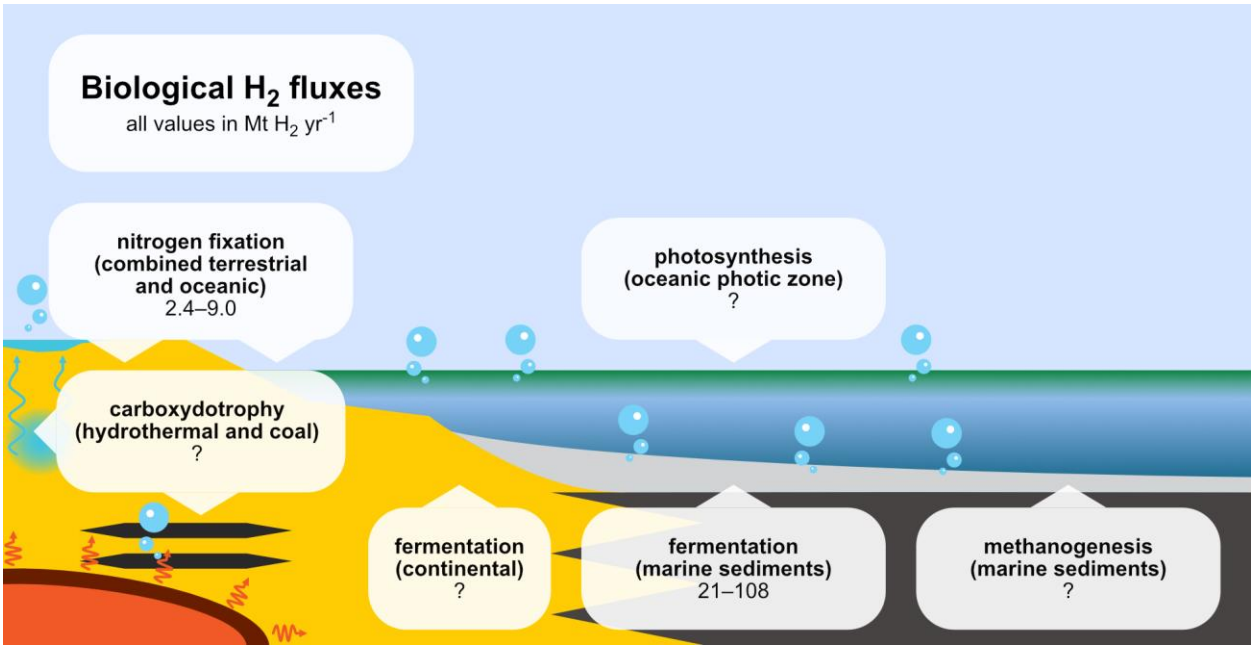

Figure 8. Fluxes of biological H_2 production in continental and oceanic environments.

While the global contribution of biology to H_2 biogeochemistry in the surface and near-surface of our planet might be important, estimates of biological H_2 fluxes, both concerning production (Section 3) and consumption (Section 7.4.1), are lacking, and for many ecosystems have never been attempted (Figure 8). For example, recent work shows that microorganisms present in soils and in the oceanic water column are capable of supplementing their energy needs using the H_2 present in trace amounts within atmospheric gases (Greening et al., 2014; Lappan et al., 2023). These recent studies suggest that the interactions of biology with H_2 reservoirs can be far more widespread than previously known, and the biological contribution to the global hydrogen cycle may have been severely underestimated. Among these interactions of biology with H_2, the biological production of H_2 remains the least constrained aspect of natural H_2 budgets.

Given the environmental distribution of H_2-producing metabolisms estimated from metagenomic studies, it is expected that biological H_2 production might be significant in a range of oxygen-poor ecosystems, such as subsurface marine sediments, sedimentary basins, anoxic aquatic environments, wetlands, and organic-rich anoxic sediments in general. Despite this, recent data suggests that the biological production of H_2 might be prevalent also in low-carbon, oligotrophic environments. Biological H_2 has also been reported from anoxic provinces in the igneous oceanic crust (Ivarsson et al., 2016). In addition, the supersaturation of H_2 in oceanic waters (Herr, 1984)

has been attributed entirely to biological production, based on isotopic evidence (Walter et al., 2016). Therefore, it is reasonable to expect that biological H_2 might be produced in a variety of other environments, although its contribution to global H_2 production remains to be assessed.

Microbial fermentation of organic carbon in anoxic environments is considered the largest contributor to biological H_2 production. Despite this, global estimates of H_2 production rates are lacking. Since a large portion of the H_2 produced by fermentations is converted to methane in anaerobic sediments and aquatic systems, it is theoretically possible to extrapolate H_2 production rates by fermentation from methane production rates. Using this approach, and considering a global aquatic ecosystem methane flux of 431 Mt CH_4 yr^{-1} (Rosentreter et al., 2021) with 10–50% of this methane deriving from hydrogenotrophic methanogenesis, H_2 production rates from fermentation in aquatic ecosystems can be estimated to be 21–108 Mt H_2 yr^{-1}.

Other metabolic pathways that produce H_2—such as nitrogen fixation, anaerobic carbon monoxide oxidation, and phosphite oxidation—are considered less important in terms of total H_2 production. For example, nitrogen fixation has been widely observed in microorganisms, although it has been less studied outside the rhizosphere. Evidence of nitrogen fixation has been reported in various subsurface environments, including sulphidic sediments, hydrothermal vents, and methane seeps. Despite its detection in these ecosystems, the true extent of nitrogen fixation remains uncertain, as are the related H_2 production rates. Current estimates suggest up to 2.4–9.0 Mt H_2 yr^{-1} (Conrad & Seiler, 1980; Greening & Grinter, 2022), although the majority of this H_2 is expected to be consumed before being released to the atmosphere (Q. Chen et al., 2015).

In spite of the widespread ability of microorganisms to produce H_2 in a variety of environmental settings, biological H_2 fluxes remain largely unconstrained (Figure 8). Indirect evidence, outlined above, suggests that microorganisms might be responsible for H_2 production rates comparable or higher than abiotic H_2 fluxes. However, the majority of the produced H_2 is expected to be consumed *in situ* by microorganisms capable of oxidising H_2 as an energy source (Section 7.5.1). Therefore, while production rates might be high, the global biological H_2 flux to the exosphere might be small. Extensive research will be required to truly constrain the role of biology in the biogeochemistry of hydrogen.

7. Subsurface migration of H_2

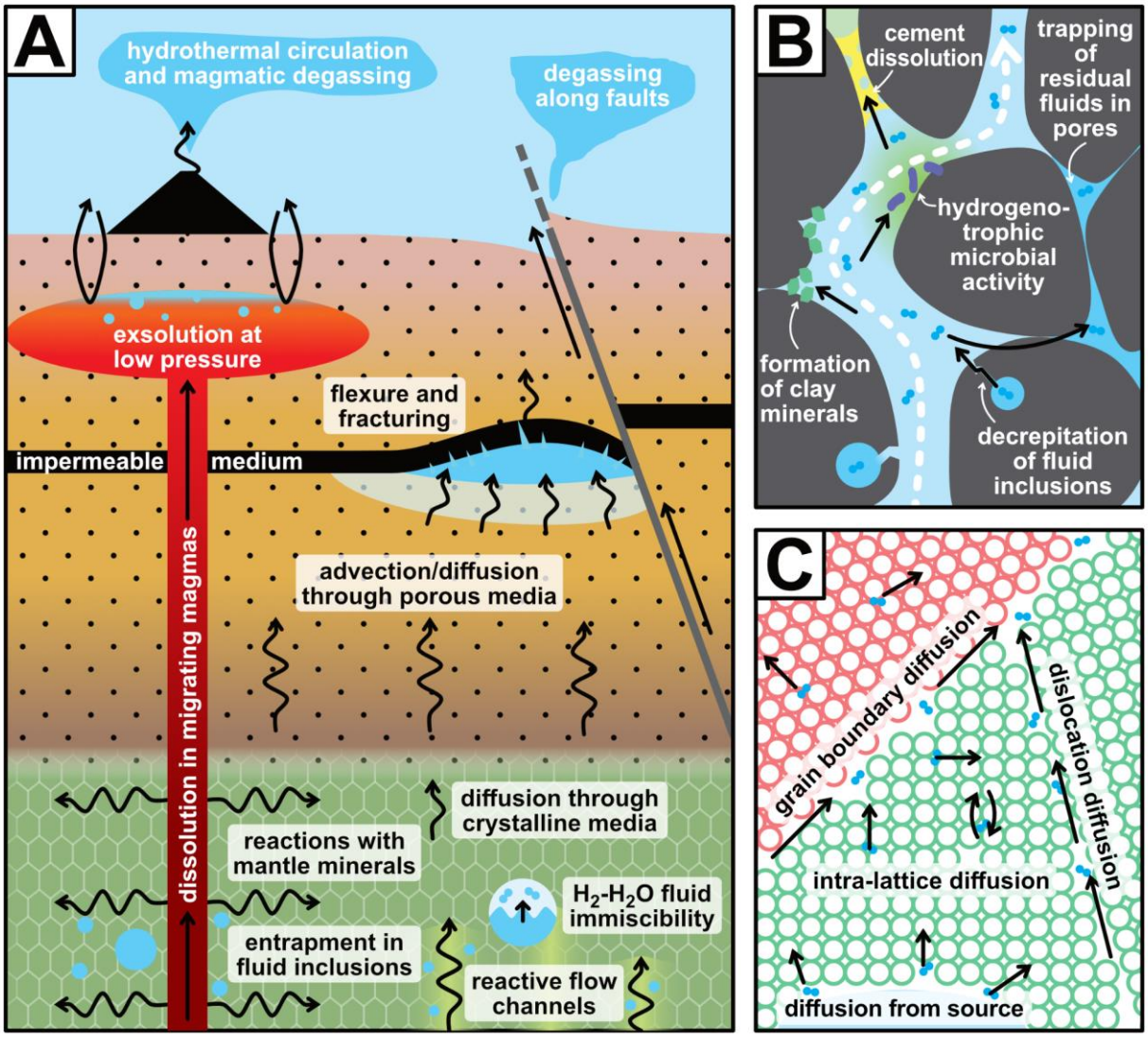

Figure 9. Schematic figure illustrating the processes that affect geological H_2 during its migration at different scales. A. Broad-scale processes (m to 10s km). B. Grain-scale processes (μm to cm). C. Lattice-scale processes (Å to nm). Black arrows broadly illustrate the direction of H_2 migration.

The subsurface migration and channelisation of H_2 are critical for its accumulation and availability as a source of energy both for microbial life and modern society. Furthermore, natural H_2 must be trapped in a manner similar to hydrocarbons in order to be economically beneficial to extract (Blay-Roger et al., 2024). In this section, we briefly summarise our current understanding on H_2 (molecular hydrogen) migration within the Earth's crust and upper mantle (Figure 9); for deep

hydrogen migration involving other forms of hydrogen (e.g., H_2O), see Mosenfelder et al., 2024; Novella et al., 2024 and references therein.

Once generated, geological H_2 migrates upwards towards the Earth's surface. Depending on the pressure-temperature conditions of formation, H_2 will either be a free gas phase, or will dissolve into an aqueous fluid phase, which will subsequently exsolve gaseous H_2 at lower pressures and temperatures (e.g., Lazar, 2020). The solubility of aqueous H_2 is a strong function of pressure, temperature, and fluid salinity (Bazarkina et al., 2020; Lopez-Lazaro et al., 2019).

Faults and fractures provide the principal avenue for abiotic H_2 escape in geologically active settings. For example, degassing of H_2, generated at depth from serpentinisation, is concentrated along thrust faults in the Pyrenees (Lefeuvre et al., 2021, 2022). Faults also provide a means of decrepitating H_2-hosting fluid inclusions in crystalline rocks and sediments; however decrepitation may also occur through a number of other mechanisms, such as solid state diffusion, strain deformation, surface erosion (Parnell & Blamey, 2017a).

7.1. Deep transport of H_2 through crystalline/impermeable media

Before H_2 can migrate through the Earth, it must escape its source region. Within the mantle and crystalline crustal basement, H_2 may be generated and entrapped within fluid inclusions (Q. Williams & Hemley, 2001), or be present within the structures of nominally anhydrous minerals such as olivine or pyroxene at a concentration of a few ppm (Figure 9C; Demouchy & Bolfan-Casanova, 2016; Moine et al., 2020; X. Yang et al., 2016). In such cases, it has been argued that intra-crystalline H_2, particularly contributing to CH_4 entrapped in fluid inclusions, may originate from diffusion into the crystalline lattice from the surrounding media (Hall & Bodnar, 1990). H_2 diffusion occurs through crystal lattice structures or along lattice defects and dislocations (Demouchy & Bolfan-Casanova, 2016). Based on molecular dynamics simulations, the diffusion of electrically neutral H_2 within the lattice of forsterite may occur at rates 1–4 orders of magnitude faster than that of H^+, whose diffusion through crystal lattices will be limited by electrostatic attraction with oxygen in mineral structures (H. Liu et al., 2024). However, such rates of diffusion (10^{-7}–10^{-10} m^2 s^{-1} at mantle temperatures) mean that diffusion is unlikely to be the principal means of large-scale H_2 transport within the mantle (H. Liu et al., 2024). Experimental investigations of H_2 diffusion through quartz (Hall & Sterner, 1995) and olivine (Mackwell & Kohlstedt, 1990) verify that diffusivity of H_2 in the mantle is low despite high temperatures and pressures; H_2 may

therefore be transported, along with other volatile species, principally through large-scale mantle convection and the movement of volatile-rich melts.

In the context of serpentinisation, H_2 escape is assisted through the increase in volume resulting from the production of serpentine from olivine. Serpentinisation is predicted to generate increased porosity as a result of fracturing opened by the stress of volume increase; the creation of a fracture mesh will facilitate the passage of water into the serpentinising region, while also removing H_2 from its source (Malvoisin et al., 2017; Yoshida et al., 2020). However, subsequent closure will result from the eventual filling of pore spaces and fractures by serpentine minerals, thereby limiting the accessibility of water into the serpentinising rock and routes permitting H_2 escape (L. Zhang et al., 2019).

In magmatic systems, H_2 is dissolved and transported within the silicate melt alongside other volatile elements (Hirschmann et al., 2012). The concentration of H_2 in silicate melts is dictated by the oxygen fugacity of the melt in addition to pressure and temperature (see Section 5.2), and H_2 has the potential to be the most mobile hydrogen component in reduced melts at magmatic temperatures (e.g., Zhang & Ni, 2010). However, H_2 may be removed from arc magmas as they ascend towards the surface by incorporation within orthopyroxene and other mantle minerals (Tollan & Hermann, 2019). At lower pressures and temperatures, H_2 solubility decreases, and exsolved H_2 will contribute towards a vapour cap above the magma. Like other volatiles, migration in the gas phase will depend on degassing through the surrounding media by faults and fractures, bubble rise, hydrothermal circulation, or eruption (e.g., Edmonds & Wallace, 2017; Edmonds & Woods, 2018).

In subduction zones, fluid flow from the devolatilising slab occurs up-dip along the subduction channel or within high-porosity channels into the mantle wedge, and is a complex interplay between fluid dynamics, rock dynamics (e.g., compaction pressures) and reactive transport driven by fluid-rock interactions (Beinlich et al., 2020; Gerya, 2022; Piccoli et al., 2021; Saffer & Tobin, 2011; C. R. Wilson et al., 2014). Shear zones also provide an avenue for H_2 migration and channelisation in high-pressure ultramafic domains (Boutier, Martinez, Sissmann, et al., 2024; Giuntoli et al., 2020). Aqueous H_2 will comprise an important component of these fluids, and will interact with the forearc mantle wedge (Vitale Brovarone et al., 2017, 2020), thereby contributing towards the H_2 which may be locked within mantle minerals. Fracturing, including processes induced by the accumulation of immiscible H_2 and companion CH_4 (Giuntoli et al., 2024; see

Section 7.1.1 and Section 7.3), can also provide avenues for H_2 to reach the Earth's surface from depth (Heinemann et al., 2021).

7.1.1. H_2 immiscibility in geological fluids

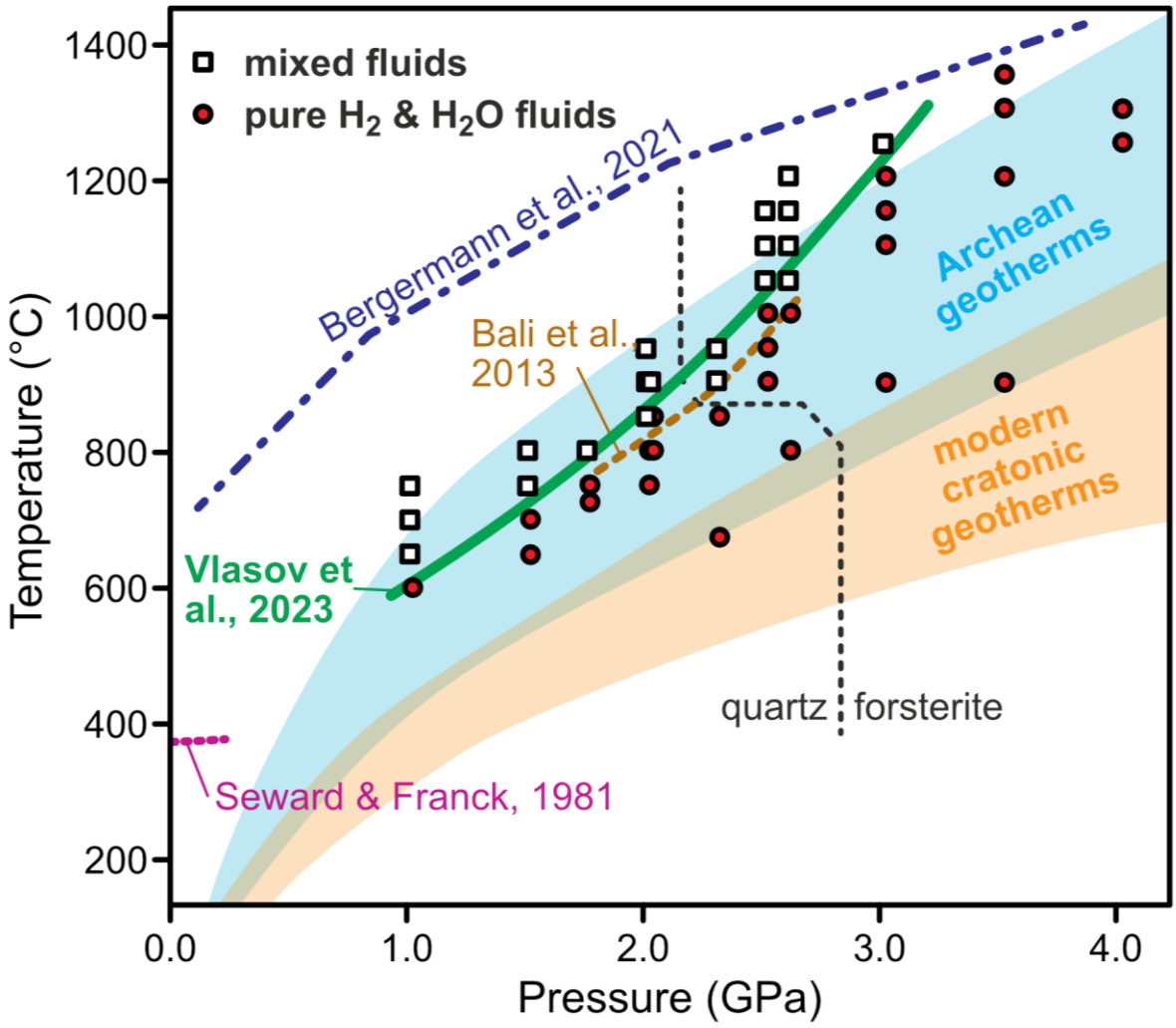

Figure 10: Critical curves and experimental data for H_2-H_2O miscibility, redrawn after Vlasov et al. (2023). Critical curves shown are Seward & Franck (1981) (purple dotted line), Bali et al. (2013) (brown dashed line), Bergermann et al. (2021) (blue dash-dotted line), and Vlasov et al. (2023) (bold solid green line). Experimental data (Bali et al., 2013; Vlasov et al., 2023) are plotted as white squares for single-phase mixed fluids and red circles for two-phase fluid inclusions (pure H_2 and/or H_2O). The grey thin dashed line separates experiments performed with quartz-hosted inclusions from those hosted in olivine in these two studies. Geotherms for modern and Archean

geotherms are redrawn after Hasterok & Chapman, (2011), Mareschal & Jaupart, (2006), and Rudnick & Nyblade (1999).

At high pressures, H_2 can be immiscible in water, with or without companion C-O-H molecules, as shown by laboratory experimental results, natural samples, and thermodynamic models (Bali et al., 2013; Giuntoli et al., 2024; J. Huang et al., 2024; Y. Li, 2017; Sverjensky et al., 2020; Vlasov et al., 2023; L. Zhang et al., 2024). The immiscibility of H_2 in aqueous fluids represents an important aspect of H_2 migration in the crust and mantle, with potential implications on global-scale geochemical processes. It was suggested that immiscible H_2-rich fluids migrate rapidly owing to their low density and low viscosity (Bali et al., 2013; Vlasov et al., 2023), although migration will depend on the lithological properties of the mantle. The decoupling of H_2 fluids from aqueous fluids and their preferential migration may promote extremely reducing environments incompatible with the redox state of a miscible H_2-bearing aqueous fluid (Bali et al., 2013). Additionally, considering H_2 escape in the early Earth (Catling et al., 2001), the fast and preferential migration of immiscible H_2 has been proposed as a possible mechanism for the early oxygenation of the Earth's upper mantle (Bali et al., 2013).

Figure 10 shows the results of experimental investigations on H_2 immiscibility in aqueous fluids (Bali et al., 2013; Vlasov et al., 2023), which demonstrate that H_2 immiscibility is possible at most early Earth and modern Earth geothermal conditions. Nevertheless, the identification of crustal and mantle rocks affected by flushing of immiscible H_2 fluids is still scarce. The reduction of carbonates in the ultramafic Lanzo Massif in the Italian Alps was ascribed to the infiltration of dry H_2 fluids resulting from serpentinisation processes (Vitale Brovarone et al., 2017). In the same locality, it was also shown that accumulation of immiscible H_2-CH_4 fluids promoted fluid overpressure and brittle fracturing at forearc depths within the Alpine subduction zone (Giuntoli et al., 2024).

7.2. Near-surface H_2 transport through porous media

Near the Earth's surface, H_2 will migrate in porous media by advection—driven by buoyancy or by pressure gradients—or by diffusion (Figure 9B; Hutchinson et al., 2024; Jackson et al., 2024). To assist in comprehending the movements and trapping of H_2 within shallow porous media, we can draw upon the extensive research performed to assess the feasibility of geological H_2 storage (for recent reviews, see Miocic et al., 2023; Perera, 2023). Within this context, H_2 is stored within geological structures and saline aquifers in a similar manner to hydrocarbons. However, the

physical properties of H_2, such as its small molecular size, low density, and low viscosity, make storage distinct, and perhaps difficult, relative to hydrocarbons (Muhammed et al., 2022; Y. Yang et al., 2024; Zivar et al., 2021). Nevertheless, important parallels can be drawn between the industrial storage of H_2 and natural H_2 behaviour in the Earth's subsurface during migration.

H_2 is efficient at migrating through porous media owing to its small molecular size; its vertical velocity through common sedimentary lithologies is twice that of methane and an order of magnitude greater than hydrocarbons (Lodhia & Clark, 2022). Migration of H_2 strongly depends on the physical and geometric properties of sedimentary lithologies that control permeability, such as rock porosity and tortuosity. Furthermore, the composition of sedimentary rocks governs any fluid-rock interactions that may occur, in turn affecting the geochemical evolution of the fluid during migration. Modelling the flow of H_2 within porous media therefore requires an understanding of how H_2 influences the dynamic interactions between rock and fluid (e.g., Hagemann et al., 2015), and how H_2 behaves in a multi-phase fluid (e.g., Bazarkina et al., 2020). Finally, temperature also is a strong control on the rate of H_2 diffusion through porous media (Y. Yang et al., 2024).

7.3. Mechanical consequences of H_2 migration and accumulation

The migration and accumulation of H_2 under structural or lithological seals may promote the weakening and cracking of overlying impermeable media (i.e., caprocks), facilitating its upward migration through the Earth (Giuntoli et al., 2024). The non-polar nature of H_2 limits its aqueous solubility, and H_2 will exsolve and contribute towards gas layers when trapped at low pressures (Heinemann et al., 2021). There remains little experimental data of H_2 breakthrough mechanisms under caprocks, although it has been suggested that fluid-rock interactions between fluids and caprocks are unlikely to result in substantial degradation (Kampman et al., 2016). Field evidence also suggests that the infiltration of H_2-rich fluids into undeformed domains may induce the localisation of ductile shear zones, which develop from microstructural changes resulting from fluid-rock dissolution-precipitation reactions (Giuntoli et al., 2020). Breakthrough mechanisms involving the build-up of pore-fluid pressure under caprocks, in a manner similar to that suggested above for crystalline lithologies in subduction settings (Giuntoli et al., 2024), may facilitate H_2 migration through caprock fractures. Diffusive losses of aqueous H_2 through caprocks are expected to be minimal, owing to the low solubility of H_2 in brines relative to hydrocarbons (Hemme & Van Berk, 2018; Jackson et al., 2024; Muhammed et al., 2022), but may be accelerated by an increase in pore fluid pressure resulting from its conversion into water (Hemme

& Van Berk, 2018). Diffusive loss of gaseous H_2 may be more probable (Perera, 2023), as is the loss of H_2 by reaction to form methane and water (Prinzhofer & Cacas-Stentz, 2023).

The mechanical effects of H_2-rock interactions are not limited to physical phenomena, but extend to a complex set of physico-chemical processes. Some of these processes are related to the effect of H_2 on the stability of rock-forming minerals and their consequent impact on rock mechanics. Although these phenomena are still little documented in the literature, a natural example is provided by the role of H_2 infiltration on carbonate breakdown, solid volume decrease, and strain localisation (Giuntoli et al., 2020; see also Galvez et al., 2013; Malvoisin et al., 2012; Peng et al., 2021 for other examples of similar reactions). H_2-mineral interactions also include a complex set of chemical-physical processes referred to as hydrogen embrittlement, which is the induction of cracking within material surfaces by hydrogen atoms (e.g., Dwivedi & Vishwakarma, 2018; Patanwar et al., 2024; Woodtli & Kieselbach, 2000). In this process, H_2 is adsorbed onto material surfaces to introduce hydrogen atoms into the structure of the material. By diffusion of hydrogen into the material in atomic/ionic form, the mechanical properties of the material, including tensile strength and fatigue strength, will be reduced, thereby making the material brittle and inducing weakness and fracturing. A related process in H_2-rich environments is that of hydrogen-assisted stress corrosion cracking: the formation and growth of cracks in a corrosive environment under tensile stress (e.g., Dilshan et al., 2024). In this process, bonds between atoms at the crack tip are broken as a result of electrochemical activity resulting from geochemical interactions (Tomkins et al., 1981). Hydrogen atoms may be liberated as a result of this electrochemical activity, thereby propagating crack advance; as a result, stress corrosion cracking is often driven by the process of hydrogen embrittlement.

At present, hydrogen embrittlement and stress corrosion cracking are best characterised for metals and polymers within hydrogen-rich environments, especially within industrial contexts (e.g., Dwivedi & Vishwakarma, 2018; Sun et al., 2025; Woodtli & Kieselbach, 2000). However high-H_2 environments in nature, such as accumulations under impermeable caprocks, are expected to be affected by processes of a similar nature (X. Chen et al., 2020). It has previously been suggested that H_2-related stress corrosion resulting from aseismic deformation may have nucleated earthquakes in Japan (Ito et al., 1999), and hydrogen embrittlement may have contributed towards the brittle failure of impermeable mechanically strong rocks (Giuntoli et al., 2024) in subduction zones. Further work will be necessary to capture the complete behaviour of H_2 on the long-term mechanical strength of silicates and other geological materials.

7.4. Migration and storage of H_2 within microcavities

Recent studies concerning our understanding of H_2 production at tectonic settings have increasingly demonstrated that microcavities and mineral fluid inclusions play a key role in the generation and migration of geological H_2 and other reduced fluid species. Furthermore, microcavities may store a significant proportion of these reduced fluids within Earth's near-surface (e.g., Andreani et al., 2023; Bourdet et al., 2023; Boutier et al., 2021; Giuntoli et al., 2024; Klein et al., 2019; Parnell & Blamey, 2017; Peng et al., 2021; Peverelli et al., 2024; Richard, 2017; Vitale Brovarone et al., 2017, 2020) and deeper (E. M. Smith et al., 2016, 2018).

H_2 formed through any of the aforementioned processes can be trapped in fluid inclusions during fluid migration (e.g., Bourdet et al., 2023; Giuntoli et al., 2024; Vitale Brovarone et al., 2017). Additionally, H_2 can be generated inside the fluid inclusions themselves through post-entrapment fluid-host interactions (e.g., Andreani et al., 2023; Boutier et al., 2021; Klein et al., 2019), fluid respeciation (Cesare, 1995), and/or the radiolytic decomposition of trapped aqueous fluids (e.g., Parnell & Blamey, 2017). H_2 may also enter pre-existing fluid inclusions through diffusion through its crystal host (e.g., Hall & Sterner, 1995; Mavrogenes & Bodnar, 1994).

However, despite the possibility for H_2 to diffuse into and out of fluid inclusions, there is ample evidence for the long-term preservation of H_2 in fluid inclusions over geological timescales and through long tectonic, magmatic, and sedimentary journeys. Parnell & Blamey (2017a) documented higher H_2 concentrations from fluid inclusions in Precambrian granitoids compared to Phanerozoic equivalents. Moreover, these authors found similar results in sedimentary rocks resulting from the erosion of Precambrian source rocks relative to Phanerozoic equivalents. An increasing number of studies have documented H_2 trapped during high-pressure metamorphism and preserved at the Earth's surface exhumed metamorphic complexes (Giuntoli et al., 2020, 2024; Peng et al., 2021; Vitale Brovarone et al., 2017, 2020), or even in ultradeep diamonds (E. M. Smith et al., 2016, 2018). The alteration of the inclusion-hosting rocks through hydrothermal, metamorphic, or mechanical processes may liberate this H_2 at multiple stages during the evolution of mantle and crustal rocks (F. Klein et al., 2019; Olivieri, 2025).

Estimating fluxes for these trapped fluids is challenging. Nevertheless, for abiotic CH_4 and associated H_2, it has been proposed that the amount of fluid inclusions passively transported by

tectonic processes is large enough to justify CH_4 venting at mid-ocean ridges (F. Klein et al., 2019).

7.5. Consumption during transport

H_2-bearing fluid migration is affected by fluid-rock reactions during transit (Figure 9). While framework minerals such as quartz and feldspar are comparatively inert, redox reactions with Fe^{3+} minerals and sulphates can consume H_2 from the migrating fluid. This in turn will affect the mechanical strength of the porous medium and the pH of the fluid, thereby driving further reaction (Truche et al., 2013). The dissolution of carbonate and sulphate cements by H_2-bearing fluids will increase porosity (Flesch et al., 2018), whereas the concurrent formation of clay minerals will decrease porosity (Z. Shi et al., 2020) and potentially adsorb up to 500 ppm H_2 (Truche et al., 2018). Reactions with graphitic carbon (Peña-Alvarez et al., 2021; Vitale Brovarone et al., 2017) and carbonate (Peng et al., 2021) will also remove H_2 from transiting fluids. Fluid-rock interactions in this regard therefore do not consistently increase or decrease porosity, but porosity changes will be strongly dependent on the chemical composition of both the fluid and the porous medium.

7.5.1. Biological consumption of H_2

The biological consumption of H_2 will affect the chemical and isotopic composition of transiting fluids in crystalline (Lima-Zaloumis et al., 2022) and porous media (Löffler et al., 2022). Microbial consumption of H_2 is a dominant mechanism of H_2 loss during underground trapping and storage, and sulphide or acetic acid formation by metabolic processes may accelerate the corrosive degradation of caprocks (Dopffel et al., 2021; Perera, 2023), although the overall consumption of H_2 will be limited by the availability of other chemical species required for microbial metabolic processes (Hemme & Van Berk, 2018). Microbiological processes will therefore affect the mineralogy, chemistry, and permeability of H_2-hosting media. To entirely avoid potential microbial consumption, H_2 fields under consideration for storage or extraction should have reservoir temperatures exceeding 122 °C (the upper limit for life; Merino et al., 2019); salinity and pH also affect the ability of deep microbial life to metabolise H_2, although their effect is not yet clear (Thaysen et al., 2021).

While the number of microbial metabolic pathways capable of producing H_2 is limited (Section 3), a large number of physiologically diverse microorganisms can utilise H_2 as a primary source of electrons for their redox reactions (Cascone et al., 2025). Due to its strong reducing capabilities, microorganisms can couple the biological oxidation of H_2 with a large number of electron

acceptors, including, but not limited to, oxygen, nitrate, nitrite, sulphate, elemental sulphur, and carbon dioxide. Additionally, microorganisms are capable of directly exchanging electrons with solid surfaces (L. Shi et al., 2016), interacting with a large number of minerals (Cosmidis & Benzerara, 2022; Ehrlich, 1996). Considering the large amount of redox couples it can create, and also considering that H_2 provides the highest amount of energy when compared to other electron donors (Cascone et al., 2025), H_2 oxidation is a key metabolism in numerous ecosystems, and it may constitute the main electron donor under certain conditions.

Biological H_2 oxidation is catalysed mainly by [NiFe]-hydrogenases. While these enzymes share a common origin for the catalytic site, they are phylogenetically diverse and vary considerably in size and complexity, and are capable of functioning under a wide range of H_2 concentrations (Greening et al., 2016). Recently, a large number of high affinity variants of [NiFe]-hydrogenases have been identified in microorganism-inhabited oxic ecosystems such as soils and the ocean water column. These enzymes are capable of efficiently acquiring electrons from the oxidation of the trace concentrations of H_2 present in atmospheric gases (Bay et al., 2021; Greening & Grinter, 2022; Lappan et al., 2023).

H_2 production and consumption in anoxic ecosystems are commonly coupled in space by microorganisms tightly sharing metabolic products. These interactions, termed syntrophic, are fundamental in several ecosystems, and are so strong that several syntrophic relationships in the past have been erroneously classified as a single species (e.g., Bryant et al., 1967). A typical example of these syntrophic interactions can be observed in marine sediments, where H_2 generated by bacterial fermentation of organic matter in sediment (see Section 3) is rapidly consumed by sulphate-reducing bacteria and methanogenic archaea (Adhikari et al., 2016; Megonigal et al., 2004; Morris et al., 2013), thereby restricting H_2 accumulation and fluxes to the seafloor.

H_2 plays a key role in a diverse range of ecosystems, but it is an essential electron donor for microbial communities present in geothermal and subsurface environments. The H_2 available for microbial oxidation at these sites has different origins depending on the geological settings, as discussed elsewhere in this manuscript. Regardless of its origin, H_2 represents a fundamental energy source for chemolithoautotrophic primary producers—microbes capable of producing biomass from inorganic carbon in the absence of light—and sustain complex microbial communities in the absence of photosynthetic primary producers. A well studied example is

represented by Subsurface Lithoautotrophic Microbial Ecosystems (SLiMEs) (Nealson et al., 2005). In SLiMEs, hydrogenotrophic microorganisms represent the base of the food web, and H_2 produced by oxidation of iron-rich rocks (Section 5.1) and/or radiolysis (Section 5.3) has been proposed as the main source sustaining these subsurface ecosystems (Sauvage et al., 2021). SLiMEs have been identified in a range of subsurface environments (Ranchou-Peyruse, 2024) including both continental and oceanic hydrothermal systems (Chapelle et al., 2002; Kelley et al., 2005; Takai et al., 2008), marine sediments (Vandieken et al., 2014), deep basaltic aquifers (Stevens & McKinley, 1995), and ophiolites (Rempfert et al., 2017).

Despite the importance of H_2 as an electron donor for microbial communities, global estimates for rates of the biological oxidation of H_2 are lacking. The data available show a high variability in oxidation rates within marine subsurface sediments (between 2×10^{-5} to 2×10^{-1} nmol H_2 d^{-1} on a per cell basis) and in clay rock formation (0.14–1.93 μmol d^{-1} per cm^3 of clay). H_2 consumption rates may be considerable in surface soils (~0.05 μmol d^{-1} per kg of soil), and possibly even higher deeper within the crust (Myagkiy et al., 2020). The only readily available data point is relative to the H_2 uptake by microbial communities in soil, estimated to be 60–70 Mt H_2 yr^{-1} (Greening & Grinter, 2022). Notably, estimates of global H_2 oxidation rates are missing for a number of diverse environments, such as water columns, marine sediments, geothermal, and subsurface environments. Lack of measurements can be partially attributed to the intrinsic difficulty of measuring microbial H_2 production and consumption at *in situ* relevant conditions for these ecosystems.

8. Implications for life in the Precambrian

The recent efforts at understanding natural H_2 generation in the modern Earth can be extrapolated to assess H_2 generation on early Earth. The production of abiotic H_2, especially from serpentinisation at mid-ocean ridges, has been considered a key energy source for early primitive hydrogenotrophic microbial life (e.g., Martin et al., 2008; Russell et al., 2010). In fact, H_2 oxidation is believed to be a metabolism that developed at the dawn of life itself (e.g., Weiss et al., 2016). However, geological processes and geochemical environments on early Earth differed significantly from the present day, necessitating a reevaluation of the circumstances in which early hydrogenotrophic microorganisms evolved and thrived. In this section we briefly summarise the key differences in H_2-generating processes between the Precambrian and the present day that may have contributed towards the emergence and development of the earliest life on Earth.

Mantle melting may have occurred at higher temperatures in the Precambrian relative to the present day (e.g., Grosch & Wilson, 2023; Sossi et al., 2016), resulting in the formation of high-Mg komatiitic magmas. Experiments (Lazar et al., 2012; Shibuya et al., 2015; Ueda et al., 2021; Yoshizaki et al., 2009), thermodynamic modelling (Leong et al., 2021), and geochemical analyses (Tamblyn & Hermann, 2023) suggest that the serpentinisation of Archean komatiites generated significantly greater quantities of H_2 relative to present-day basalts (>315 mmol H_2 per kg komatiite versus 50 mmol H_2 per kg basalt). The serpentinisation of komatiites could have therefore contributed significantly to H_2 generation at/near mid-ocean ridge environments, with possible fluxes of the order of ~5×10^{12} mol H_2 yr^{-1} (~10 Mt H_2 yr^{-1}; Kasting, 2013) and ~2.59×10^{12} mol H_2 yr^{-1} (~5.2 Mt H_2 yr^{-1}; Ueda et al., 2021); for comparison, the H_2 generated by serpentinisation of abyssal peridotite at present-day mid-ocean ridges is ~3 Mt H_2 yr^{-1} (Section 6.1; Worman et al., 2020). However, such large H_2 fluxes may have been affected by the partitioning of ferrous iron directly into carbonates during low-temperature serpentinisation, which limits its oxidation in komatiites (Ueda et al., 2021). The partitioning of komatiitic aluminium also affects H_2 generation from komatiite serpentinisation by favouring Fe^{2+}-bearing smectite formation instead of the formation of Fe^{3+}-bearing magnetite (Shibuya et al., 2015; Ueda et al., 2021).

Ocean water chemistry also differed on early Earth (e.g., Albarede et al., 2020). For example, sulphate concentrations were believed to be significantly lower in reduced Archean oceans (e.g., Anbar & Knoll, 2002; Canfield, 1998; Hurtgen et al., 2002). As Fe^{2+} solubility is strongly dependent on oceanic sulphate concentrations, Fe^{2+} fluxes from Precambrian mid-ocean ridge vents were therefore expected to be higher than the present-day (Kump & Seyfried, 2005), possessing the reducing power to generate H_2 from seawater (Sleep & Bird, 2007). Furthermore, prior to the evolution of silica-secreting organisms such as sponges and radiolaria, concentrations of aqueous SiO_2 in ocean water would have been higher in the Precambrian than the present-day. The low-temperature (<200 °C) oxidation of Fe^{2+} in oceanic lithosphere may have been restricted by elevated aqueous SiO_2 concentrations, which limits the oxidation and uptake of Fe^{3+} in serpentine minerals in lieu of Si (Section 5.1.1; Tutolo et al., 2020). This could therefore imply that H_2 generation at ridge centres and sites of komatiite formation in the Archean was significantly higher than the present day, whereas off-axis H_2 generation was lower.

During periods of global glaciation in the Neoproterozoic—'Snowball Earth' events—subglacial microbial life on the continents may have been sustained through the abiotic generation of H_2 (Parnell & McMahon, 2016). In particular, radiolysis (Sherwood Lollar et al., 2014) and rock

commutation by glacial erosion (Macdonald et al., 2018; Telling et al., 2015) have been emphasised as key H_2-generating processes that can sustain subglacial life. The precipitation of Precambrian BIFs, the product of oxygenation events in otherwise anoxic ocean environments, would have resulted from limited ocean-atmosphere exchange during these periods of global glaciation (Ilyin, 2009), and also more generally before the oxygenation of Earth's surface at 2.4–2.0 Ga (e.g., Klein, 2005). Although such formations are rare on present-day Earth, the oxidation of siderite and magnetite within BIFs (Section 6.4.5; Geymond et al., 2022; Malvoisin & Brunet, 2023) during a timeframe when they were more widespread could provide a key source of H_2 for Precambrian microbial life.

9. Summary and conclusions

The abiotic fluxes in this review are summarised in Figure 7 and Table 2. By combining the reported ranges in the literature, we evaluate abiotic H_2 fluxes at geological settings as ~39 to >63 Mt H_2 yr^{-1}. This estimate exceeds the 23 ± 8 Mt H_2 yr^{-1} estimate of Zgonnik (2020), and our upper bound of 63 Mt H_2 yr^{-1} is more than double the equivalent of Zgonnik. This is a result of recent developments in quantifying new environments of H_2 formation that are not considered by Zgonnik, such as subduction zones (e.g., Merdith et al., 2023; Vitale Brovarone et al., 2017, 2020) and continental rifts (Z. Liu et al., 2023; Zwaan et al., 2025), and in particular oceanic radiolysis (Sauvage et al., 2021; Worman et al., 2020). At the present day, it is estimated that subduction of oceanic lithosphere contributes 1,000–2,000 Mt H_2O yr^{-1} (Faccenda, 2014; van Keken et al., 2011). Our H_2 fluxes translate to an equivalent output of 351–567< Mt H_2O yr^{-1}, which is equivalent to 18–57< % of the annual flux of hydrogen subducted back into the mantle in the form of water.

Significant uncertainties, often ranging several orders of magnitude, remain in quantifying the fluxes of H_2 at these different settings, for example, the abiotic H_2 generated in subduction zone settings from serpentinisation and other redox reactions, including graphite-saturated fluid equilibria (Section 6.2). This is a by-product of the approaches taken to determine fluxes at individual settings, which often rely on extrapolation from laboratory experiments, field observations at specific sites, and numerical models based on the observations from the former two approaches. Further uncertainty arises from limited observation periods of H_2 fluxing, which may fluctuate substantially with time at some localities (I. Moretti, Prinzhofer, et al., 2021). There are also additional implicit environments where abiotic H_2 can be generated which are not discussed in detail within this review or others, principally because these sources have yet to be characterised, for example, fluxes of H_2 resulting from processes during present-day orogenesis.

The total flux presented here is therefore likely to represent a minimum value, which will only increase with progressive research into natural H_2 generation—a sentiment we share with Ellis & Gelman (2024). We anticipate that the resolution of abiotic H_2 fluxes will improve substantially in the near future, as more and more interest is garnered in the exploration and exploitation of natural H_2 as an anthropogenic energy carrier (Blay-Roger et al., 2024). Geochemical datasets on tracers such as H_2 isotopes (Section 1.1; e.g., Lin et al., 2005; Milkov, 2022)—still scarce in the literature—or coupled H_2-noble gas data, will likely improve our resolution not only on the fluxes, but also on the different origins of H_2 in geobiological fluids. Recent developments such as H_2 clumped isotopes (Mangenot et al., 2023) may potentially provide new avenues to resolve pending questions on the origin of H_2 in the crust.

In comparison to our abiotic H_2 range of 39–63< Mt H_2 yr^{-1}, the H_2 released into the atmosphere through industrial processes is of a similar magnitude, with typical estimates of ~15 Mt H_2 yr^{-1} (Constant et al., 2009; Ehhalt & Rohrer, 2009; Patterson et al., 2020). When included with total non-abiotic fluxes of H_2 into the atmosphere (77.3 ± 13.2 Mt H_2 yr^{-1}, including both biogenic and anthropogenic sources) (Patterson et al., 2020; Pieterse et al., 2011), our range suggests that a significant proportion (30–50%) of exospheric H_2 fluxes may of abiotic natural origin. It is therefore clear that abiotic H_2, regardless of our present resolution of its fluxes, is an important component of the present-day reduced hydrogen cycle. By comparison, biological H_2 remains largely unconstrained in most ecosystems, and both the biological contribution to the production of H_2 and consumption of abiotic H_2 remains to be assessed.

Finally, we make note that our global assessed fluxes do not indicate the presence of H_2 accumulations already present within the Earth, instead highlighting settings where high concentrations of H_2 are likely to be identified. The natural world may host 10^3 to 10^{10} Mt of underground natural H_2 resources produced over millions or billions of years, and the extraction of even a small portion of this mass, if confirmed, would be sufficient to alleviate present-day H_2 industrial demands (Ellis & Gelman, 2024). Furthermore, our H_2 fluxes provide no indication as to whether such accumulations could be considered renewable from an energy point of view (i.e., in that H_2 may be replenished by natural processes at least as quickly as it is consumed), especially if H_2-generating processes are stimulated, e.g., by water injection (Osselin et al., 2022). Whether natural H_2 production is potentially rapid enough to fulfil renewable resource criteria and to meet future extraction rates remains an open question, and future studies must consider the

concentrations, production rates, and timescales required for industrially viable H_2 accumulations to arise.

In this review, we have highlighted the importance of abiotic H_2 as a reducing agent, as an energy source for primitive microbial life at the present day and in the geological past, and as a clean energy carrier. With the recent discovery of a liquid layer of water in the Martian crust (Wright et al., 2024), we emphasise that the abiotic H_2-forming processes we have discussed in this manuscript could therefore have the potential to possibly sustain a Martian deep biosphere parallel to that which we observe on Earth, with exciting implications for life elsewhere in the universe. The identification and characterisation of abiotic H_2 is therefore a vital component in a multitude of disciplines.

Acknowledgements

This work is part of a project that has received funding from the European Research Council (ERC) under the European Union's Horizon 2020 research and innovation program to AVB (Grant No. 864045; DeepSeep) and DG (Grant No. 948972; COEVOLVE). A MUR FARE grant (Grant No. R20ZIYMPAR; DRYNK) to AVB and MUR PRIN2022 grant (Grant No. 20224YR3AZ; HYDECARB) to AVB and DG are also acknowledged.

Figure 3 is created using the Thermotopes-COH software (Boutier, Martinez, Daniel, et al., 2024) and the *matplotlib* Python 3 library (Hunter, 2007; The Matplotlib Development Team, 2024). Figure 4 is created with QGIS v3.38.3 (QGIS Association, 2024), Crameri scientific colormaps v8.0.1 (Crameri, 2023; Crameri et al., 2020), and GIS datasets graciously provided by A. Merdith and S. Zahirovic. The datafiles used to perform the calculations exhibited in Section 6.5 and Figure 6 are available online in a Zenodo data repository in both Excel and Jupyter Notebook (Python 3) format (doi.org/10.5281/zenodo.14834771), and we thank A. Copley, T. Hirose, S. Worman, and M.-A. Filip for providing assistance with these calculations. Finally, we acknowledge the extensive discussions with the participants of the 5th SerpentineDays conference in Granada (September 2024) that greatly motivated and benefitted this manuscript.

References

Abers, G. A., van Keken, P. E., & Hacker, B. R. (2017). The cold and relatively dry nature of mantle forearcs in subduction zones. *Nature Geoscience*, *10*(5), 333–337. https://doi.org/10.1038/ngeo2922

Abrajano, T. A., Sturchio, N. C., Bohlke, J. K., Lyon, G. L., Poreda, R. J., & Stevens, C. M. (1988). Methane-hydrogen gas seeps, Zambales Ophiolite, Philippines: Deep or shallow origin? *Chemical Geology*, *71*(1), 211–222. https://doi.org/10.1016/0009-2541(88)90116-7

Adhikari, R. R., Glombitza, C., Nickel, J. C., Anderson, C. H., Dunlea, A. G., Spivack, A. J., Murray, R. W., D'Hondt, S., & Kallmeyer, J. (2016). Hydrogen Utilization Potential in Subsurface Sediments. *Frontiers in Microbiology*, *7*. https://doi.org/10.3389/fmicb.2016.00008

Aiuppa, A., Fischer, T. P., Plank, T., Robidoux, P., & Di Napoli, R. (2017). Along-arc, inter-arc and arc-to-arc variations in volcanic gas CO_2/S_T ratios reveal dual source of carbon in arc volcanism. *Earth-Science Reviews*, *168*, 24–47. https://doi.org/10.1016/j.earscirev.2017.03.005

Aiuppa, A., & Moussallam, Y. (2024). Hydrogen and hydrogen sulphide in volcanic gases: Abundance, processes, and atmospheric fluxes. *Comptes Rendus. Géoscience*, *356*(S1), 1–23. https://doi.org/10.5802/crgeos.235

Aiuppa, A., Shinohara, H., Tamburello, G., Giudice, G., Liuzzo, M., & Moretti, R. (2011). Hydrogen in the gas plume of an open-vent volcano, Mount Etna, Italy. *Journal of Geophysical Research: Solid Earth*, *116*(B10). https://doi.org/10.1029/2011JB008461

Albarede, F., Thibon, F., Blichert-Toft, J., & Tsikos, H. (2020). Chemical archeoceanography. *Chemical Geology*, *548*, 119625. https://doi.org/10.1016/j.chemgeo.2020.119625

Albers, E., Bach, W., Klein, F., Menzies, C. D., Lucassen, F., & Teagle, D. A. H. (2019). Fluid–rock interactions in the shallow Mariana forearc: Carbon cycling and redox conditions. *Solid Earth*, *10*(3), 907–930. https://doi.org/10.5194/se-10-907-2019

Albers, E., Bach, W., Pérez-Gussinyé, M., McCammon, C., & Frederichs, T. (2021). Serpentinization-Driven H_2 Production From Continental Break-Up to Mid-Ocean Ridge Spreading: Unexpected High Rates at the West Iberia Margin. *Frontiers in Earth Science*, *9*. https://doi.org/10.3389/feart.2021.673063

Alexander, C. M. O., Bowden, R., Fogel, M. L., Howard, K. T., Herd, C. D. K., & Nittler, L. R. (2012). The Provenances of Asteroids, and Their Contributions to the Volatile Inventories of the Terrestrial Planets. *Science*, *337*(6095), 721–723. https://doi.org/10.1126/science.1223474

Alt, J. C. (2003). Hydrothermal fluxes at mid-ocean ridges and on ridge flanks. *Comptes Rendus Geoscience*, *335*(10), 853–864. https://doi.org/10.1016/j.crte.2003.02.001

Andreani, M., Montagnac, G., Fellah, C., Hao, J., Vandier, F., Daniel, I., Pisapia, C., Galipaud, J., Lilley, M. D., Früh Green, G. L., Borensztajn, S., & Ménez, B. (2023). The rocky road to organics needs drying. *Nature Communications*, *14*(1), Article 1. https://doi.org/10.1038/s41467-023-36038-6

Andreani, M., Muñoz, M., Marcaillou, C., & Delacour, A. (2013). µXANES study of iron redox state in serpentine during oceanic serpentinization. *Lithos*, *178*, 70–83. https://doi.org/10.1016/j.lithos.2013.04.008

Arai, T., Okusawa, T., & Tsukahara, H. (2001). Behavior of gases in the Nojima Fault Zone revealed from the chemical composition and carbon isotope ratio of gases extracted from DPRI 1800 m drill core. *Island Arc*, *10*(3–4), 430–438. https://doi.org/10.1111/j.1440-1738.2001.00341.x

Arrouvel, C., & Prinzhofer, A. (2021). Genesis of natural hydrogen: New insights from thermodynamic simulations. *International Journal of Hydrogen Energy*, *46*(36), 18780–18794. https://doi.org/10.1016/j.ijhydene.2021.03.057

Bach, W., & Edwards, K. J. (2003). Iron and sulfide oxidation within the basaltic ocean crust: Implications for chemolithoautotrophic microbial biomass production. *Geochimica et Cosmochimica Acta*, *67*(20), 3871–3887. https://doi.org/10.1016/S0016-7037(03)00304-1

Bach, W., Paulick, H., Garrido, C. J., Ildefonse, B., Meurer, W. P., & Humphris, S. E. (2006). Unraveling the sequence of serpentinization reactions: Petrography, mineral chemistry, and petrophysics of serpentinites from MAR 15°N (ODP Leg 209, Site 1274). *Geophysical Research Letters*, *33*(13). https://doi.org/10.1029/2006GL025681

Bachaud, P., Meiller, C., Brosse, E., Durand, I., & Beaumont, V. (2017). Modeling of Hydrogen Genesis in Ophiolite Massif. *Procedia Earth and Planetary Science*, *17*, 265–268. https://doi.org/10.1016/j.proeps.2016.12.051

Baciu, C., & Etiope, G. (2024). A direct observation of a hydrogen-rich pressurized reservoir within an ophiolite (Tișovița, Romania). *International Journal of Hydrogen Energy*, *73*, 402–406. https://doi.org/10.1016/j.ijhydene.2024.06.065

Bali, E., Audétat, A., & Keppler, H. (2013). Water and hydrogen are immiscible in Earth's mantle. *Nature*, *495*(7440), 220–222. https://doi.org/10.1038/nature11908

Barbier, S., Huang, F., Andreani, M., Tao, R., Hao, J., Eleish, A., Prabhu, A., Minhas, O., Fontaine, K., Fox, P., & Daniel, I. (2020). A Review of H_2, CH_4, and Hydrocarbon Formation in

Experimental Serpentinization Using Network Analysis. *Frontiers in Earth Science*, *8*. https://www.frontiersin.org/articles/10.3389/feart.2020.00209

Bay, S. K., Dong, X., Bradley, J. A., Leung, P. M., Grinter, R., Jirapanjawat, T., Arndt, S. K., Cook, P. L. M., LaRowe, D. E., Nauer, P. A., Chiri, E., & Greening, C. (2021). Trace gas oxidizers are widespread and active members of soil microbial communities. *Nature Microbiology*, *6*(2), 246–256. https://doi.org/10.1038/s41564-020-00811-w

Bayrakci, G., Minshull, T. A., Sawyer, D. S., Reston, T. J., Klaeschen, D., Papenberg, C., Ranero, C., Bull, J. M., Davy, R. G., Shillington, D. J., Perez-Gussinye, M., & Morgan, J. K. (2016). Fault-controlled hydration of the upper mantle during continental rifting. *Nature Geoscience*, *9*(5), 384–388. https://doi.org/10.1038/ngeo2671

Bazarkina, E. F., Chou, I.-M., Goncharov, A. F., & Akinfiev, N. N. (2020). The Behavior of H_2 in Aqueous Fluids under High Temperature and Pressure. *Elements*, *16*(1), 33–38. https://doi.org/10.2138/gselements.16.1.33

Beinlich, A., John, T., Vrijmoed, J. C., Tominaga, M., Magna, T., & Podladchikov, Y. Y. (2020). Instantaneous rock transformations in the deep crust driven by reactive fluid flow. *Nature Geoscience*, *13*(4), 307–311. https://doi.org/10.1038/s41561-020-0554-9

Bergermann, A., French, M., & Redmer, R. (2021). Gibbs-ensemble Monte Carlo simulation of H_2 –H_2 O mixtures. *Physical Chemistry Chemical Physics*, *23*(22), 12637–12643. https://doi.org/10.1039/D1CP00515D

Berman, R. G. (1988). Internally-Consistent Thermodynamic Data for Minerals in the System Na_2O-K_2O-CaO-MgO-FeO-Fe_2O_3-Al_2O_3-SiO_2-TiO_2-H_2O-CO_2. *Journal of Petrology*, *29*(2), 445–522. https://doi.org/10.1093/petrology/29.2.445

Beyssac, O., Rouzaud, J.-N., Goffé, B., Brunet, F., & Chopin, C. (2002). Graphitization in a high-pressure, low-temperature metamorphic gradient: A Raman microspectroscopy and HRTEM study. *Contributions to Mineralogy and Petrology*, *143*(1), 19–31. https://doi.org/10.1007/s00410-001-0324-7

Bird, P. (2003). An updated digital model of plate boundaries. *Geochemistry, Geophysics, Geosystems*, *4*(3). https://doi.org/10.1029/2001GC000252

Blair, C. C., D'Hondt, S., Spivack, A. J., & Kingsley, R. H. (2007). Radiolytic Hydrogen and Microbial Respiration in Subsurface Sediments. *Astrobiology*, *7*(6), 951–970. https://doi.org/10.1089/ast.2007.0150

Blakely, R. J., Brocher, T. M., & Wells, R. E. (2005). Subduction-zone magnetic anomalies and implications for hydrated forearc mantle. *Geology*, *33*(6), 445. https://doi.org/10.1130/G21447.1

Blay-Roger, R., Bach, W., Bobadilla, L. F., Reina, T. R., Odriozola, J. A., Amils, R., & Blay, V. (2024). Natural hydrogen in the energy transition: Fundamentals, promise, and enigmas. *Renewable and Sustainable Energy Reviews*, *189*, 113888. https://doi.org/10.1016/j.rser.2023.113888

Bonatti, E., & Michael, P. J. (1989). Mantle peridotites from continental rifts to ocean basins to subduction zones. *Earth and Planetary Science Letters*, *91*(3), 297–311. https://doi.org/10.1016/0012-821X(89)90005-8

Boreham, C. J., & Davies, J. B. (2020). Carbon and hydrogen isotopes of the wet gases produced by gamma-ray-induced polymerisation of methane: Insights into radiogenic mechanism and natural gas formation. *Radiation Physics and Chemistry*, *168*, 108546. https://doi.org/10.1016/j.radphyschem.2019.108546

Boreham, C. J., Edwards, D. S., Czado, K., Rollet, N., Wang, L., Van Der Wielen, S., Champion, D., Blewett, R., Feitz, A., & Henson, P. A. (2021). Hydrogen in Australian natural gas: Occurrences, sources and resources. *The APPEA Journal*, *61*(1), 163. https://doi.org/10.1071/AJ20044

Boreham, C. J., Edwards, D. S., Feitz, A. J., Murray, A. P., Mahlstedt, N., & Horsfield, B. (2023). Modelling of hydrogen gas generation from overmature organic matter in the Cooper Basin, Australia. *The APPEA Journal*, *63*(2), S351–S356. https://doi.org/10.1071/AJ22084

Boreham, C. J., Sohn, J. H., Cox, N., Williams, J., Hong, Z., & Kendrick, M. A. (2021). Hydrogen and hydrocarbons associated with the Neoarchean Frog's Leg Gold Camp, Yilgarn Craton, Western Australia. *Chemical Geology*, *575*, 120098. https://doi.org/10.1016/j.chemgeo.2021.120098

Boschi, C., Bonatti, E., Ligi, M., Brunelli, D., Cipriani, A., Dallai, L., D'Orazio, M., Früh-Green, G. L., Tonarini, S., Barnes, J. D., & Bedini, R. M. (2013). Serpentinization of mantle peridotites along an uplifted lithospheric section, Mid Atlantic Ridge at 11° N. *Lithos*, *178*, 3–23. https://doi.org/10.1016/j.lithos.2013.06.003

Bostock, M. G., Hyndman, R. D., Rondenay, S., & Peacock, S. M. (2002). An inverted continental Moho and serpentinization of the forearc mantle. *Nature*, *417*(6888), 536–538. https://doi.org/10.1038/417536a

Bouquet, A., Glein, C. R., Wyrick, D., & Waite, J. H. (2017). Alternative Energy: Production of H_2 by Radiolysis of Water in the Rocky Cores of Icy Bodies. *The Astrophysical Journal Letters*, *840*(1), L8. https://doi.org/10.3847/2041-8213/aa6d56

Bourdet, J., Piane, C. D., Wilske, C., Mallants, D., Suckow, A., Questiaux, D., Gerber, C., Crane,

P., Deslandes, A., Martin, L., & Aleshin, M. (2023). Natural hydrogen in low temperature geofluids in a Precambrian granite, South Australia. Implications for hydrogen generation and movement in the upper crust. *Chemical Geology*, *638*, 121698. https://doi.org/10.1016/j.chemgeo.2023.121698

Boutier, A., Martinez, I., Daniel, I., Tumiati, S., Siron, G., & Vitale Brovarone, A. (2024). Thermotopes-COH—A software for carbon isotope modeling and speciation of COH fluids. *Computers & Geosciences*, 105533. https://doi.org/10.1016/j.cageo.2024.105533

Boutier, A., Martinez, I., Sissmann, O., Agostini, S., Daniel, I., Van Baalen, M., Mana, S., & Vitale Brovarone, A. (2024). Complexity of graphite formation in response to metamorphic methane generation and transformation in an orogenic ultramafic body. *Geochimica et Cosmochimica Acta*, *364*, 166–183. https://doi.org/10.1016/j.gca.2023.10.028

Boutier, A., Vitale Brovarone, A., Martinez, I., Sissmann, O., & Mana, S. (2021). High-pressure serpentinization and abiotic methane formation in metaperidotite from the Appalachian subduction, northern Vermont. *Lithos*, *396–397*, 106190. https://doi.org/10.1016/j.lithos.2021.106190

Broadley, M. W., Bekaert, D. V., Piani, L., Füri, E., & Marty, B. (2022). Origin of life-forming volatile elements in the inner Solar System. *Nature*, *611*(7935), 245–255. https://doi.org/10.1038/s41586-022-05276-x

Brune, S., Kolawole, F., Olive, J.-A., Stamps, D. S., Buck, W. R., Buiter, S. J. H., Furman, T., & Shillington, D. J. (2023). Geodynamics of continental rift initiation and evolution. *Nature Reviews Earth & Environment*, 1–19. https://doi.org/10.1038/s43017-023-00391-3

Brune, S., Williams, S. E., & Müller, R. D. (2017). Potential links between continental rifting, CO_2 degassing and climate change through time. *Nature Geoscience*, *10*(12), 941–946. https://doi.org/10.1038/s41561-017-0003-6

Bryant, M. P., Wolin, E. A., Wolin, M. J., & Wolfe, R. S. (1967). *Methanobacillus omelianskii*, a symbiotic association of two species of bacteria. *Archiv Für Mikrobiologie*, *59*(1), 20–31. https://doi.org/10.1007/BF00406313

Bryce, C., Blackwell, N., Schmidt, C., Otte, J., Huang, Y.-M., Kleindienst, S., Tomaszewski, E., Schad, M., Warter, V., Peng, C., Byrne, J. M., & Kappler, A. (2018). Microbial anaerobic Fe(II) oxidation – Ecology, mechanisms and environmental implications. *Environmental Microbiology*, *20*(10), 3462–3483. https://doi.org/10.1111/1462-2920.14328

Buck, E. C., Wittman, R. S., Skomurski, F. N., Cantrell, K. J., McNamara, B. K., & Soderquist, C. Z. (2012). *Radiolysis Process Model* (PNNL-21554). Pacific Northwest National Lab. (PNNL), Richland, WA (United States). https://doi.org/10.2172/1069211

Burgisser, A., Alletti, M., & Scaillet, B. (2015). Simulating the behavior of volatiles belonging to the C–O–H–S system in silicate melts under magmatic conditions with the software D-Compress. *Computers & Geosciences*, *79*, 1–14. https://doi.org/10.1016/j.cageo.2015.03.002

Burgisser, A., & Scaillet, B. (2007). Redox evolution of a degassing magma rising to the surface. *Nature*, *445*(7124), 194–197. https://doi.org/10.1038/nature05509

Burton, M. R., Sawyer, G. M., & Granieri, D. (2013). Deep Carbon Emissions from Volcanoes. *Reviews in Mineralogy and Geochemistry*, *75*(1), 323–354. https://doi.org/10.2138/rmg.2013.75.11

Buseck, P. R., & Beyssac, O. (2014). From Organic Matter to Graphite: Graphitization. *Elements*, *10*(6), 421–426. https://doi.org/10.2113/gselements.10.6.421

Campbell, B. J., Li, C., Sessions, A. L., & Valentine, D. L. (2009). Hydrogen isotopic fractionation in lipid biosynthesis by H_2-consuming *Desulfobacterium autotrophicum*. *Geochimica et Cosmochimica Acta*, *73*(10), 2744–2757. https://doi.org/10.1016/j.gca.2009.02.034

Campbell, J. (1978). Pyrolysis of Subbituminous Coal in Relation to In-Situ Gasification. *Fuel*, *57*, 217–224. https://doi.org/10.1016/0016-2361(78)90119-9

Canfield, D. E., Rosing, M. T., & Bjerrum, C. (2006). Early anaerobic metabolisms. *Philosophical Transactions of the Royal Society B: Biological Sciences*, *361*(1474), 1819–1836. https://doi.org/10.1098/rstb.2006.1906

Cannat, M., Fontaine, F., & Escartín, J. (2010). Serpentinization and Associated Hydrogen And Methane Fluxes at Slow Spreading Ridges. In *Diversity Of Hydrothermal Systems On Slow Spreading Ocean Ridges* (pp. 241–264). American Geophysical Union (AGU). https://doi.org/10.1029/2008GM000760

Capriolo, M., Marzoli, A., Aradi, L. E., Ackerson, M. R., Bartoli, O., Callegaro, S., Dal Corso, J., Ernesto, M., Gouvêa Vasconcellos, E. M., De Min, A., Newton, R. J., & Szabó, C. (2021). Massive methane fluxing from magma–sediment interaction in the end-Triassic Central Atlantic Magmatic Province. *Nature Communications*, *12*(1), 5534. https://doi.org/10.1038/s41467-021-25510-w

Carlin, W., Malvoisin, B., Brunet, F., Lanson, B., Findling, N., Lanson, M., Fargetton, T., Jeannin, L., & Lhote, O. (2024). Kinetics of low-temperature H_2 production in ultramafic rocks by ferroan brucite oxidation. *Geochemical Perspectives Letters*, *29*, 27–32. https://doi.org/10.7185/geochemlet.2408

Carlson, R. L., & Miller, D. J. (2003). Mantle wedge water contents estimated from seismic velocities in partially serpentinized peridotites. *Geophysical Research Letters*, *30*(5).

https://doi.org/10.1029/2002GL016600

Carlson, R. W., Garnero, E., Harrison, T. M., Li, J., Manga, M., McDonough, W. F., Mukhopadhyay, S., Romanowicz, B., Rubie, D., Williams, Q., & Zhong, S. (2014). How Did Early Earth Become Our Modern World? *Annual Review of Earth and Planetary Sciences*, *42*(1), 151–178. https://doi.org/10.1146/annurev-earth-060313-055016

Carn, S. A., Fioletov, V. E., McLinden, C. A., Li, C., & Krotkov, N. A. (2017). A decade of global volcanic SO_2 emissions measured from space. *Scientific Reports*, *7*, 44095. https://doi.org/10.1038/srep44095

Carrillo Ramirez, A., Gonzalez Penagos, F., Rodriguez, G., & Moretti, I. (2023). Natural H_2 Emissions in Colombian Ophiolites: First Findings. *Geosciences*, *13*(12), Article 12. https://doi.org/10.3390/geosciences13120358

Cascone, M., Gargallo, G. C., Migliaccio, F., Corso, D., Tonietti, L., Cordone, A., Pietrini, I., Franchi, E., Carpani, G., Benedetto, A. di, Luciani, G., Anzelmo, G., Giovannelli, A., Iacopini, D., Parente, M., Edlmann, K., Moracci, M., & Giovannelli, D. (2025). *Hydrogenotrophic metabolisms in the subsurface and their implications for underground hydrogen storage and natural hydrogen prospecting*. https://eartharxiv.org/repository/view/8350/

Catling, D. C., Zahnle, K. J., & McKay, C. P. (2001). Biogenic Methane, Hydrogen Escape, and the Irreversible Oxidation of Early Earth. *Science*, *293*(5531), 839–843. https://doi.org/10.1126/science.1061976

Cesare, B. (1995). Graphite precipitation in C—O—H fluid inclusions: Closed system compositional and density changes, and thermobarometric implications. *Contributions to Mineralogy and Petrology*, *122*(1), 25–33. https://doi.org/10.1007/s004100050110

Chapelle, F. H., O'Neill, K., Bradley, P. M., Methé, B. A., Ciufo, S. A., Knobel, L. L., & Lovley, D. R. (2002). A hydrogen-based subsurface microbial community dominated by methanogens. *Nature*, *415*(6869), 312–315. https://doi.org/10.1038/415312a

Charlou, J. L., Donval, J. P., Konn, C., OndréAs, H., Fouquet, Y., Jean-Baptiste, P., & Fourré, E. (2010). High production and fluxes of H_2 and CH_4 and evidence of abiotic hydrocarbon synthesis by serpentinization in ultramafic-hosted hydrothermal systems on the Mid-Atlantic Ridge. In *Diversity Of Hydrothermal Systems On Slow Spreading Ocean Ridges* (pp. 265–296). American Geophysical Union (AGU). https://doi.org/10.1029/2008GM000752

Chen, Q., Popa, M. E., Batenburg, A. M., & Röckmann, T. (2015). Isotopic signatures of production and uptake of H_2 by soil. *Atmospheric Chemistry and Physics*, *15*(22), 13003–

13021. https://doi.org/10.5194/acp-15-13003-2015

Chorlton, L. B. (2007). *Generalized geology of the world: Bedrock domains and major faults in GIS format: a small-scale world geology map with an extended geological attribute database* [Dataset]. Geological Survey of Canada, Open File, 5529, 48. https://doi.org/10.4095/223767

Christensen, D. H., & Ruff, L. J. (1988). Seismic coupling and outer rise earthquakes. *Journal of Geophysical Research: Solid Earth*, *93*(B11), 13421–13444. https://doi.org/10.1029/JB093iB11p13421

Christie, D. M., Carmichael, I. S. E., & Langmuir, C. H. (1986). Oxidation states of mid-ocean ridge basalt glasses. *Earth and Planetary Science Letters*, *79*(3), 397–411. https://doi.org/10.1016/0012-821X(86)90195-0

Combaudon, V., Moretti, I., Kleine, B. I., & Stefánsson, A. (2022). Hydrogen emissions from hydrothermal fields in Iceland and comparison with the Mid-Atlantic Ridge. *International Journal of Hydrogen Energy*, *47*(18), 10217–10227. https://doi.org/10.1016/j.ijhydene.2022.01.101

Connolly, J. a. D., & Cesare, B. (1993). C-O-H-S fluid composition and oxygen fugacity in graphitic metapelites. *Journal of Metamorphic Geology*, *11*(3), 379–388. https://doi.org/10.1111/j.1525-1314.1993.tb00155.x

Conrad, R. (1996). Anaerobic hydrogen metabolism in aquatic sediments. *Internationale Vereinigung Für Theoretische Und Angewandte Limnologie: Mitteilungen*, *25*(1), 15–24. https://doi.org/10.1080/05384680.1996.11904063

Conrad, R., & Seiler, W. (1980). Contribution of hydrogen production by biological nitrogen fixation to the global hydrogen budget. *Journal of Geophysical Research: Oceans*, *85*(C10), 5493–5498. https://doi.org/10.1029/JC085iC10p05493

Constant, P., Poissant, L., & Villemur, R. (2009). Tropospheric H_2 budget and the response of its soil uptake under the changing environment. *Science of The Total Environment*, *407*(6), 1809–1823. https://doi.org/10.1016/j.scitotenv.2008.10.064

Coogan, L. A. (2007). 3.19—The Lower Oceanic Crust. In H. D. Holland & K. K. Turekian (Eds.), *Treatise on Geochemistry* (pp. 1–45). Pergamon. https://doi.org/10.1016/B978-008043751-4/00230-3

Cosmidis, J., & Benzerara, K. (2022). Why do microbes make minerals? *Comptes Rendus. Géoscience*, *354*(G1), 1–39. https://doi.org/10.5802/crgeos.107

Crameri, F. (2023). *Scientific colour maps* (Version 8.0.1) [Computer software]. Zenodo. https://doi.org/10.5281/zenodo.8409685

Crameri, F., Shephard, G. E., & Heron, P. J. (2020). The misuse of colour in science communication. *Nature Communications*, *11*(1), 5444.

D'Alessandro, W., Yüce, G., Italiano, F., Bellomo, S., Gülbay, A. H., Yasin, D. U., & Gagliano, A. L. (2018). Large compositional differences in the gases released from the Kizildag ophiolitic body (Turkey): Evidences of prevailingly abiogenic origin. *Marine and Petroleum Geology*, *89*, 174–184. https://doi.org/10.1016/j.marpetgeo.2016.12.017

Dalla Torre, M., Ferreiro Mählmann, R., & Ernst, W. G. (1997). Experimental study on the pressure dependence of vitrinite maturation. *Geochimica et Cosmochimica Acta*, *61*(14), 2921–2928. https://doi.org/10.1016/S0016-7037(97)00104-X

Damm, C., & Peukert, W. (2009). Kinetics of Radical Formation during the Mechanical Activation of Quartz. *Langmuir*, *25*(4), 2264–2270. https://doi.org/10.1021/la803502x

Dandar, O., Okamoto, A., Uno, M., Oyanagi, R., Nagaya, T., Burenjargal, U., Miyamoto, T., & Tsuchiya, N. (2019). Formation of secondary olivine after orthopyroxene during hydration of mantle wedge: Evidence from the Khantaishir Ophiolite, western Mongolia. *Contributions to Mineralogy and Petrology*, *174*(11), 86. https://doi.org/10.1007/s00410-019-1623-1

Darrah, T. H., Tedesco, D., Tassi, F., Vaselli, O., Cuoco, E., & Poreda, R. J. (2013). Gas chemistry of the Dallol region of the Danakil Depression in the Afar region of the northern-most East African Rift. *Chemical Geology*, *339*, 16–29. https://doi.org/10.1016/j.chemgeo.2012.10.036

Das, S. (2013). Critical Review of Water Radiolysis Processes, Dissociation Products, and Possible Impacts on the Local Environment: A Geochemist's Perspective. *Australian Journal of Chemistry*, *66*(5), 522–529. https://doi.org/10.1071/CH13012

de Moor, J. M., Fischer, T. P., Sharp, Z. D., King, P. L., Wilke, M., Botcharnikov, R. E., Cottrell, E., Zelenski, M., Marty, B., Klimm, K., Rivard, C., Ayalew, D., Ramirez, C., & Kelley, K. A. (2013). Sulfur degassing at Erta Ale (Ethiopia) and Masaya (Nicaragua) volcanoes: Implications for degassing processes and oxygen fugacities of basaltic systems. *Geochemistry, Geophysics, Geosystems*, *14*(10), 4076–4108. https://doi.org/10.1002/ggge.20255

Debret, B., Andreani, M., Muñoz, M., Bolfan-Casanova, N., Carlut, J., Nicollet, C., Schwartz, S., & Trcera, N. (2014). Evolution of Fe redox state in serpentine during subduction. *Earth and Planetary Science Letters*, *400*, 206–218. https://doi.org/10.1016/j.epsl.2014.05.038

Debret, B., Muriel, A., & Godard, M. (2024). A review of abyssal serpentinite geochemistry and geodynamics. *Earth-Science Reviews*, 104910.

https://doi.org/10.1016/j.earscirev.2024.104910
Demouchy, S., & Bolfan-Casanova, N. (2016). Distribution and transport of hydrogen in the lithospheric mantle: A review. *Lithos*, *240–243*, 402–425. https://doi.org/10.1016/j.lithos.2015.11.012
Deschamps, F., Godard, M., Guillot, S., & Hattori, K. (2013). Geochemistry of subduction zone serpentinites: A review. *Lithos*, *178*, 96–127. https://doi.org/10.1016/j.lithos.2013.05.019
DeShon, H. R., & Schwartz, S. Y. (2004). Evidence for serpentinization of the forearc mantle wedge along the Nicoya Peninsula, Costa Rica. *Geophysical Research Letters*, *31*(21). https://doi.org/10.1029/2004GL021179
Deville, E., Mohamed Hassan, K., Moussa Ahmed, K., Prinzhofer, A., Pelissier, N., Guélard, J., Noirez, S., Mohamed Magareh, H., & Omar Said, I. (2023). H_2 generation *versus* H_2 consumption in volcanic gas systems: A case study in the Afar hot spot in Djibouti. *Applied Geochemistry*, *156*, 105761. https://doi.org/10.1016/j.apgeochem.2023.105761
DeWitt, J., McMahon, S., & Parnell, J. (2022). The Effect of Grain Size on Porewater Radiolysis. *Earth and Space Science*, *9*(6), e2021EA002024. https://doi.org/10.1029/2021EA002024
D'Hondt, S., Spivack, A. J., Pockalny, R., Ferdelman, T. G., Fischer, J. P., Kallmeyer, J., Abrams, L. J., Smith, D. C., Graham, D., Hasiuk, F., Schrum, H., & Stancin, A. M. (2009). Subseafloor sedimentary life in the South Pacific Gyre. *Proceedings of the National Academy of Sciences*, *106*(28), 11651–11656. https://doi.org/10.1073/pnas.0811793106
Dick, H. J. B., Lin, J., & Schouten, H. (2003). An ultraslow-spreading class of ocean ridge. *Nature*, *426*(6965), 405–412. https://doi.org/10.1038/nature02128
Diehl, A., & Bach, W. (2020). MARHYS (MARine HYdrothermal Solutions) Database: A Global Compilation of Marine Hydrothermal Vent Fluid, End Member, and Seawater Compositions. *Geochemistry, Geophysics, Geosystems*, *21*(12), e2020GC009385. https://doi.org/10.1029/2020GC009385
Diehl, A., & Bach, W. (2023). *MARHYS Database 3.0* [Dataset]. PANGAEA. https://doi.org/10.1594/PANGAEA.958978
Dogan, T., Mori, T., Tsunomori, F., & Notsu, K. (2007). Soil H_2 and CO_2 Surveys at Several Active Faults in Japan. *Pure and Applied Geophysics*, *164*(12), 2449–2463. https://doi.org/10.1007/s00024-007-0277-5
Dopffel, N., Jansen, S., & Gerritse, J. (2021). Microbial side effects of underground hydrogen storage – Knowledge gaps, risks and opportunities for successful implementation. *International Journal of Hydrogen Energy*, *46*(12), 8594–8606. https://doi.org/10.1016/j.ijhydene.2020.12.058

Drobner, E., Huber, H., Wächtershäuser, G., Rose, D., & Stetter, K. O. (1990). Pyrite formation linked with hydrogen evolution under anaerobic conditions. *Nature*, *346*(6286), 742–744. https://doi.org/10.1038/346742a0

Dubessy, J., Pagel, M., Beny, J.-M., Christensen, H., Hickel, B., Kosztolanyi, C., & Poty, B. (1988). Radiolysis evidenced by H_2-O_2 and H_2-bearing fluid inclusions in three uranium deposits. *Geochimica et Cosmochimica Acta*, *52*(5), 1155–1167. https://doi.org/10.1016/0016-7037(88)90269-4

Dzaugis, M. E., Spivack, A. J., & D'Hondt, S. (2018). Radiolytic H_2 Production in Martian Environments. *Astrobiology*, *18*(9), 1137–1146. https://doi.org/10.1089/ast.2017.1654

Dzaugis, M. E., Spivack, A. J., Dunlea, A. G., Murray, R. W., & D'Hondt, S. (2016). Radiolytic Hydrogen Production in the Subseafloor Basaltic Aquifer. *Frontiers in Microbiology*, *7*. https://www.frontiersin.org/articles/10.3389/fmicb.2016.00076

Ebinger, C. J. (2005). Continental break-up: The East African perspective. *Astronomy & Geophysics*, *46*(2), 2.16-2.21. https://doi.org/10.1111/j.1468-4004.2005.46216.x

Edmonds, M. (2008). New geochemical insights into volcanic degassing. *Philosophical Transactions of the Royal Society A: Mathematical, Physical and Engineering Sciences*, *366*(1885), 4559–4579. https://doi.org/10.1098/rsta.2008.0185

Edmonds, M., & Wallace, P. J. (2017). Volatiles and Exsolved Vapor in Volcanic Systems. *Elements*, *13*(1), 29–34. https://doi.org/10.2113/gselements.13.1.29

Edmonds, M., & Woods, A. W. (2018). Exsolved volatiles in magma reservoirs. *Journal of Volcanology and Geothermal Research*, *368*, 13–30. https://doi.org/10.1016/j.jvolgeores.2018.10.018

Edwards, K. J., Wheat, C. G., & Sylvan, J. B. (2011). Under the sea: Microbial life in volcanic oceanic crust. *Nature Reviews Microbiology*, *9*(10), 703–712. https://doi.org/10.1038/nrmicro2647

Ehhalt, D. H., & Rohrer, F. (2009). The tropospheric cycle of H_2: A critical review. *Tellus B: Chemical and Physical Meteorology*, *61*(3), 500–535. https://doi.org/10.1111/j.1600-0889.2009.00416.x

Ehrlich, H. L. (1996). How microbes influence mineral growth and dissolution. *Chemical Geology*, *132*(1), 5–9. https://doi.org/10.1016/S0009-2541(96)00035-6

Elderfield, H., & Schultz, A. (1996). Mid-Ocean Ridge Hydrothermal Fluxes and the Chemical Composition of the Ocean. *Annual Review of Earth and Planetary Sciences*, *24*(1), 191–224. https://doi.org/10.1146/annurev.earth.24.1.191

Ellis, G. S., & Gelman, S. E. (2024). Model predictions of global geologic hydrogen resources.

Science Advances, *10*(50), eado0955. https://doi.org/10.1126/sciadv.ado0955

Ellison, E. T., Templeton, A. S., Zeigler, S. D., Mayhew, L. E., Kelemen, P. B., Matter, J. M., & Party, T. O. D. P. S. (2021). Low-Temperature Hydrogen Formation During Aqueous Alteration of Serpentinized Peridotite in the Samail Ophiolite. *Journal of Geophysical Research: Solid Earth*, *126*(6), e2021JB021981. https://doi.org/10.1029/2021JB021981

Ely, T. D., Leong, J. M., Canovas, P. A., & Shock, E. L. (2023). Huge Variation in H_2 Generation During Seawater Alteration of Ultramafic Rocks. *Geochemistry, Geophysics, Geosystems*, *24*(3), e2022GC010658. https://doi.org/10.1029/2022GC010658

Emmanuel, S., & Ague, J. J. (2007). Implications of present-day abiogenic methane fluxes for the early Archean atmosphere. *Geophysical Research Letters*, *34*(15). https://doi.org/10.1029/2007GL030532

Emmanuel, S., & Berkowitz, B. (2006). Suppression and stimulation of seafloor hydrothermal convection by exothermic mineral hydration. *Earth and Planetary Science Letters*, *243*(3), 657–668. https://doi.org/10.1016/j.epsl.2006.01.028

Epstein, G. S., Condit, C. B., Stoner, R. K., Holt, A. F., & Guevara, V. E. (2024). Evolving Subduction Zone Thermal Structure Drives Extensive Forearc Mantle Wedge Hydration. *AGU Advances*, *5*(4), e2023AV001121. https://doi.org/10.1029/2023AV001121

Espitalié, J., Senga Makadi, K., & Trichet, J. (1984). Role of the mineral matrix during kerogen pyrolysis. *Organic Geochemistry*, *6*, 365–382. https://doi.org/10.1016/0146-6380(84)90059-7

Etiope, G. (2023). Massive release of natural hydrogen from a geological seep (Chimaera, Turkey): Gas advection as a proxy of subsurface gas migration and pressurised accumulations. *International Journal of Hydrogen Energy*, *48*(25), 9172–9184. https://doi.org/10.1016/j.ijhydene.2022.12.025

Etiope, G. (2024). Natural hydrogen extracted from ophiolitic rocks: A first dataset. *International Journal of Hydrogen Energy*, *78*, 368–372. https://doi.org/10.1016/j.ijhydene.2024.06.292

Evans, B. W. (2004). The Serpentinite Multisystem Revisited: Chrysotile Is Metastable. *International Geology Review*, *46*(6), 479–506. https://doi.org/10.2747/0020-6814.46.6.479

Evans, B. W. (2010). Lizardite versus antigorite serpentinite: Magnetite, hydrogen, and life(?). *Geology*, *38*(10), 879–882. https://doi.org/10.1130/G31158.1

Evans, B. W., Hattori, K., & Baronnet, A. (2013). Serpentinite: What, Why, Where? *Elements*, *9*(2), 99–106. https://doi.org/10.2113/gselements.9.2.99

Faccenda, M. (2014). Water in the slab: A trilogy. *Tectonophysics*, *614*, 1–30.

https://doi.org/10.1016/j.tecto.2013.12.020

Fischer, T. P., Arellano, S., Carn, S., Aiuppa, A., Galle, B., Allard, P., Lopez, T., Shinohara, H., Kelly, P., Werner, C., Cardellini, C., & Chiodini, G. (2019). The emissions of CO_2 and other volatiles from the world's subaerial volcanoes. *Scientific Reports*, *9*(1), 1–11. https://doi.org/10.1038/s41598-019-54682-1

Fischer, T. P., & Chiodini, G. (2015). Volcanic, Magmatic and Hydrothermal Gases. In *The Encyclopedia of Volcanoes* (pp. 779–797). Elsevier. https://doi.org/10.1016/B978-0-12-385938-9.00045-6

Flesch, S., Pudlo, D., Albrecht, D., Jacob, A., & Enzmann, F. (2018). Hydrogen underground storage—Petrographic and petrophysical variations in reservoir sandstones from laboratory experiments under simulated reservoir conditions. *International Journal of Hydrogen Energy*, *43*(45), 20822–20835. https://doi.org/10.1016/j.ijhydene.2018.09.112

Foley, S. F., & Fischer, T. P. (2017). An essential role for continental rifts and lithosphere in the deep carbon cycle. *Nature Geoscience*, *10*(12), 897–902. https://doi.org/10.1038/s41561-017-0002-7

Frery, E., Langhi, L., Maison, M., & Moretti, I. (2021). Natural hydrogen seeps identified in the North Perth Basin, Western Australia. *International Journal of Hydrogen Energy*, *46*(61), 31158–31173. https://doi.org/10.1016/j.ijhydene.2021.07.023

Freund, F., Dickinson, J. T., & Cash, M. (2002). Hydrogen in Rocks: An Energy Source for Deep Microbial Communities. *Astrobiology*, *2*(1), 83–92. https://doi.org/10.1089/153110702753621367

Froidl, F., Littke, R., Grohmann, S., Baniasad, A., Böcker, J., Hartkopf-Fröder, C., & Weniger, P. (2021). Kerogen composition and origin, oil and gas generation potential of the Berriasian Wealden Shales of the Lower Saxony Basin. *International Journal of Coal Geology*, *246*, 103831. https://doi.org/10.1016/j.coal.2021.103831

Frost, B. R. (1991). Introduction to oxygen fugacity and its petrologic importance. *Reviews in Mineralogy and Geochemistry*, *25*, 1–9.

Frost, B. R., & Beard, J. S. (2007). On Silica Activity and Serpentinization. *Journal of Petrology*, *48*(7), 1351–1368. https://doi.org/10.1093/petrology/egm021

Frost, D. J., & McCammon, C. A. (2008). The Redox State of Earth's Mantle. *Annual Review of Earth and Planetary Sciences*, *36*(Volume 36, 2008), 389–420. https://doi.org/10.1146/annurev.earth.36.031207.124322

Früh-Green, G. L., Connolly, J. A. D., Plas, A., Kelley, D. S., & Grobéty, B. (2004). Serpentinization of oceanic peridotites: Implications for geochemical cycles and biological

activity. In W. S. D. Wilcock, E. F. DeLong, D. S. Kelley, J. A. Baross, & S. Craig Cary (Eds.), *Geophysical Monograph Series* (Vol. 144, pp. 119–136). American Geophysical Union. https://doi.org/10.1029/144GM08

Früh-Green, G. L., Plas, A., & Lécuyer, C. (1996). Petrologic and stable isotope constraints on hydrothermal alteration and serpentinization of the EPR shallow mantle at Hess Deep (Site 895). In C. Mevel, K. M. Gillis, J. F. Allan, & P. S. Meyer (Eds.), *Proceedings of the Ocean Drilling Program, 147 Scientific Results* (Vol. 147). Ocean Drilling Program. https://doi.org/10.2973/odp.proc.sr.147.1996

Fryer, P. (2012). Serpentinite Mud Volcanism: Observations, Processes, and Implications. *Annual Review of Marine Science*, *4*(1), 345–373. https://doi.org/10.1146/annurev-marine-120710-100922

Fryer, P., Wheat, C. G., Williams, T., Kelley, C., Johnson, K., Ryan, J., Kurz, W., Shervais, J., Albers, E., Bekins, B., Debret, B., Deng, J., Dong, Y., Eickenbusch, P., Frery, E., Ichiyama, Y., Johnston, R., Kevorkian, R., Magalhaes, V., … Pomponi, S. (2020). Mariana serpentinite mud volcanism exhumes subducted seamount materials: Implications for the origin of life. *Philosophical Transactions of the Royal Society A: Mathematical, Physical and Engineering Sciences*, *378*(2165), 20180425. https://doi.org/10.1098/rsta.2018.0425

Fullerton, K. M., Schrenk, M. O., Yücel, M., Manini, E., Basili, M., Rogers, T. J., Fattorini, D., Di Carlo, M., d'Errico, G., Regoli, F., Nakagawa, M., Vetriani, C., Smedile, F., Ramírez, C., Miller, H., Morrison, S. M., Buongiorno, J., Jessen, G. L., Steen, A. D., … Lloyd, K. G. (2021). Effect of tectonic processes on biosphere–geosphere feedbacks across a convergent margin. *Nature Geoscience*, *14*(5), 301–306. https://doi.org/10.1038/s41561-021-00725-0

Furnes, H., & Dilek, Y. (2022). Archean versus Phanerozoic oceanic crust formation and tectonics: Ophiolites through time. *Geosystems and Geoenvironment*, *1*(1), 100004. https://doi.org/10.1016/j.geogeo.2021.09.004

Furnes, H., & Staudigel, H. (1999). Biological mediation in ocean crust alteration: How deep is the deep biosphere? *Earth and Planetary Science Letters*, *166*(3), 97–103. https://doi.org/10.1016/S0012-821X(99)00005-9

Furnes, H., Staudigel, H., Thorseth, I. H., Torsvik, T., Muehlenbachs, K., & Tumyr, O. (2001). Bioalteration of basaltic glass in the oceanic crust. *Geochemistry, Geophysics, Geosystems*, *2*(8). https://doi.org/10.1029/2000GC000150

Gaillard, F., Bernadou, F., Roskosz, M., Bouhifd, M. A., Marrocchi, Y., Iacono-Marziano, G., Moreira, M., Scaillet, B., & Rogerie, G. (2022). Redox controls during magma ocean

degassing. *Earth and Planetary Science Letters*, *577*, 117255. https://doi.org/10.1016/j.epsl.2021.117255

Gaillard, F., Scaillet, B., & Arndt, N. T. (2011). Atmospheric oxygenation caused by a change in volcanic degassing pressure. *Nature*, *478*(7368), 229–232. https://doi.org/10.1038/nature10460

Gallant, R. M., & Von Damm, K. L. (2006). Geochemical controls on hydrothermal fluids from the Kairei and Edmond Vent Fields, 23°–25°S, Central Indian Ridge. *Geochemistry, Geophysics, Geosystems*, *7*(6). https://doi.org/10.1029/2005GC001067

Gaucher, E. C. (2020). New Perspectives in the Industrial Exploration for Native Hydrogen. *Elements*, *16*(1), 8–9. https://doi.org/10.2138/gselements.16.1.8

Genda, H., & Ikoma, M. (2008). Origin of the ocean on the Earth: Early evolution of water D/H in a hydrogen-rich atmosphere. *Icarus*, *194*(1), 42–52. https://doi.org/10.1016/j.icarus.2007.09.007

Gerlach, T. M. (1993). Oxygen buffering of Kilauea volcanic gases and the oxygen fugacity of Kilauea basalt. *Geochimica et Cosmochimica Acta*, *57*(4), 795–814. https://doi.org/10.1016/0016-7037(93)90169-W

Gerya, T. (2022). Numerical modeling of subduction: State of the art and future directions. *Geosphere*, *18*(2), 503–561. https://doi.org/10.1130/GES02416.1

Geymond, U., Briolet, T., Combaudon, V., Sissmann, O., Martinez, I., Duttine, M., & Moretti, I. (2023). Reassessing the role of magnetite during natural hydrogen generation. *Frontiers in Earth Science*, *11*. https://doi.org/10.3389/feart.2023.1169356

Geymond, U., Ramanaidou, E., Lévy, D., Ouaya, A., & Moretti, I. (2022). Can Weathering of Banded Iron Formations Generate Natural Hydrogen? Evidence from Australia, Brazil and South Africa. *Minerals*, *12*(2), Article 2. https://doi.org/10.3390/min12020163

Giggenbach, W. F. (1987). Redox processes governing the chemistry of fumarolic gas discharges from White Island, New Zealand. *Applied Geochemistry*, *2*(2), 143–161. https://doi.org/10.1016/0883-2927(87)90030-8

Giggenbach, W. F. (1996). Chemical Composition of Volcanic Gases. In R. Scarpa & R. I. Tilling (Eds.), *Monitoring and Mitigation of Volcano Hazards* (pp. 221–256). Springer. https://doi.org/10.1007/978-3-642-80087-0_7

Gilat, A. L., & Vol, A. (2005). Primordial hydrogen-helium degassing, an overlooked major energy source for internal terrestrial processes. *HAIT Journal of Science and Engineering B*, *2*(1–2), 125–167.

Gilat, A. L., & Vol, A. (2012). Degassing of primordial hydrogen and helium as the major energy

source for internal terrestrial processes. *Geoscience Frontiers*, *3*(6), 911–921. https://doi.org/10.1016/j.gsf.2012.03.009

Gillis, K. M., Snow, J. E., Klaus, A., Abe, N., Adrião, Á. B., Akizawa, N., Ceuleneer, G., Cheadle, M. J., Faak, K., Falloon, T. J., Friedman, S. A., Godard, M., Guerin, G., Harigane, Y., Horst, A. J., Hoshide, T., Ildefonse, B., Jean, M. M., John, B. E., … Wintsch, R. P. (2014). Primitive layered gabbros from fast-spreading lower oceanic crust. *Nature*, *505*(7482), 204–207. https://doi.org/10.1038/nature12778

Giuntoli, F., Menegon, L., Siron, G., Cognigni, F., Leroux, H., Compagnoni, R., Rossi, M., & Vitale Brovarone, A. (2024). Methane-hydrogen-rich fluid migration may trigger seismic failure in subduction zones at forearc depths. *Nature Communications*, *15*(1), Article 1. https://doi.org/10.1038/s41467-023-44641-w

Giuntoli, F., Vitale Brovarone, A., & Menegon, L. (2020). Feedback between high-pressure genesis of abiotic methane and strain localization in subducted carbonate rocks. *Scientific Reports*, *10*(1), 9848. https://doi.org/10.1038/s41598-020-66640-3

Glein, C. R., & Zolotov, M. Yu. (2020). Hydrogen, Hydrocarbons, and Habitability Across the Solar System. *Elements*, *16*(1), 47–52. https://doi.org/10.2138/gselements.16.1.47

Global Volcanism Program. (2024). *Volcanoes of the World* (Version 5.2.3) [Dataset]. Smithsonian Institution. https://doi.org/10.5479/si.GVP.VOTW5-2024.5.2

Gluyas, J. G., Humphreys, M., Karolytė, R., Cheng, A., Sherwood Lollar, B., & Ballentine, C. (2025). Exploring for hydrogen, helium and lithium: Is it as easy as 1, 2, 3? *Energy Geoscience Conference Series*, *1*(1), egc1-2024–13. https://doi.org/10.1144/egc1-2024-13

Gold, T. (1992). The deep, hot biosphere. *Proceedings of the National Academy of Sciences*, *89*(13), 6045–6049. https://doi.org/10.1073/pnas.89.13.6045

Goodwin, A. M. (1996). *Principles of Precambrian Geology*. Elsevier.

Greening, C., Berney, M., Hards, K., Cook, G. M., & Conrad, R. (2014). A soil actinobacterium scavenges atmospheric H_2 using two membrane-associated, oxygen-dependent [NiFe] hydrogenases. *Proceedings of the National Academy of Sciences*, *111*(11), 4257–4261. https://doi.org/10.1073/pnas.1320586111

Greening, C., Biswas, A., Carere, C. R., Jackson, C. J., Taylor, M. C., Stott, M. B., Cook, G. M., & Morales, S. E. (2016). Genomic and metagenomic surveys of hydrogenase distribution indicate H_2 is a widely utilised energy source for microbial growth and survival. *The ISME Journal*, *10*(3), 761–777. https://doi.org/10.1038/ismej.2015.153

Greening, C., & Grinter, R. (2022). Microbial oxidation of atmospheric trace gases. *Nature*

Reviews Microbiology, *20*(9), 513–528. https://doi.org/10.1038/s41579-022-00724-x

Gregory, S. P., Barnett, M. J., Field, L. P., & Milodowski, A. E. (2019). Subsurface Microbial Hydrogen Cycling: Natural Occurrence and Implications for Industry. *Microorganisms*, *7*(2), Article 2. https://doi.org/10.3390/microorganisms7020053

Grevemeyer, I., Ranero, C. R., & Ivandic, M. (2018). Structure of oceanic crust and serpentinization at subduction trenches. *Geosphere*, *14*(2), 395–418. https://doi.org/10.1130/GES01537.1

Grosch, E. G., & Wilson, A. (2023). The discovery and petrogenetic significance of komatiites. *Journal of African Earth Sciences*, *205*, 105002. https://doi.org/10.1016/j.jafrearsci.2023.105002

Grozeva, N. G., Klein, F., Seewald, J. S., & Sylva, S. P. (2020). Chemical and isotopic analyses of hydrocarbon-bearing fluid inclusions in olivine-rich rocks. *Philosophical Transactions of the Royal Society A: Mathematical, Physical and Engineering Sciences*, *378*(2165), 20180431. https://doi.org/10.1098/rsta.2018.0431

Gu, T., Pamato, M. G., Novella, D., Alvaro, M., Fournelle, J., Brenker, F. E., Wang, W., & Nestola, F. (2022). Hydrous peridotitic fragments of Earth's mantle 660 km discontinuity sampled by a diamond. *Nature Geoscience*, *15*(11), 950–954. https://doi.org/10.1038/s41561-022-01024-y

Hacker, B. R. (2008). H_2O subduction beyond arcs. *Geochemistry, Geophysics, Geosystems*, *9*(3). https://doi.org/10.1029/2007GC001707

Hackmann, T. J. (2024). The vast landscape of carbohydrate fermentation in prokaryotes. *FEMS Microbiology Reviews*, *48*(4), fuae016. https://doi.org/10.1093/femsre/fuae016

Hagemann, B., Rasoulzadeh, M., Panfilov, M., Ganzer, L., & Reitenbach, V. (2015). Mathematical modeling of unstable transport in underground hydrogen storage. *Environmental Earth Sciences*, *73*(11), 6891–6898. https://doi.org/10.1007/s12665-015-4414-7

Hall, D. L., & Bodnar, R. J. (1990). Methane in fluid inclusions from granulites: A product of hydrogen diffusion? *Geochimica et Cosmochimica Acta*, *54*(3), 641–651. https://doi.org/10.1016/0016-7037(90)90360-W

Hall, D. L., & Sterner, S. M. (1995). Experimental diffusion of hydrogen into synthetic fluid inclusions in quartz. *Journal of Metamorphic Geology*, *13*(3), 345–355. https://doi.org/10.1111/j.1525-1314.1995.tb00224.x

Hallis, L. J., Huss, G. R., Nagashima, K., Taylor, G. J., Halldórsson, S. A., Hilton, D. R., Mottl, M. J., & Meech, K. J. (2015). Evidence for primordial water in Earth's deep mantle. *Science*, *350*(6262), 795–797. https://doi.org/10.1126/science.aac4834

Halmer, M. M., Schmincke, H.-U., & Graf, H.-F. (2002). The annual volcanic gas input into the atmosphere, in particular into the stratosphere: A global data set for the past 100 years. *Journal of Volcanology and Geothermal Research*, *115*(3), 511–528. https://doi.org/10.1016/S0377-0273(01)00318-3

Halpaap, F., Rondenay, S., Perrin, A., Goes, S., Ottemöller, L., Austrheim, H., Shaw, R., & Eeken, T. (2019). Earthquakes track subduction fluids from slab source to mantle wedge sink. *Science Advances*, *5*(4), eaav7369. https://doi.org/10.1126/sciadv.aav7369

Hao, J., Sverjensky, D. A., & Hazen, R. M. (2019). Redox states of Archean surficial environments: The importance of $H_{2,g}$ instead of $O_{2,g}$ for weathering reactions. *Chemical Geology*, *521*, 49–58. https://doi.org/10.1016/j.chemgeo.2019.05.022

Hassan, Q., Algburi, S., Sameen, A. Z., Jaszczur, M., & Salman, H. M. (2024). Hydrogen as an energy carrier: Properties, storage methods, challenges, and future implications. *Environment Systems and Decisions*, *44*(2), 327–350. https://doi.org/10.1007/s10669-023-09932-z

Hasterok, D., & Chapman, D. S. (2011). Heat production and geotherms for the continental lithosphere. *Earth and Planetary Science Letters*, *307*(1), 59–70. https://doi.org/10.1016/j.epsl.2011.04.034

Hatakeyama, K., Katayama, I., Hirauchi, K., & Michibayashi, K. (2017). Mantle hydration along outer-rise faults inferred from serpentinite permeability. *Scientific Reports*, *7*(1), Article 1. https://doi.org/10.1038/s41598-017-14309-9

Hay Mele, B., Monticelli, M., Leone, S., Bastoni, D., Barosa, B., Cascone, M., Migliaccio, F., Montemagno, F., Ricciardelli, A., Tonietti, L., Rotundi, A., Cordone, A., & Giovannelli, D. (2023). Oxidoreductases and metal cofactors in the functioning of the earth. *Essays in Biochemistry*, *67*(4), 653–670. https://doi.org/10.1042/EBC20230012

Heinemann, N., Alcalde, J., M. Miocic, J., T. Hangx, S. J., Kallmeyer, J., Ostertag-Henning, C., Hassanpouryouzband, A., M. Thaysen, E., J. Strobel, G., Schmidt-Hattenberger, C., Edlmann, K., Wilkinson, M., Bentham, M., Haszeldine, R. S., Carbonell, R., & Rudloff, A. (2021). Enabling large-scale hydrogen storage in porous media – the scientific challenges. *Energy & Environmental Science*, *14*(2), 853–864. https://doi.org/10.1039/D0EE03536J

Hekinian, R., Chaigneau, M., & Cheminee, J. L. (1973). Popping Rocks and Lava Tubes from the Mid-Atlantic Rift Valley at 36° N. *Nature*, *245*(5425), Article 5425. https://doi.org/10.1038/245371a0

Hemme, C., & Van Berk, W. (2018). Hydrogeochemical Modeling to Identify Potential Risks of Underground Hydrogen Storage in Depleted Gas Fields. *Applied Sciences*, *8*(11), Article

11. https://doi.org/10.3390/app8112282

Henley, R. W., & Fischer, T. P. (2021). Sulfur sequestration and redox equilibria in volcanic gases. *Journal of Volcanology and Geothermal Research*, *414*, 107181. https://doi.org/10.1016/j.jvolgeores.2021.107181

Herr, F. L. (1984). Dissolved hydrogen in Eurasian Arctic waters. *Tellus B*, *36B*(1), 55–66. https://doi.org/10.1111/j.1600-0889.1984.tb00052.x

Hirose, T., Kawagucci, S., & Suzuki, K. (2011). Mechanoradical H_2 generation during simulated faulting: Implications for an earthquake-driven subsurface biosphere. *Geophysical Research Letters*, *38*(17). https://doi.org/10.1029/2011GL048850

Hirose, T., Kawagucci, S., & Suzuki, K. (2012). Correction to "Mechanoradical H_2 generation during simulated faulting: Implications for an earthquake-driven subsurface biosphere." *Geophysical Research Letters*, *39*(23). https://doi.org/10.1029/2012GL054539

Hirschmann, M. M., Withers, A. C., Ardia, P., & Foley, N. T. (2012). Solubility of molecular hydrogen in silicate melts and consequences for volatile evolution of terrestrial planets. *Earth and Planetary Science Letters*, *345–348*, 38–48. https://doi.org/10.1016/j.epsl.2012.06.031

Holden, J., Breier, J., Rogers, K., Schulte, M., & Toner, B. (2012). Biogeochemical Processes at Hydrothermal Vents: Microbes and Minerals, Bioenergetics, and Carbon Fluxes. *Oceanography*, *25*(1), 196–208. https://doi.org/10.5670/oceanog.2012.18

Holland, G., Lollar, B. S., Li, L., Lacrampe-Couloume, G., Slater, G. F., & Ballentine, C. J. (2013). Deep fracture fluids isolated in the crust since the Precambrian era. *Nature*, *497*(7449), 357–360. https://doi.org/10.1038/nature12127

Holland, H. D. (2002). Volcanic gases, black smokers, and the great oxidation event. *Geochimica et Cosmochimica Acta*, *66*(21), 3811–3826. https://doi.org/10.1016/S0016-7037(02)00950-X

Holloway, J. R. (1984). Graphite-CH_4-H_2O-CO_2 equilibria at low-grade metamorphic conditions. *Geology*, *12*(8), 455–458. https://doi.org/10.1130/0091-7613(1984)12<455:GEALMC>2.0.CO;2

Holloway, J. R. (2004). Redox reactions in seafloor basalts: Possible insights into silicic hydrothermal systems. *Chemical Geology*, *210*(1), 225–230. https://doi.org/10.1016/j.chemgeo.2004.06.009

Holloway, J. R., & O'Day, P. A. (2000). Production of CO_2 and H_2 by Diking-Eruptive Events at Mid-Ocean Ridges: Implications for Abiotic Organic Synthesis and Global Geochemical Cycling. *International Geology Review*, *42*(8), 673–683.

https://doi.org/10.1080/00206810009465105
Holt, A. F., & Condit, C. B. (2021). Slab Temperature Evolution Over the Lifetime of a Subduction Zone. *Geochemistry, Geophysics, Geosystems*, *22*(6), e2020GC009476. https://doi.org/10.1029/2020GC009476
Horibe, Y., & Craig, H. (1995). DH fractionation in the system methane-hydrogen-water. *Geochimica et Cosmochimica Acta*, *59*(24), 5209–5217. https://doi.org/10.1016/0016-7037(95)00391-6
Horsfield, B., Mahlstedt, N., Weniger, P., Misch, D., Vranjes-Wessely, S., Han, S., & Wang, C. (2022). Molecular hydrogen from organic sources in the deep Songliao Basin, P.R. China. *International Journal of Hydrogen Energy*, *47*(38), 16750–16774. https://doi.org/10.1016/j.ijhydene.2022.02.208
Huang, J., Sverjensky, D. A., Daniel, I., & Vitale Brovarone, A. (2024). Reaction path model of the formation of abiotic immiscible hydrocarbon fluids in subducted carbonated serpentinites, Lanzo Massif (Western Italian Alps). *Lithos*, 107498. https://doi.org/10.1016/j.lithos.2024.107498
Huang, R., Ding, X., Sun, W., & Shang, X. (2021). Contrasted Effect of Spinel and Pyroxene on Molecular Hydrogen (H_2) Production during Serpentinization of Olivine. *Minerals*, *11*(8), Article 8. https://doi.org/10.3390/min11080794
Huang, R., Shang, X., Zhao, Y., Sun, W., & Liu, X. (2023). Effect of Fluid Salinity on Reaction Rate and Molecular Hydrogen (H_2) Formation During Peridotite Serpentinization at 300°C. *Journal of Geophysical Research: Solid Earth*, *128*(3), e2022JB025218. https://doi.org/10.1029/2022JB025218
Huang, R., Song, M., Ding, X., Zhu, S., Zhan, W., & Sun, W. (2017). Influence of pyroxene and spinel on the kinetics of peridotite serpentinization. *Journal of Geophysical Research: Solid Earth*, *122*(9), 7111–7126. https://doi.org/10.1002/2017JB014231
Huang, R., Sun, W., Ding, X., Zhao, Y., Li, Y., & Shang, X. (2024). The influence of silica on reaction rates and molecular hydrogen (H_2) generation during olivine hydrothermal alteration. *Science China Earth Sciences*, *67*(1), 222–233. https://doi.org/10.1007/s11430-023-1172-9
Huang, R., Sun, W., Ding, X., Zhao, Y., & Song, M. (2020). Effect of pressure on the kinetics of peridotite serpentinization. *Physics and Chemistry of Minerals*, *47*(7), 33. https://doi.org/10.1007/s00269-020-01101-x
Huang, R., Sun, W., Song, M., & Ding, X. (2019). Influence of pH on Molecular Hydrogen (H_2) Generation and Reaction Rates during Serpentinization of Peridotite and Olivine.

Minerals, *9*(11), Article 11. https://doi.org/10.3390/min9110661

Huizenga, J.-M. (2001). Thermodynamic modelling of C–O–H fluids. *Lithos*, *55*(1–4), 101–114. https://www.sciencedirect.com/science/article/pii/S0024493700000402

Humphris, S. E., & Klein, F. (2018). Progress in Deciphering the Controls on the Geochemistry of Fluids in Seafloor Hydrothermal Systems. *Annual Review of Marine Science*, *10*(Volume 10, 2018), 315–343. https://doi.org/10.1146/annurev-marine-121916-063233

Hunter, J. D. (2007). Matplotlib: A 2D Graphics Environment. *Computing in Science & Engineering*, *9*(3), 90–95. Computing in Science & Engineering. https://doi.org/10.1109/MCSE.2007.55

Hutchinson, I. P., Jackson, O., Stocks, A. E., Barnicoat, A. C., & Lawrence, S. R. (2024). Greenstones as a source of hydrogen in cratonic sedimentary basins. *Geological Society, London, Special Publications*, *547*(1), SP547-2023–2039. https://doi.org/10.1144/SP547-2023-39

Hyndman, R. D., & Peacock, S. M. (2003). Serpentinization of the forearc mantle. *Earth and Planetary Science Letters*, *212*(3), 417–432. https://doi.org/10.1016/S0012-821X(03)00263-2

Iacono-Marziano, G., Gaillard, F., Scaillet, B., Polozov, A. G., Marecal, V., Pirre, M., & Arndt, N. T. (2012). Extremely reducing conditions reached during basaltic intrusion in organic matter-bearing sediments. *Earth and Planetary Science Letters*, *357–358*, 319–326. https://doi.org/10.1016/j.epsl.2012.09.052

Iacono-Marziano, G., Marecal, V., Pirre, M., Gaillard, F., Arteta, J., Scaillet, B., & Arndt, N. T. (2012). Gas emissions due to magma–sediment interactions during flood magmatism at the Siberian Traps: Gas dispersion and environmental consequences. *Earth and Planetary Science Letters*, *357–358*, 308–318. https://doi.org/10.1016/j.epsl.2012.09.051

IEA. (2024). *Global Hydrogen Review 2024*. International Energy Agency.

Ikuta, D., Ohtani, E., Sano-Furukawa, A., Shibazaki, Y., Terasaki, H., Yuan, L., & Hattori, T. (2019). Interstitial hydrogen atoms in face-centered cubic iron in the Earth's core. *Scientific Reports*, *9*(1), 7108. https://doi.org/10.1038/s41598-019-43601-z

Ilyin, A. V. (2009). Neoproterozoic banded iron formations. *Lithology and Mineral Resources*, *44*(1), 78–86. https://doi.org/10.1134/S0024490209010064

Ito, T., Nagamine, K., Yamamoto, K., Adachi, M., & Kawabe, I. (1999). Preseismic hydrogen gas anomalies caused by stress-corrosion process preceding earthquakes. *Geophysical Research Letters*, *26*(13), 2009–2012. https://doi.org/10.1029/1999GL900407

Ivarsson, M., Schnürer, A., Bengtson, S., & Neubeck, A. (2016). Anaerobic Fungi: A Potential

Source of Biological H_2 in the Oceanic Crust. *Frontiers in Microbiology*, *7*. https://doi.org/10.3389/fmicb.2016.00674

Jackson, O., Lawrence, S. R., Hutchinson, I. P., Stocks, A. E., Barnicoat, A. C., & Powney, M. (2024). Natural hydrogen: Sources, systems and exploration plays. *Geoenergy*, *2*(1), geoenergy2024. https://doi.org/10.1144/geoenergy2024-002

Jian, H., Canales, J. P., Dunn, R., & Nedimović, M. R. (2024). Hydrothermal flow and serpentinization in oceanic core complexes controlled by mafic intrusions. *Nature Geoscience*, 1–6. https://doi.org/10.1038/s41561-024-01444-y

Johnson, H. P., & Pruis, M. J. (2003). Fluxes of fluid and heat from the oceanic crustal reservoir. *Earth and Planetary Science Letters*, *216*(4), 565–574. https://doi.org/10.1016/S0012-821X(03)00545-4

Kaim, V., & Kaur-Ghumaan, S. (2019). Manganese Complexes: Hydrogen Generation and Oxidation. *European Journal of Inorganic Chemistry*, *2019*(48), 5041–5051. https://doi.org/10.1002/ejic.201900988

Kameda, J., Saruwatari, K., Tanaka, H., & Tsunomori, F. (2004). Mechanisms of hydrogen generation during the mechanochemical treatment of biotite within D_2O media. *Earth, Planets and Space*, *56*(12), 1241–1245. https://doi.org/10.1186/BF03353346

Kampman, N., Busch, A., Bertier, P., Snippe, J., Hangx, S., Pipich, V., Di, Z., Rother, G., Harrington, J. F., Evans, J. P., Maskell, A., Chapman, H. J., & Bickle, M. J. (2016). Observational evidence confirms modelling of the long-term integrity of CO_2-reservoir caprocks. *Nature Communications*, *7*(1), 12268. https://doi.org/10.1038/ncomms12268

Karolytė, R., Warr, O., Van Heerden, E., Flude, S., De Lange, F., Webb, S., Ballentine, C. J., & Sherwood Lollar, B. (2022). The role of porosity in H_2/He production ratios in fracture fluids from the Witwatersrand Basin, South Africa. *Chemical Geology*, *595*, 120788. https://doi.org/10.1016/j.chemgeo.2022.120788

Kasting, J. F. (2013). What caused the rise of atmospheric O_2? *Chemical Geology*, *362*, 13–25. https://doi.org/10.1016/j.chemgeo.2013.05.039

Kasting, J. F., & Canfield, D. E. (2012). The Global Oxygen Cycle. In *Fundamentals of Geobiology* (pp. 93–104). John Wiley & Sons, Ltd. https://doi.org/10.1002/9781118280874.ch7

Kawagucci, S., Toki, T., Ishibashi, J., Takai, K., Ito, M., Oomori, T., & Gamo, T. (2010). Isotopic variation of molecular hydrogen in 20°–375°C hydrothermal fluids as detected by a new analytical method. *Journal of Geophysical Research: Biogeosciences*, *115*(G3). https://doi.org/10.1029/2009JG001203

Kawano, S., Katayama, I., & Okazaki, K. (2011). Permeability anisotropy of serpentinite and fluid

pathways in a subduction zone. *Geology*, *39*(10), 939–942. https://doi.org/10.1130/G32173.1

Keir, R. S. (2010). A note on the fluxes of abiogenic methane and hydrogen from mid-ocean ridges. *Geophysical Research Letters*, *37*(24). https://doi.org/10.1029/2010GL045362

Kelley, D. S., Karson, J. A., Früh-Green, G. L., Yoerger, D. R., Shank, T. M., Butterfield, D. A., Hayes, J. M., Schrenk, M. O., Olson, E. J., Proskurowski, G., Jakuba, M., Bradley, A., Larson, B., Ludwig, K., Glickson, D., Buckman, K., Bradley, A. S., Brazelton, W. J., Roe, K., … Sylva, S. P. (2005). A Serpentinite-Hosted Ecosystem: The Lost City Hydrothermal Field. *Science*, *307*(5714), 1428–1434. https://doi.org/10.1126/science.1102556

Kietäväinen, R., & Purkamo, L. (2015). The origin, source, and cycling of methane in deep crystalline rock biosphere. *Frontiers in Microbiology*, *6*. https://www.frontiersin.org/journals/microbiology/articles/10.3389/fmicb.2015.00725

Kita, I., Matsuo, S., & Wakita, H. (1982). H_2 generation by reaction between H_2O and crushed rock: An experimental study on H_2 degassing from the active fault zone. *Journal of Geophysical Research: Solid Earth*, *87*(B13), 10789–10795. https://doi.org/10.1029/JB087iB13p10789

Klein, C. (2005). Some Precambrian banded iron-formations (BIFs) from around the world: Their age, geologic setting, mineralogy, metamorphism, geochemistry, and origins. *American Mineralogist*, *90*(10), 1473–1499. https://doi.org/10.2138/am.2005.1871

Klein, F., Bach, W., Humphris, S. E., Kahl, W.-A., Jöns, N., Moskowitz, B., & Berquó, T. S. (2014). Magnetite in seafloor serpentinite—Some like it hot. *Geology*, *42*(2), 135–138. https://doi.org/10.1130/G35068.1

Klein, F., Bach, W., Jöns, N., McCollom, T., Moskowitz, B., & Berquó, T. (2009). Iron partitioning and hydrogen generation during serpentinization of abyssal peridotites from 15°N on the Mid-Atlantic Ridge. *Geochimica et Cosmochimica Acta*, *73*(22), 6868–6893. https://doi.org/10.1016/j.gca.2009.08.021

Klein, F., Bach, W., & McCollom, T. M. (2013). Compositional controls on hydrogen generation during serpentinization of ultramafic rocks. *Lithos*, *178*, 55–69. https://doi.org/10.1016/j.lithos.2013.03.008

Klein, F., Grozeva, N. G., & Seewald, J. S. (2019). Abiotic methane synthesis and serpentinization in olivine-hosted fluid inclusions. *Proceedings of the National Academy of Sciences*, *116*(36), 17666–17672. https://doi.org/10.1073/pnas.1907871116

Klein, F., Grozeva, N. G., Seewald, J. S., McCollom, T. M., Humphris, S. E., Moskowitz, B., Berquo, T. S., & Kahl, W.-A. (2015). Experimental constraints on fluid-rock reactions

during incipient serpentinization of harzburgite. *American Mineralogist*, *100*(4), 991–1002. https://doi.org/10.2138/am-2015-5112

Klein, F., Schroeder, T., John, C. M., Davis, S., Humphris, S. E., Seewald, J. S., Sichel, S., Bach, W., & Brunelli, D. (2024). Mineral carbonation of peridotite fueled by magmatic degassing and melt impregnation in an oceanic transform fault. *Proceedings of the National Academy of Sciences*, *121*(8), e2315662121. https://doi.org/10.1073/pnas.2315662121

Klein, F., Tarnas, J. D., & Bach, W. (2020). Abiotic Sources of Molecular Hydrogen on Earth. *Elements*, *16*(1), 19–24. https://doi.org/10.2138/gselements.16.1.19

Koepenick, K. W., Brantley, S. L., Thompson, J. M., Rowe, G. L., Nyblade, A. A., & Moshy, C. (1996). Volatile emissions from the crater and flank of Oldoinyo Lengai volcano, Tanzania. *Journal of Geophysical Research: Solid Earth*, *101*(B6), 13819–13830. https://doi.org/10.1029/96JB00173

Konn, C., Charlou, J. l., Holm, N. g., & Mousis, O. (2015). The Production of Methane, Hydrogen, and Organic Compounds in Ultramafic-Hosted Hydrothermal Vents of the Mid-Atlantic Ridge. *Astrobiology*, *15*(5), 381–399. https://doi.org/10.1089/ast.2014.1198

Korenaga, J. (2017). On the extent of mantle hydration caused by plate bending. *Earth and Planetary Science Letters*, *457*, 1–9. https://doi.org/10.1016/j.epsl.2016.10.011

Lappan, R., Shelley, G., Islam, Z. F., Leung, P. M., Lockwood, S., Nauer, P. A., Jirapanjawat, T., Ni, G., Chen, Y.-J., Kessler, A. J., Williams, T. J., Cavicchioli, R., Baltar, F., Cook, P. L. M., Morales, S. E., & Greening, C. (2023). Molecular hydrogen in seawater supports growth of diverse marine bacteria. *Nature Microbiology*, *8*(4), 581–595. https://doi.org/10.1038/s41564-023-01322-0

Larin, N., Zgonnik, V., Rodina, S., Deville, E., Prinzhofer, A., & Larin, V. N. (2015). Natural Molecular Hydrogen Seepage Associated with Surficial, Rounded Depressions on the European Craton in Russia. *Natural Resources Research*, *24*(3), 369–383. https://doi.org/10.1007/s11053-014-9257-5

Larin, V. N. (1993). *Hydridic earth: The new geology of our primordially hydrogen-rich planet* (C. W. Hunt, Trans.). Polar Pub.

LaVerne, J. A., & Tandon, L. (2005). H_2 and Cl_2 Production in the Radiolysis of Calcium and Magnesium Chlorides and Hydroxides. *The Journal of Physical Chemistry A*, *109*(12), 2861–2865. https://doi.org/10.1021/jp044166o

Lazar, C. (2020). Using Silica Activity to Model Redox-dependent Fluid Compositions in Serpentinites from 100 to 700 °C and from 1 to 20 kbar. *Journal of Petrology*, *61*(11–12), egaa101. https://doi.org/10.1093/petrology/egaa101

Lazar, C., McCollom, T. M., & Manning, C. E. (2012). Abiogenic methanogenesis during experimental komatiite serpentinization: Implications for the evolution of the early Precambrian atmosphere. *Chemical Geology*, *326–327*, 102–112. https://doi.org/10.1016/j.chemgeo.2012.07.019

Le Bayon, R., Brey, G. P., Ernst, W. G., & Mählmann, R. F. (2011). Experimental kinetic study of organic matter maturation: Time and pressure effects on vitrinite reflectance at 400°C. *Organic Geochemistry*, *42*(4), 340–355. https://doi.org/10.1016/j.orggeochem.2011.01.011

Lee, C.-T. A., Leeman, W. P., Canil, D., & Li, Z.-X. A. (2005). Similar V/Sc Systematics in MORB and Arc Basalts: Implications for the Oxygen Fugacities of their Mantle Source Regions. *Journal of Petrology*, *46*(11), 2313–2336. https://doi.org/10.1093/petrology/egi056

Lee, H., Muirhead, J. D., Fischer, T. P., Ebinger, C. J., Kattenhorn, S. A., Sharp, Z. D., & Kianji, G. (2016). Massive and prolonged deep carbon emissions associated with continental rifting. *Nature Geoscience*, *9*(2), 145–149. https://doi.org/10.1038/ngeo2622

Lee, S., Kang, N., Park, M., Hwang, J. Y., Yun, S. H., & Jeong, H. Y. (2018). A review on volcanic gas compositions related to volcanic activities and non-volcanological effects. *Geosciences Journal*, *22*(1), 183–197. https://doi.org/10.1007/s12303-017-0056-y

Lefeldt, M., Ranero, C. R., & Grevemeyer, I. (2012). Seismic evidence of tectonic control on the depth of water influx into incoming oceanic plates at subduction trenches. *Geochemistry, Geophysics, Geosystems*, *13*(5). https://doi.org/10.1029/2012GC004043

Lefeuvre, N., Thomas, E., Truche, L., Donzé, F.-V., Cros, T., Dupuy, J., Pinzon-Rincon, L., & Rigollet, C. (2024). Characterizing Natural Hydrogen Occurrences in the Paris Basin From Historical Drilling Records. *Geochemistry, Geophysics, Geosystems*, *25*(5), e2024GC011501. https://doi.org/10.1029/2024GC011501

Lefeuvre, N., Truche, L., Donzé, F.-V., Ducoux, M., Barré, G., Fakoury, R.-A., Calassou, S., & Gaucher, E. C. (2021). Native H_2 Exploration in the Western Pyrenean Foothills. *Geochemistry, Geophysics, Geosystems*, *22*(8), e2021GC009917. https://doi.org/10.1029/2021GC009917

Lefeuvre, N., Truche, L., Donzé, F.-V., Gal, F., Tremosa, J., Fakoury, R.-A., Calassou, S., & Gaucher, E. C. (2022). Natural hydrogen migration along thrust faults in foothill basins: The North Pyrenean Frontal Thrust case study. *Applied Geochemistry*, *145*, 105396. https://doi.org/10.1016/j.apgeochem.2022.105396

Leong, J. A. M., Ely, T., & Shock, E. L. (2021). Decreasing extents of Archean serpentinization contributed to the rise of an oxidized atmosphere. *Nature Communications*, *12*(1), Article

1. https://doi.org/10.1038/s41467-021-27589-7

Leong, J. A. M., Nielsen, M., McQueen, N., Karolytė, R., Hillegonds, D. J., Ballentine, C., Darrah, T., McGillis, W., & Kelemen, P. (2023). H_2 and CH_4 outgassing rates in the Samail ophiolite, Oman: Implications for low-temperature, continental serpentinization rates. *Geochimica et Cosmochimica Acta*, *347*, 1–15. https://doi.org/10.1016/j.gca.2023.02.008

Lévy, D., Roche, V., Pasquet, G., Combaudon, V., Geymond, U., Loiseau, K., & Moretti, I. (2023). Natural H_2 exploration: Tools and workflows to characterize a play. *Science and Technology for Energy Transition*, *78*, 27. https://doi.org/10.2516/stet/2023021

Li, X., Krooss, B. M., Ostertag-Henning, C., Weniger, P., & Littke, R. (2018). Liberation of hydrogen-containing gases during closed system pyrolysis of immature organic matter-rich shales. *International Journal of Coal Geology*, *185*, 23–32. https://doi.org/10.1016/j.coal.2017.11.001

Li, X., Krooss, B. M., Weniger, P., & Littke, R. (2015). Liberation of molecular hydrogen (H_2) and methane (CH_4) during non-isothermal pyrolysis of shales and coals: Systematics and quantification. *International Journal of Coal Geology*, *137*, 152–164. https://doi.org/10.1016/j.coal.2014.11.011

Li, X., Krooss, B. M., Weniger, P., & Littke, R. (2017). Molecular hydrogen (H_2) and light hydrocarbon gases generation from marine and lacustrine source rocks during closed-system laboratory pyrolysis experiments. *Journal of Analytical and Applied Pyrolysis*, *126*, 275–287. https://doi.org/10.1016/j.jaap.2017.05.019

Li, Y. (2017). Immiscible C-H-O fluids formed at subduction zone conditions. *Geochemical Perspectives Letters*, 12–21. https://doi.org/10.7185/geochemlet.1702

Li, Y., Du, J., Wang, X., Zhou, X., Xie, C., & Cui, Y. (2013). Spatial Variations of Soil Gas Geochemistry in the Tangshan Area of Northern China. *Terrestrial, Atmospheric and Oceanic Sciences*, *24*(3), 323. https://doi.org/10.3319/TAO.2012.11.26.01(TT)

Li, Y., Vočadlo, L., Sun, T., & Brodholt, J. P. (2020). The Earth's core as a reservoir of water. *Nature Geoscience*, *13*(6), 453–458. https://doi.org/10.1038/s41561-020-0578-1

Li, Z.-X. A., & Lee, C.-T. A. (2004). The constancy of upper mantle fO_2 through time inferred from V/Sc ratios in basalts. *Earth and Planetary Science Letters*, *228*(3), 483–493. https://doi.org/10.1016/j.epsl.2004.10.006

Liang, Y., Cui, W., Masuda, Y., Hirose, T., & Tsuji, T. (2024). *Identifying General Reaction Conditions for Mechanoradical Natural Hydrogen Production*. Research Square. https://doi.org/10.21203/rs.3.rs-4001833/v1

Liggins, P., Shorttle, O., & Rimmer, P. B. (2020). Can volcanism build hydrogen-rich early

atmospheres? *Earth and Planetary Science Letters*, *550*, 116546. https://doi.org/10.1016/j.epsl.2020.116546

Lilley, M. D., Butterfield, D. A., Lupton, J. E., & Olson, E. J. (2003). Magmatic events can produce rapid changes in hydrothermal vent chemistry. *Nature*, *422*(6934), 878–881. https://doi.org/10.1038/nature01569

Lima-Zaloumis, J., Neubeck, A., Ivarsson, M., Bose, M., Greenberger, R., Templeton, A. S., Czaja, A. D., Kelemen, P. B., & Edvinsson, T. (2022). Microbial biosignature preservation in carbonated serpentine from the Samail Ophiolite, Oman. *Communications Earth & Environment*, *3*(1), 1–11. https://doi.org/10.1038/s43247-022-00551-1

Lin, H.-T., Cowen, J. P., Olson, E. J., Lilley, M. D., Jungbluth, S. P., Wilson, S. T., & Rappé, M. S. (2014). Dissolved hydrogen and methane in the oceanic basaltic biosphere. *Earth and Planetary Science Letters*, *405*, 62–73. https://doi.org/10.1016/j.epsl.2014.07.037

Lin, L.-H., Hall, J., Lippmann-Pipke, J., Ward, J. A., Sherwood Lollar, B., DeFlaun, M., Rothmel, R., Moser, D., Gihring, T. M., Mislowack, B., & Onstott, T. C. (2005). Radiolytic H_2 in continental crust: Nuclear power for deep subsurface microbial communities. *Geochemistry, Geophysics, Geosystems*, *6*(7). https://doi.org/10.1029/2004GC000907

Lin, L.-H., Slater, G. F., Sherwood Lollar, B., Lacrampe-Couloume, G., & Onstott, T. C. (2005). The yield and isotopic composition of radiolytic H_2, a potential energy source for the deep subsurface biosphere. *Geochimica et Cosmochimica Acta*, *69*(4), 893–903. https://doi.org/10.1016/j.gca.2004.07.032

Lippmann-Pipke, J., Sherwood Lollar, B., Niedermann, S., Stroncik, N. A., Naumann, R., van Heerden, E., & Onstott, T. C. (2011). Neon identifies two billion year old fluid component in Kaapvaal Craton. *Chemical Geology*, *283*(3), 287–296. https://doi.org/10.1016/j.chemgeo.2011.01.028

Liu, H., Zhang, B., Fei, H., & Liu, L. (2024). A first-principles molecular dynamics study of molecular hydrogen diffusion in Fe-free olivine. *Geoscience Frontiers*, 101926. https://doi.org/10.1016/j.gsf.2024.101926

Liu, Q., Wei, Y., Li, P., Huang, X., Meng, Q., Wu, X., Zhu, D., Xu, H., Fu, Y., Zhu, D., Zhang, W., & Jin, Z. (2025). Natural hydrogen in the volcanic-bearing sedimentary basin: Origin, conversion, and production rates. *Science Advances*. https://www.science.org/doi/10.1126/sciadv.adr6771

Liu, Z., Perez-Gussinye, M., García-Pintado, J., Mezri, L., & Bach, W. (2023). Mantle serpentinization and associated hydrogen flux at North Atlantic magma-poor rifted margins. *Geology*. https://doi.org/10.1130/G50722.1

Lodhia, B. H., & Clark, S. R. (2022). Computation of vertical fluid mobility of CO_2 , methane, hydrogen and hydrocarbons through sandstones and carbonates. *Scientific Reports*, *12*(1), 10216. https://doi.org/10.1038/s41598-022-14234-6

Löffler, M., Schrader, M., Lüders, K., Werban, U., Hornbruch, G., Dahmke, A., Vogt, C., & Richnow, H. H. (2022). Stable Hydrogen Isotope Fractionation of Hydrogen in a Field Injection Experiment: Simulation of a Gaseous H2 Leakage. *ACS Earth and Space Chemistry*, *6*(3), 631–641. https://doi.org/10.1021/acsearthspacechem.1c00254

Lopez-Lazaro, C., Bachaud, P., Moretti, I., & Ferrando, N. (2019). Predicting the phase behavior of hydrogen in NaCl brines by molecular simulation for geological applications. *BSGF - Earth Sciences Bulletin*, *190*, 7. https://doi.org/10.1051/bsgf/2019008

Lorant, F., & Behar, F. (2002). Late Generation of Methane from Mature Kerogens. *Energy & Fuels*, *16*(2), 412–427. https://doi.org/10.1021/ef010126x

Lupton, F. S., Conrad, R., & Zeikus, J. G. (1984). Physiological function of hydrogen metabolism during growth of sulfidogenic bacteria on organic substrates. *Journal of Bacteriology*, *159*(3), 843–849. https://doi.org/10.1128/jb.159.3.843-849.1984

Luxem, K. E., Leavitt, W. D., & Zhang, X. (2020). Large Hydrogen Isotope Fractionation Distinguishes Nitrogenase-Derived Methane from Other Methane Sources. *Applied and Environmental Microbiology*, *86*(19), e00849-20. https://doi.org/10.1128/AEM.00849-20

Macdonald, M. L., Wadham, J. L., Telling, J., & Skidmore, M. L. (2018). Glacial Erosion Liberates Lithologic Energy Sources for Microbes and Acidity for Chemical Weathering Beneath Glaciers and Ice Sheets. *Frontiers in Earth Science*, *6*. https://doi.org/10.3389/feart.2018.00212

Mackwell, S. J., & Kohlstedt, D. L. (1990). Diffusion of hydrogen in olivine: Implications for water in the mantle. *Journal of Geophysical Research: Solid Earth*, *95*(B4), 5079–5088. https://doi.org/10.1029/JB095iB04p05079

Mahlstedt, N., Horsfield, B., Weniger, P., Misch, D., Shi, X., Noah, M., & Boreham, C. (2022). Molecular hydrogen from organic sources in geological systems. *Journal of Natural Gas Science and Engineering*, *105*, 104704. https://doi.org/10.1016/j.jngse.2022.104704

Maiga, O., Deville, E., Laval, J., Prinzhofer, A., & Diallo, A. B. (2023). Characterization of the spontaneously recharging natural hydrogen reservoirs of Bourakebougou in Mali. *Scientific Reports*, *13*(1), 11876. https://doi.org/10.1038/s41598-023-38977-y

Malvoisin, B., Brantut, N., & Kaczmarek, M.-A. (2017). Control of serpentinisation rate by reaction-induced cracking. *Earth and Planetary Science Letters*, *476*, 143–152. https://doi.org/10.1016/j.epsl.2017.07.042

Malvoisin, B., & Brunet, F. (2023). Barren ground depressions, natural H_2 and orogenic gold deposits: Spatial link and geochemical model. *Science of The Total Environment*, *856*, 158969. https://doi.org/10.1016/j.scitotenv.2022.158969

Mann, P., & Taira, A. (2004). Global tectonic significance of the Solomon Islands and Ontong Java Plateau convergent zone. *Tectonophysics*, *389*(3), 137–190. https://doi.org/10.1016/j.tecto.2003.10.024

Marcaillou, C., Muñoz, M., Vidal, O., Parra, T., & Harfouche, M. (2011). Mineralogical evidence for H_2 degassing during serpentinization at 300 °C/300 bar. *Earth and Planetary Science Letters*, *303*(3), 281–290. https://doi.org/10.1016/j.epsl.2011.01.006

Mareschal, J.-C., & Jaupart, C. (2006). Archean Thermal Regime and Stabilization of the Cratons. In *Archean Geodynamics and Environments* (pp. 61–73). American Geophysical Union (AGU). https://doi.org/10.1029/164GM06

Martin, C., Flores, K. E., Vitale Brovarone, A., Angiboust, S., & Harlow, G. E. (2020). Deep mantle serpentinization in subduction zones: Insight from in situ B isotopes in slab and mantle wedge serpentinites. *Chemical Geology*, *545*, 119637. https://doi.org/10.1016/j.chemgeo.2020.119637

Martin, W., Baross, J., Kelley, D., & Russell, M. J. (2008). Hydrothermal vents and the origin of life. *Nature Reviews Microbiology*, *6*(11), 805–814. https://doi.org/10.1038/nrmicro1991

Martin, W., & Müller, M. (1998). The hydrogen hypothesis for the first eukaryote. *Nature*, *392*(6671), 37–41. https://doi.org/10.1038/32096

Marty, B. (2012). The origins and concentrations of water, carbon, nitrogen and noble gases on Earth. *Earth and Planetary Science Letters*, *313–314*, 56–66. https://doi.org/10.1016/j.epsl.2011.10.040

Marty, B., Avice, G., Sano, Y., Altwegg, K., Balsiger, H., Hässig, M., Morbidelli, A., Mousis, O., & Rubin, M. (2016). Origins of volatile elements (H, C, N, noble gases) on Earth and Mars in light of recent results from the ROSETTA cometary mission. *Earth and Planetary Science Letters*, *441*, 91–102. https://doi.org/10.1016/j.epsl.2016.02.031

Matthews, K. J., Maloney, K. T., Zahirovic, S., Williams, S. E., Seton, M., & Müller, R. D. (2016). Global plate boundary evolution and kinematics since the late Paleozoic. *Global and Planetary Change*, *146*, 226–250. https://doi.org/10.1016/j.gloplacha.2016.10.002

Mavrogenes, J. A., & Bodnar, R. J. (1994). Hydrogen movement into and out of fluid inclusions in quartz: Experimental evidence and geologic implications. *Geochimica et Cosmochimica Acta*, *58*(1), 141–148. https://doi.org/10.1016/0016-7037(94)90452-9

Mayhew, L. E., & Ellison, E. T. (2020). A synthesis and meta-analysis of the Fe chemistry of

serpentinites and serpentine minerals. *Philosophical Transactions of the Royal Society A: Mathematical, Physical and Engineering Sciences*, *378*(2165), 20180420. https://doi.org/10.1098/rsta.2018.0420

Mayhew, L. E., Ellison, E. T., McCollom, T. M., Trainor, T. P., & Templeton, A. S. (2013). Hydrogen generation from low-temperature water–rock reactions. *Nature Geoscience*, *6*(6), 478–484. https://doi.org/10.1038/ngeo1825

McCaig, A. M. (1988). Deep fluid circulation in fault zones. *Geology*, *16*(10), 867–870. https://doi.org/10.1130/0091-7613(1988)016<0867:DFCIFZ>2.3.CO;2

McCammon, C. (2005). The Paradox of Mantle Redox. *Science*, *308*(5723), 807–808. https://doi.org/10.1126/science.1110532

McCollom, T. M. (2003). Formation of meteorite hydrocarbons from thermal decomposition of siderite ($FeCO_3$). *Geochimica et Cosmochimica Acta*, *67*(2), 311–317. https://doi.org/10.1016/S0016-7037(02)00945-6

McCollom, T. M. (2013). Laboratory Simulations of Abiotic Hydrocarbon Formation in Earth's Deep Subsurface. *Reviews in Mineralogy and Geochemistry*, *75*(1), 467–494. https://doi.org/10.2138/rmg.2013.75.15

McCollom, T. M., & Bach, W. (2009). Thermodynamic constraints on hydrogen generation during serpentinization of ultramafic rocks. *Geochimica et Cosmochimica Acta*, *73*(3), 856–875. https://doi.org/10.1016/j.gca.2008.10.032

McCollom, T. M., & Donaldson, C. (2016). Generation of Hydrogen and Methane during Experimental Low-Temperature Reaction of Ultramafic Rocks with Water. *Astrobiology*, *16*(6), 389–406. https://doi.org/10.1089/ast.2015.1382

McCollom, T. M., Klein, F., Moskowitz, B., Berquó, T. S., Bach, W., & Templeton, A. S. (2020). Hydrogen generation and iron partitioning during experimental serpentinization of an olivine–pyroxene mixture. *Geochimica et Cosmochimica Acta*, *282*, 55–75. https://doi.org/10.1016/j.gca.2020.05.016

McCollom, T. M., Klein, F., & Ramba, M. (2022). Hydrogen generation from serpentinization of iron-rich olivine on Mars, icy moons, and other planetary bodies. *Icarus*, *372*, 114754. https://doi.org/10.1016/j.icarus.2021.114754

McCollom, T. M., Klein, F., Robbins, M., Moskowitz, B., Berquó, T. S., Jöns, N., Bach, W., & Templeton, A. (2016). Temperature trends for reaction rates, hydrogen generation, and partitioning of iron during experimental serpentinization of olivine. *Geochimica et Cosmochimica Acta*, *181*, 175–200. https://doi.org/10.1016/j.gca.2016.03.002

McCollom, T. M., Klein, F., Solheid, P., & Moskowitz, B. (2020). The effect of pH on rates of

reaction and hydrogen generation during serpentinization. *Philosophical Transactions of the Royal Society A: Mathematical, Physical and Engineering Sciences*, *378*(2165), 20180428. https://doi.org/10.1098/rsta.2018.0428

McCollom, T. M., & Seewald, J. S. (2013). Serpentinites, Hydrogen, and Life. *Elements*, *9*(2), 129–134. https://doi.org/10.2113/gselements.9.2.129

McDermott, J. M., Sylva, S. P., Ono, S., German, C. R., & Seewald, J. S. (2018). Geochemistry of fluids from Earth's deepest ridge-crest hot-springs: Piccard hydrothermal field, Mid-Cayman Rise. *Geochimica et Cosmochimica Acta*, *228*, 95–118. https://doi.org/10.1016/j.gca.2018.01.021

McDonough, W. F., & Sun, S. -s. (1995). The composition of the Earth. *Chemical Geology*, *120*, 223–253. https://doi.org/10.1016/0009-2541(94)00140-4

McMahon, S., Parnell, J., & Blamey, N. J. F. (2016). Evidence for Seismogenic Hydrogen Gas, a Potential Microbial Energy Source on Earth and Mars. *Astrobiology*, *16*(9), 690–702. https://doi.org/10.1089/ast.2015.1405

Megonigal, J. P., Hines, M. E., & Visscher, P. T. (2004). Anaerobic metabolism: Linkages to trace gases and aerobic processes. *Biogeochemistry*.

Ménez, B. (2020). Abiotic Hydrogen and Methane: Fuels for Life. *Elements*, *16*(1), 39–46. https://doi.org/10.2138/gselements.16.1.39

Merdith, A. S., Daniel, I., Sverjensky, D., Andreani, M., Mather, B., Williams, S., & Vitale Brovarone, A. (2023). Global Hydrogen Production During High-Pressure Serpentinization of Subducting Slabs. *Geochemistry, Geophysics, Geosystems*, *24*(10), e2023GC010947. https://doi.org/10.1029/2023GC010947

Merdith, A. S., del Real, P. G., Daniel, I., Andreani, M., Wright, N. M., & Coltice, N. (2020). Pulsated Global Hydrogen and Methane Flux at Mid-Ocean Ridges Driven by Pangea Breakup. *Geochemistry, Geophysics, Geosystems*, *21*(4), e2019GC008869. https://doi.org/10.1029/2019GC008869

Michalski, J. R., Cuadros, J., Niles, P. B., Parnell, J., Deanne Rogers, A., & Wright, S. P. (2013). Groundwater activity on Mars and implications for a deep biosphere. *Nature Geoscience*, *6*(2), Article 2. https://doi.org/10.1038/ngeo1706

Milesi, V., Guyot, F., Brunet, F., Richard, L., Recham, N., Benedetti, M., Dairou, J., & Prinzhofer, A. (2015). Formation of CO_2, H_2 and condensed carbon from siderite dissolution in the 200–300°C range and at 50 MPa. *Geochimica et Cosmochimica Acta*, *154*, 201–211. https://doi.org/10.1016/j.gca.2015.01.015

Milesi, V., Prinzhofer, A., Guyot, F., Benedetti, M., & Rodrigues, R. (2016). Contribution of

siderite–water interaction for the unconventional generation of hydrocarbon gases in the Solimões basin, north-west Brazil. *Marine and Petroleum Geology*, *71*, 168–182. https://doi.org/10.1016/j.marpetgeo.2015.12.022

Milkov, A. V. (2022). Molecular hydrogen in surface and subsurface natural gases: Abundance, origins and ideas for deliberate exploration. *Earth-Science Reviews*, *230*, 104063. https://doi.org/10.1016/j.earscirev.2022.104063

Miller, H. M., Mayhew, L. E., Ellison, E. T., Kelemen, P., Kubo, M., & Templeton, A. S. (2017). Low temperature hydrogen production during experimental hydration of partially-serpentinized dunite. *Geochimica et Cosmochimica Acta*, *209*, 161–183. https://doi.org/10.1016/j.gca.2017.04.022

Miller, N. C., & Lizarralde, D. (2016). Finite-frequency wave propagation through outer rise fault zones and seismic measurements of upper mantle hydration. *Geophysical Research Letters*, *43*(15), 7982–7990. https://doi.org/10.1002/2016GL070083

Miller, N. C., Lizarralde, D., Collins, J. A., Holbrook, W. S., & Van Avendonk, H. J. A. (2021). Limited Mantle Hydration by Bending Faults at the Middle America Trench. *Journal of Geophysical Research: Solid Earth*, *126*(1), e2020JB020982. https://doi.org/10.1029/2020JB020982

Minshull, T. A. (2009). Geophysical characterisation of the ocean–continent transition at magma-poor rifted margins. *Comptes Rendus. Géoscience*, *341*(5), 382–393. https://doi.org/10.1016/j.crte.2008.09.003

Miocic, J., Heinemann, N., Edlmann, K., Scafidi, J., Molaei, F., & Alcalde, J. (2023). Underground hydrogen storage: A review. *Geological Society, London, Special Publications*, *528*(1), 73–86. https://doi.org/10.1144/SP528-2022-88

Miozzi, F., & Tumiati, S. (2020). Aqueous concentration of CO_2 in carbon-saturated fluids as a highly sensitive oxybarometer. *Geochemical Perspectives Letters*, *16*, 30–34. https://doi.org/10.7185/geochemlet.2040

Moine, B. N., Bolfan-Casanova, N., Radu, I. B., Ionov, D. A., Costin, G., Korsakov, A. V., Golovin, A. V., Oleinikov, O. B., Deloule, E., & Cottin, J. Y. (2020). Molecular hydrogen in minerals as a clue to interpret ∂D variations in the mantle. *Nature Communications*, *11*(1), 3604. https://doi.org/10.1038/s41467-020-17442-8

Moretti, I., Baby, P., Alvarez Zapata, P., & Mendoza, R. V. (2023). Subduction and Hydrogen Release: The Case of Bolivian Altiplano. *Geosciences*, *13*(4), Article 4. https://doi.org/10.3390/geosciences13040109

Moretti, I., Bouton, N., Ammouial, J., & Carrillo Ramirez, A. (2024). The H_2 potential of the

Colombian coals in natural conditions. *International Journal of Hydrogen Energy*, *77*, 1443–1456. https://doi.org/10.1016/j.ijhydene.2024.06.225

Moretti, I., Brouilly, E., Loiseau, K., Prinzhofer, A., & Deville, E. (2021). Hydrogen Emanations in Intracratonic Areas: New Guide Lines for Early Exploration Basin Screening. *Geosciences*, *11*(3), Article 3. https://doi.org/10.3390/geosciences11030145

Moretti, I., Prinzhofer, A., Françolin, J., Pacheco, C., Rosanne, M., Rupin, F., & Mertens, J. (2021). Long-term monitoring of natural hydrogen superficial emissions in a Brazilian cratonic environment. Sporadic large pulses versus daily periodic emissions. *International Journal of Hydrogen Energy*, *46*(5), 3615–3628. https://doi.org/10.1016/j.ijhydene.2020.11.026

Moretti, R., & Papale, P. (2004). On the oxidation state and volatile behavior in multicomponent gas–melt equilibria. *Chemical Geology*, *213*(1), 265–280. https://doi.org/10.1016/j.chemgeo.2004.08.048

Mörner, N.-A., & Etiope, G. (2002). Carbon degassing from the lithosphere. *Global and Planetary Change*, *33*(1), 185–203. https://doi.org/10.1016/S0921-8181(02)00070-X

Morris, B. E. L., Henneberger, R., Huber, H., & Moissl-Eichinger, C. (2013). Microbial syntrophy: Interaction for the common good. *FEMS Microbiology Reviews*, *37*(3), 384–406. https://doi.org/10.1111/1574-6976.12019

Mottl, M. J., Komor, S. C., Fryer, P., & Moyer, C. L. (2003). Deep-slab fluids fuel extremophilic Archaea on a Mariana forearc serpentinite mud volcano: Ocean Drilling Program Leg 195. *Geochemistry, Geophysics, Geosystems*, *4*(11). https://doi.org/10.1029/2003GC000588

Moussallam, Y., Oppenheimer, C., Aiuppa, A., Giudice, G., Moussallam, M., & Kyle, P. (2012). Hydrogen emissions from Erebus volcano, Antarctica. *Bulletin of Volcanology*, *74*(9), 2109–2120. https://doi.org/10.1007/s00445-012-0649-2

Moussallam, Y., Oppenheimer, C., & Scaillet, B. (2019). On the relationship between oxidation state and temperature of volcanic gas emissions. *Earth and Planetary Science Letters*, *520*, 260–267. https://doi.org/10.1016/j.epsl.2019.05.036

Moussallam, Y., Oppenheimer, C., & Scaillet, B. (2024). A novel approach to volcano surveillance using gas geochemistry. *Comptes Rendus. Géoscience*, *356*(S1), 1–14. https://doi.org/10.5802/crgeos.158

Muhammed, N. S., Haq, B., Al Shehri, D., Al-Ahmed, A., Rahman, M. M., & Zaman, E. (2022). A review on underground hydrogen storage: Insight into geological sites, influencing factors and future outlook. *Energy Reports*, *8*, 461–499. https://doi.org/10.1016/j.egyr.2021.12.002

Mukhopadhyay, S., & Parai, R. (2019). Noble Gases: A Record of Earth's Evolution and Mantle

Dynamics. *Annual Review of Earth and Planetary Sciences*, *47*(Volume 47, 2019), 389–419. https://doi.org/10.1146/annurev-earth-053018-060238

Murray, J., Clément, A., Fritz, B., Schmittbuhl, J., Bordmann, V., & Fleury, J. M. (2020). Abiotic hydrogen generation from biotite-rich granite: A case study of the Soultz-sous-Forêts geothermal site, France. *Applied Geochemistry*, *119*, 104631. https://doi.org/10.1016/j.apgeochem.2020.104631

Myagkiy, A., Brunet, F., Popov, C., Krüger, R., Guimarães, H., Sousa, R. S., Charlet, L., & Moretti, I. (2020). H_2 dynamics in the soil of a H_2-emitting zone (São Francisco Basin, Brazil): Microbial uptake quantification and reactive transport modelling. *Applied Geochemistry*, *112*, 104474. https://doi.org/10.1016/j.apgeochem.2019.104474

Naliboff, J. B., Billen, M. I., Gerya, T., & Saunders, J. (2013). Dynamics of outer-rise faulting in oceanic-continental subduction systems. *Geochemistry, Geophysics, Geosystems*, *14*(7), 2310–2327. https://doi.org/10.1002/ggge.20155

Nealson, K. H., Inagaki, F., & Takai, K. (2005). Hydrogen-driven subsurface lithoautotrophic microbial ecosystems (SLiMEs): Do they exist and why should we care? *Trends in Microbiology*, *13*(9), 405–410. https://doi.org/10.1016/j.tim.2005.07.010

Nehemia, V., Davidi, S., & Cohen, H. (1999). Emission of hydrogen gas from weathered steam coal piles via formaldehyde as a precursor: I. Oxidative decomposition of formaldehyde catalyzed by coal – batch reactor studies. *Fuel*, *78*(7), 775–780. https://doi.org/10.1016/S0016-2361(98)00219-1

Neubeck, A., Duc, N. T., Bastviken, D., Crill, P., & Holm, N. G. (2011). Formation of H_2 and CH_4 by weathering of olivine at temperatures between 30 and 70°C. *Geochemical Transactions*, *12*(1), 6. https://doi.org/10.1186/1467-4866-12-6

Neubeck, A., Duc, N. T., Hellevang, H., Oze, C., Bastviken, D., Bacsik, Z., & Holm, N. G. (2014). Olivine alteration and H_2 production in carbonate-rich, low temperature aqueous environments. *Planetary and Space Science*, *96*, 51–61. https://doi.org/10.1016/j.pss.2014.02.014

Ni, Y., Ma, Q., Ellis, G. S., Dai, J., Katz, B., Zhang, S., & Tang, Y. (2011). Fundamental studies on kinetic isotope effect (KIE) of hydrogen isotope fractionation in natural gas systems. *Geochimica et Cosmochimica Acta*, *75*(10), 2696–2707. https://doi.org/10.1016/j.gca.2011.02.016

Novella, D., Demouchy, S., & Bolfan-Casanova, N. (2024). Deep Hydrogen Reservoirs and Longevity. *Elements*, *20*(4), 235–240. https://doi.org/10.2138/gselements.20.4.235

Novelli, P. C., Lang, P. M., Masarie, K. A., Hurst, D. F., Myers, R., & Elkins, J. W. (1999). Molecular

hydrogen in the troposphere: Global distribution and budget. *Journal of Geophysical Research: Atmospheres*, *104*(D23), 30427–30444. https://doi.org/10.1029/1999JD900788

Nozaka, T. (2018). Compositional variation of olivine related to high–temperature serpentinization of peridotites: Evidence from the Oeyama ophiolite. *Journal of Mineralogical and Petrological Sciences*, *113*(5), 219–231. https://doi.org/10.2465/jmps.180420

Okland, I., Huang, S., Thorseth, I. H., & Pedersen, R. B. (2014). Formation of H_2, CH_4 and N-species during low-temperature experimental alteration of ultramafic rocks. *Chemical Geology*, *387*, 22–34. https://doi.org/10.1016/j.chemgeo.2014.08.003

Olivieri, O. S. (2025). *Characterization of H_2 and hydrocarbons trapped in exhumed metamorphic rocks: Origin and fluxes of energy sources in subduction zones* [PhD thesis]. University of Bologna.

Onstott, T. C., McGown, D., Kessler, J., Lollar, B. S., Lehmann, K. K., & Clifford, S. M. (2006). Martian CH_4: Sources, Flux, and Detection. *Astrobiology*, *6*(2), 377–395. https://doi.org/10.1089/ast.2006.6.377

Oppenheimer, C. (2003). Volcanic Degassing. In R. L. Rudnick (Ed.), *The Crust* (Vol. 3). Elsevier.

Oppenheimer, C., Scaillet, B., Woods, A., Sutton, A. J., Elias, T., & Moussallam, Y. (2018). Influence of eruptive style on volcanic gas emission chemistry and temperature. *Nature Geoscience*, *11*(9), 678–681. https://doi.org/10.1038/s41561-018-0194-5

Osburn, M. R., Dawson, K. S., Fogel, M. L., & Sessions, A. L. (2016). Fractionation of Hydrogen Isotopes by Sulfate- and Nitrate-Reducing Bacteria. *Frontiers in Microbiology*, *7*. https://doi.org/10.3389/fmicb.2016.01166

Osselin, F., Soulaine, C., Fauguerolles, C., Gaucher, E. C., Scaillet, B., & Pichavant, M. (2022). Orange hydrogen is the new green. *Nature Geoscience*, *15*(10), 765–769. https://doi.org/10.1038/s41561-022-01043-9

Palme, H., Lodders, K., & Jones, A. (2014). Solar System Abundances of the Elements. In *Treatise on Geochemistry* (pp. 15–36). Elsevier. https://doi.org/10.1016/B978-0-08-095975-7.00118-2

Parkes, R. J., Berlendis, S., Roussel, E. G., Bahruji, H., Webster, G., Oldroyd, A., Weightman, A. J., Bowker, M., Davies, P. R., & Sass, H. (2019). Rock-crushing derived hydrogen directly supports a methanogenic community: Significance for the deep biosphere. *Environmental Microbiology Reports*, *11*(2), 165–172. https://doi.org/10.1111/1758-2229.12723

Parkes, R. J., Linnane, C. D., Webster, G., Sass, H., Weightman, A. J., Hornibrook, E. R. C., & Horsfield, B. (2011). Prokaryotes stimulate mineral H_2 formation for the deep biosphere

and subsequent thermogenic activity. *Geology*, *39*(3), 219–222. https://doi.org/10.1130/G31598.1

Parkes, R. J., Wellsbury, P., Mather, I. D., Cobb, S. J., Cragg, B. A., Hornibrook, E. R. C., & Horsfield, B. (2007). Temperature activation of organic matter and minerals during burial has the potential to sustain the deep biosphere over geological timescales. *Organic Geochemistry*, *38*(6), 845–852. https://doi.org/10.1016/j.orggeochem.2006.12.011

Parnell, J., & Blamey, N. (2017a). Global hydrogen reservoirs in basement and basins. *Geochemical Transactions*, *18*(1), 2. https://doi.org/10.1186/s12932-017-0041-4

Parnell, J., & Blamey, N. (2017b). Hydrogen from Radiolysis of Aqueous Fluid Inclusions during Diagenesis. *Minerals*, *7*(8), Article 8. https://doi.org/10.3390/min7080130

Parnell, J., & McMahon, S. (2016). Physical and chemical controls on habitats for life in the deep subsurface beneath continents and ice. *Philosophical Transactions of the Royal Society A: Mathematical, Physical and Engineering Sciences*, *374*(2059), 20140293. https://doi.org/10.1098/rsta.2014.0293

Pasquet, G., Houssein Hassan, R., Sissmann, O., Varet, J., & Moretti, I. (2022). An Attempt to Study Natural H_2 Resources across an Oceanic Ridge Penetrating a Continent: The Asal–Ghoubbet Rift (Republic of Djibouti). *Geosciences*, *12*(1), Article 1. https://doi.org/10.3390/geosciences12010016

Pasquet, G., Idriss, A. M., Ronjon-Magand, L., Ranchou-Peyruse, M., Guignard, M., Duttine, M., Ranchou-Peyruse, A., & Moretti, I. (2023). Natural hydrogen potential and basaltic alteration in the Asal–Ghoubbet rift, Republic of Djibouti. *BSGF - Earth Sciences Bulletin*, *194*, 9. https://doi.org/10.1051/bsgf/2023004

Pastina, B., LaVerne, J. A., & Pimblott, S. M. (1999). Dependence of Molecular Hydrogen Formation in Water on Scavengers of the Precursor to the Hydrated Electron. *The Journal of Physical Chemistry A*, *103*(29), 5841–5846. https://doi.org/10.1021/jp991222q

Patterson, J. D., Aydin, M., Crotwell, A. M., Petron, G., Severinghaus, J. P., & Saltzman, E. S. (2020). Atmospheric History of H_2 Over the Past Century Reconstructed From South Pole Firn Air. *Geophysical Research Letters*, *47*(14), e2020GL087787. https://doi.org/10.1029/2020GL087787

Peacock, S. M., & Bostock, M. G. (2024). Serpentinization of the forearc mantle wedge in subduction zones: Revisiting Roy D. Hyndman's seminal contributions 25 years later. *Canadian Journal of Earth Sciences*, cjes-2024-0082. https://doi.org/10.1139/cjes-2024-0082

Peacock, S. M., & Hyndman, R. D. (1999). Hydrous minerals in the mantle wedge and the

maximum depth of subduction thrust earthquakes. *Geophysical Research Letters*, *26*(16), 2517–2520. https://doi.org/10.1029/1999GL900558

Peng, W., Zhang, L., Tumiati, S., Vitale Brovarone, A., Hu, H., Cai, Y., & Shen, T. (2021). Abiotic methane generation through reduction of serpentinite-hosted dolomite: Implications for carbon mobility in subduction zones. *Geochimica et Cosmochimica Acta*, *311*, 119–140. https://doi.org/10.1016/j.gca.2021.07.033

Perera, M. S. A. (2023). A review of underground hydrogen storage in depleted gas reservoirs: Insights into various rock-fluid interaction mechanisms and their impact on the process integrity. *Fuel*, *334*, 126677. https://doi.org/10.1016/j.fuel.2022.126677

Perk, N. W., Coogan, L. A., Karson, J. A., Klein, E. M., & Hanna, H. D. (2007). Petrology and geochemistry of primitive lower oceanic crust from Pito Deep: Implications for the accretion of the lower crust at the Southern East Pacific Rise. *Contributions to Mineralogy and Petrology*, *154*(5), 575–590. https://doi.org/10.1007/s00410-007-0210-z

Pester, N. J., Conrad, M. E., Knauss, K. G., & DePaolo, D. J. (2018). Kinetics of D/H isotope fractionation between molecular hydrogen and water. *Geochimica et Cosmochimica Acta*, *242*, 191–212. https://doi.org/10.1016/j.gca.2018.09.015

Petersen, J. M., Zielinski, F. U., Pape, T., Seifert, R., Moraru, C., Amann, R., Hourdez, S., Girguis, P. R., Wankel, S. D., Barbe, V., Pelletier, E., Fink, D., Borowski, C., Bach, W., & Dubilier, N. (2011). Hydrogen is an energy source for hydrothermal vent symbioses. *Nature*, *476*(7359), 176–180. https://doi.org/10.1038/nature10325

Peverelli, V., Olivieri, O. S., Tsujimori, T., Giovannelli, D., Shi, G., Cannaò, E., Piccoli, F., & Vitale Brovarone, A. (2024). Cold-subduction biogeodynamics boosts deep energy delivery to the forearc. *Geochimica et Cosmochimica Acta*. https://doi.org/10.1016/j.gca.2024.10.004

Pfeffer, W. T., Arendt, A. A., Bliss, A., Bolch, T., Cogley, J. G., Gardner, A. S., Hagen, J.-O., Hock, R., Kaser, G., Kienholz, C., Miles, E. S., Moholdt, G., Mölg, N., Paul, F., Radić, V., Rastner, P., Raup, B. H., Rich, J., Sharp, M. J., & The Randolph Consortium. (2014). The Randolph Glacier Inventory: A globally complete inventory of glaciers. *Journal of Glaciology*, *60*(221), 537–552. https://doi.org/10.3189/2014JoG13J176

Piani, L., Marrocchi, Y., Rigaudier, T., Vacher, L. G., Thomassin, D., & Marty, B. (2020). Earth's water may have been inherited from material similar to enstatite chondrite meteorites. *Science*, *369*(6507), 1110–1113. https://doi.org/10.1126/science.aba1948

Piccoli, F., Ague, J. J., Chu, X., Tian, M., & Vitale Brovarone, A. (2021). Field-Based Evidence for Intra-Slab High-Permeability Channel Formation at Eclogite-Facies Conditions During Subduction. *Geochemistry, Geophysics, Geosystems*, *22*(3), e2020GC009520.

https://doi.org/10.1029/2020GC009520

Pierrehumbert, R., & Gaidos, E. (2011). Hydrogen Greenhouse Planets Beyond The Habitable Zone. *The Astrophysical Journal Letters*, *734*(1), L13. https://doi.org/10.1088/2041-8205/734/1/L13

Pieterse, G., Krol, M. C., Batenburg, A. M., Steele, L. P., Krummel, P. B., Langenfelds, R. L., & Röckmann, T. (2011). Global modelling of H_2 mixing ratios and isotopic compositions with the TM5 model. *Atmospheric Chemistry and Physics*, *11*(14), 7001–7026. https://doi.org/10.5194/acp-11-7001-2011

Plümper, O., King, H. E., Geisler, T., Liu, Y., Pabst, S., Savov, I. P., Rost, D., & Zack, T. (2017). Subduction zone forearc serpentinites as incubators for deep microbial life. *Proceedings of the National Academy of Sciences*, *114*(17), 4324–4329. https://doi.org/10.1073/pnas.1612147114

Potter, J., Salvi, S., & Longstaffe, F. J. (2013). Abiogenic hydrocarbon isotopic signatures in granitic rocks: Identifying pathways of formation. *Lithos*, *182–183*, 114–124. https://doi.org/10.1016/j.lithos.2013.10.001

Preiner, M., Xavier, J. C., Sousa, F. L., Zimorski, V., Neubeck, A., Lang, S. Q., Greenwell, H. C., Kleinermanns, K., Tüysüz, H., McCollom, T. M., Holm, N. G., & Martin, W. F. (2018). Serpentinization: Connecting Geochemistry, Ancient Metabolism and Industrial Hydrogenation. *Life*, *8*(4), Article 4. https://doi.org/10.3390/life8040041

Price, H., Jaeglé, L., Rice, A., Quay, P., Novelli, P. C., & Gammon, R. (2007). Global budget of molecular hydrogen and its deuterium content: Constraints from ground station, cruise, and aircraft observations. *Journal of Geophysical Research: Atmospheres*, *112*(D22). https://doi.org/10.1029/2006JD008152

Prigent, C., Warren, J. M., Kohli, A. H., & Teyssier, C. (2020). Fracture-mediated deep seawater flow and mantle hydration on oceanic transform faults. *Earth and Planetary Science Letters*, *532*, 115988. https://doi.org/10.1016/j.epsl.2019.115988

Prinzhofer, A., & Cacas-Stentz, M.-C. (2023). Natural hydrogen and blend gas: A dynamic model of accumulation. *International Journal of Hydrogen Energy*, *48*(57), 21610–21623. https://doi.org/10.1016/j.ijhydene.2023.03.060

Prinzhofer, A., Rigollet, C., Lefeuvre, N., Françolin, J., & Valadão de Miranda, P. E. (2024). Maricá (Brazil), the new natural hydrogen play which changes the paradigm of hydrogen exploration. *International Journal of Hydrogen Energy*, *62*, 91–98. https://doi.org/10.1016/j.ijhydene.2024.02.263

Prinzhofer, A., Tahara Cissé, C. S., & Diallo, A. B. (2018). Discovery of a large accumulation of

natural hydrogen in Bourakebougou (Mali). *International Journal of Hydrogen Energy*, *43*(42), 19315–19326. https://doi.org/10.1016/j.ijhydene.2018.08.193

Proskurowski, G., Lilley, M. D., Kelley, D. S., & Olson, E. J. (2006). Low temperature volatile production at the Lost City Hydrothermal Field, evidence from a hydrogen stable isotope geothermometer. *Chemical Geology*, *229*(4), 331–343. https://doi.org/10.1016/j.chemgeo.2005.11.005

QGIS Association. (2024). *QGIS Geographic Information System* (Version 3.38.3) [Computer software]. http://www.qgis.org

Ramirez, R. M., & Kaltenegger, L. (2017). A Volcanic Hydrogen Habitable Zone. *The Astrophysical Journal Letters*, *837*(1), L4. https://doi.org/10.3847/2041-8213/aa60c8

Ranero, C. R., Phipps Morgan, J., McIntosh, K., & Reichert, C. (2003). Bending-related faulting and mantle serpentinization at the Middle America trench. *Nature*, *425*(6956), 367–373. https://doi.org/10.1038/nature01961

Reed, M., & Palandri, J. (2008). Hydrogen Produced by Reduction of H_2O in Rock Reaction: Peridotite vs Basalt. *AIP Conference Proceedings*, *987*. https://doi.org/10.1063/1.2896951

Rempfert, K. R., Miller, H. M., Bompard, N., Nothaft, D., Matter, J. M., Kelemen, P., Fierer, N., & Templeton, A. S. (2017). Geological and Geochemical Controls on Subsurface Microbial Life in the Samail Ophiolite, Oman. *Frontiers in Microbiology*, *8*. https://doi.org/10.3389/fmicb.2017.00056

Reston, T. J., & McDermott, K. G. (2011). Successive detachment faults and mantle unroofing at magma-poor rifted margins. *Geology*, *39*(11), 1071–1074. https://doi.org/10.1130/G32428.1

Reynolds, J. G., Crawford, R. W., & Burnham, A. K. (1991). Analysis of oil shale and petroleum source rock pyrolysis by triple quadrupole mass spectrometry: Comparisons of gas evolution at the heating rate of 10.degree.C/min. *Energy & Fuels*, *5*(3), 507–523. https://doi.org/10.1021/ef00027a025

RGI 7.0 Consortium. (2023). *Randolph Glacier Inventory—A Dataset of Global Glacier Outlines, Version 7.0.* [Dataset]. NSIDC: National Snow and Ice Data Center. https://doi.org/doi:10.5067/f6jmovy5navz

Ricci, A., Kleine, B. I., Fiebig, J., Gunnarsson-Robin, J., Mativo Kamunya, K., Mountain, B., & Stefánsson, A. (2022). Equilibrium and kinetic controls on molecular hydrogen abundance and hydrogen isotope fractionation in hydrothermal fluids. *Earth and Planetary Science Letters*, *579*, 117338. https://doi.org/10.1016/j.epsl.2021.117338

Richard, A. (2017). Radiolytic (H_2, O_2) and other Trace Gases (CO_2, CH_4, C_2H_6, N_2) in Fluid

Inclusions from Unconformity-related U Deposits. *Procedia Earth and Planetary Science*, *17*, 273–276. https://doi.org/10.1016/j.proeps.2016.12.053

Rickard, D., & Luther, G. W. (1997). Kinetics of pyrite formation by the H_2S oxidation of iron (II) monosulfide in aqueous solutions between 25 and 125°C: The mechanism. *Geochimica et Cosmochimica Acta*, *61*(1), 135–147. https://doi.org/10.1016/S0016-7037(96)00322-5

Robert, F. (2003). The D/H Ratio in Chondrites. *Space Science Reviews*, *106*(1), 87–101. https://doi.org/10.1023/A:1024629402715

Rogers, T. J., Buongiorno, J., Jessen, G. L., Schrenk, M. O., Fordyce, J. A., de Moor, J. M., Ramírez, C. J., Barry, P. H., Yücel, M., Selci, M., Cordone, A., Giovannelli, D., & Lloyd, K. G. (2023). Chemolithoautotroph distributions across the subsurface of a convergent margin. *The ISME Journal*, *17*(1), Article 1. https://doi.org/10.1038/s41396-022-01331-7

Rohrbach, A., Ballhaus, C., Golla–Schindler, U., Ulmer, P., Kamenetsky, V. S., & Kuzmin, D. V. (2007). Metal saturation in the upper mantle. *Nature*, *449*(7161), 456–458. https://doi.org/10.1038/nature06183

Rohrbach, A., Ballhaus, C., Ulmer, P., Golla-Schindler, U., & Schönbohm, D. (2011). Experimental Evidence for a Reduced Metal-saturated Upper Mantle. *Journal of Petrology*, *52*(4), 717–731. https://doi.org/10.1093/petrology/egq101

Rosentreter, J. A., Borges, A. V., Deemer, B. R., Holgerson, M. A., Liu, S., Song, C., Melack, J., Raymond, P. A., Duarte, C. M., Allen, G. H., Olefeldt, D., Poulter, B., Battin, T. I., & Eyre, B. D. (2021). Half of global methane emissions come from highly variable aquatic ecosystem sources. *Nature Geoscience*, *14*(4), 225–230. https://doi.org/10.1038/s41561-021-00715-2

Rubie, D. C., Frost, D. J., Mann, U., Asahara, Y., Nimmo, F., Tsuno, K., Kegler, P., Holzheid, A., & Palme, H. (2011). Heterogeneous accretion, composition and core–mantle differentiation of the Earth. *Earth and Planetary Science Letters*, *301*(1), 31–42. https://doi.org/10.1016/j.epsl.2010.11.030

Rudnick, R., & Nyblade, A. A. (1999). The thickness and heat production of Archean lithosphere, constraints from xenolith thermobarometry and surface heat flow. In Y. Fei, C. M. Bertka, & B. O. Mysen (Eds.), *Mantle Petrology: Field Observations and High Pressure Experimentation: A Tribute to Francis R. (Joe) Boyd* (pp. 3–12). The Geochemical Society.

Rüpke, L. H., & Hasenclever, J. (2017). Global rates of mantle serpentinization and H_2 production at oceanic transform faults in 3-D geodynamic models. *Geophysical Research Letters*, *44*(13), 6726–6734. https://doi.org/10.1002/2017GL072893

Rüpke, L. H., Morgan, J. P., Hort, M., & Connolly, J. A. D. (2004). Serpentine and the subduction

zone water cycle. *Earth and Planetary Science Letters*, *223*(1), 17–34. https://doi.org/10.1016/j.epsl.2004.04.018

Russell, M. J., Hall, A. J., & Martin, W. (2010). Serpentinization as a source of energy at the origin of life. *Geobiology*, *8*(5), 355–371. https://doi.org/10.1111/j.1472-4669.2010.00249.x

Russell, M. J., & Ponce, A. (2020). Six 'Must-Have' Minerals for Life's Emergence: Olivine, Pyrrhotite, Bridgmanite, Serpentine, Fougerite and Mackinawite. *Life*, *10*(11), Article 11. https://doi.org/10.3390/life10110291

Saffer, D. M., & Tobin, H. J. (2011). Hydrogeology and Mechanics of Subduction Zone Forearcs: Fluid Flow and Pore Pressure. *Annual Review of Earth and Planetary Sciences*, *39*(1), 157–186. https://doi.org/10.1146/annurev-earth-040610-133408

Salvi, S., & Williams-Jones, A. E. (1997). Fischer-Tropsch synthesis of hydrocarbons during sub-solidus alteration of the Strange Lake peralkaline granite, Quebec/Labrador, Canada. *Geochimica et Cosmochimica Acta*, *61*(1), 83–99. https://doi.org/10.1016/S0016-7037(96)00313-4

Saruwatari, K., Kameda, J., & Tanaka, H. (2004). Generation of hydrogen ions and hydrogen gas in quartz–water crushing experiments: An example of chemical processes in active faults. *Physics and Chemistry of Minerals*, *31*(3), 176–182. https://doi.org/10.1007/s00269-004-0382-2

Saspiturry, N., Allanic, C., & Peyrefitte, A. (2024). Serpentinization and Magmatic Distribution in a Hyperextended Rift Suture: Implication for Natural Hydrogen Exploration (Mauléon Basin, Pyrenees). *Tectonics*, *43*(8), e2024TC008385. https://doi.org/10.1029/2024TC008385

Sato, M., Sutton, A. J., & McGee, K. A. (1984). Anomalous hydrogen emissions from the San Andreas fault observed at the Cienega Winery, central California. *Pure and Applied Geophysics*, *122*(2), 376–391. https://doi.org/10.1007/BF00874606

Sato, M., Sutton, A. J., McGee, K. A., & Russell-Robinson, S. (1986). Monitoring of hydrogen along the San Andreas and Calaveras faults in central California in 1980–1984. *Journal of Geophysical Research: Solid Earth*, *91*(B12), 12315–12326. https://doi.org/10.1029/JB091iB12p12315

Sauvage, J. F., Flinders, A., Spivack, A. J., Pockalny, R., Dunlea, A. G., Anderson, C. H., Smith, D. C., Murray, R. W., & D'Hondt, S. (2021). The contribution of water radiolysis to marine sedimentary life. *Nature Communications*, *12*(1), 1297. https://doi.org/10.1038/s41467-021-21218-z

Savary, V., & Pagel, M. (1997). The effects of water radiolysis on local redox conditions in the

Oklo, Gabon, natural fission reactors 10 and 16. *Geochimica et Cosmochimica Acta*, *61*(21), 4479–4494. https://doi.org/10.1016/S0016-7037(97)00261-5

Scambelluri, M., & Tonarini, S. (2012). Boron isotope evidence for shallow fluid transfer across subduction zones by serpentinized mantle. *Geology*, *40*(10), 907–910. https://doi.org/10.1130/G33233.1

Schut, G., Peters, J., Boyd, E., & Adams, M. (2014). Hydrogen Metabolism and the Evolution of Biological Respiration: Two separate families of enzymes that oxidize hydrogen and also produce it arose through convergent evolution. *Microbe Magazine*, *9*, 361–367. https://doi.org/10.1128/microbe.9.361.1

Schwartz, S., Guillot, S., Reynard, B., Lafay, R., Debret, B., Nicollet, C., Lanari, P., & Auzende, A. L. (2013). Pressure–temperature estimates of the lizardite/antigorite transition in high pressure serpentinites. *Lithos*, *178*, 197–210. https://doi.org/10.1016/j.lithos.2012.11.023

Schwarzenbach, E. M., Früh-Green, G. L., Bernasconi, S. M., Alt, J. C., & Plas, A. (2013). Serpentinization and carbon sequestration: A study of two ancient peridotite-hosted hydrothermal systems. *Chemical Geology*, *351*, 115–133. https://doi.org/10.1016/j.chemgeo.2013.05.016

Seward, T. M., & Franck, E. U. (1981). The system hydrogen—Water up to 440°C and 2500 bar pressure. *Berichte Der Bunsengesellschaft Für Physikalische Chemie*, *85*(1), 2–7. https://doi.org/10.1002/bbpc.19810850103

Sharp, Z. D., McCubbin, F. M., & Shearer, C. K. (2013). A hydrogen-based oxidation mechanism relevant to planetary formation. *Earth and Planetary Science Letters*, *380*, 88–97. https://doi.org/10.1016/j.epsl.2013.08.015

Sherwood Lollar, B., Lacrampe-Couloume, G., Slater, G. F., Ward, J., Moser, D. P., Gihring, T. M., Lin, L.-H., & Onstott, T. C. (2006). Unravelling abiogenic and biogenic sources of methane in the Earth's deep subsurface. *Chemical Geology*, *226*(3), 328–339. https://doi.org/10.1016/j.chemgeo.2005.09.027

Sherwood Lollar, B., Onstott, T. C., Lacrampe-Couloume, G., & Ballentine, C. J. (2014). The contribution of the Precambrian continental lithosphere to global H_2 production. *Nature*, *516*(7531), 379–382. https://doi.org/10.1038/nature14017

Sherwood Lollar, B., Voglesonger, K., Lin, L.-H., Lacrampe-Couloume, G., Telling, J., Abrajano, T. A., Onstott, T. C., & Pratt, L. M. (2007). Hydrogeologic Controls on Episodic H_2 Release from Precambrian Fractured Rocks—Energy for Deep Subsurface Life on Earth and Mars. *Astrobiology*, *7*(6), 971–986. https://doi.org/10.1089/ast.2006.0096

Sherwood Lollar, B., Warr, O., & Higgins, P. M. (2024). The Hidden Hydrogeosphere: The

Contribution of Deep Groundwater to the Planetary Water Cycle. *Annual Review of Earth and Planetary Sciences*, *52*(1), null. https://doi.org/10.1146/annurev-earth-040722-102252

Shi, L., Dong, H., Reguera, G., Beyenal, H., Lu, A., Liu, J., Yu, H.-Q., & Fredrickson, J. K. (2016). Extracellular electron transfer mechanisms between microorganisms and minerals. *Nature Reviews Microbiology*, *14*(10), 651–662. https://doi.org/10.1038/nrmicro.2016.93

Shi, Z., Jessen, K., & Tsotsis, T. T. (2020). Impacts of the subsurface storage of natural gas and hydrogen mixtures. *International Journal of Hydrogen Energy*, *45*(15), 8757–8773. https://doi.org/10.1016/j.ijhydene.2020.01.044

Shibuya, T., Yoshizaki, M., Sato, M., Shimizu, K., Nakamura, K., Omori, S., Suzuki, K., Takai, K., Tsunakawa, H., & Maruyama, S. (2015). Hydrogen-rich hydrothermal environments in the Hadean ocean inferred from serpentinization of komatiites at 300 °C and 500 bar. *Progress in Earth and Planetary Science*, *2*(1), 46. https://doi.org/10.1186/s40645-015-0076-z

Shillington, D. J., Bécel, A., Nedimović, M. R., Kuehn, H., Webb, S. C., Abers, G. A., Keranen, K. M., Li, J., Delescluse, M., & Mattei-Salicrup, G. A. (2015). Link between plate fabric, hydration and subduction zone seismicity in Alaska. *Nature Geoscience*, *8*(12), Article 12. https://doi.org/10.1038/ngeo2586

Silva, R. C., Snowdon, L. R., Huang, H., Nightingale, M., Becker, V., Taylor, S., Mayer, B., Pedersen, J. H., di Primio, R., & Larter, S. (2019). Radiolysis as a source of ^{13}C depleted natural gases in the geosphere. *Organic Geochemistry*, *138*, 103911. https://doi.org/10.1016/j.orggeochem.2019.103911

Siron, G., Blanchard, M., Aufort, J., Williams, S., & Vitale-Brovarone, A. (2024). *Decoupling of high-pressure H_2 production from serpentinization and magnetite in subduction zones*. Research Square. https://doi.org/10.21203/rs.3.rs-4973494/v1

Skelton, A., Whitmarsh, R., Arghe, F., Crill, P., & Koyi, H. (2005). Constraining the rate and extent of mantle serpentinization from seismic and petrological data: Implications for chemosynthesis and tectonic processes. *Geofluids*, *5*(3), 153–164. https://doi.org/10.1111/j.1468-8123.2005.00111.x

Sleep, N. H., & Bird, D. K. (2007). Niches of the pre-photosynthetic biosphere and geologic preservation of Earth's earliest ecology. *Geobiology*, *5*(2), 101–117. https://doi.org/10.1111/j.1472-4669.2007.00105.x

Sleep, N. H., & Zoback, M. D. (2007). Did Earthquakes Keep the Early Crust Habitable? *Astrobiology*, *7*(6), 1023–1032. https://doi.org/10.1089/ast.2006.0091

Smetannikov, A. F. (2011). Hydrogen generation during the radiolysis of crystallization water in carnallite and possible consequences of this process. *Geochemistry International*, *49*(9), 916–924. https://doi.org/10.1134/S0016702911070081

Smith, E. M., Shirey, S. B., Nestola, F., Bullock, E. S., Wang, J., Richardson, S. H., & Wang, W. (2016). Large gem diamonds from metallic liquid in Earth's deep mantle. *Science*, *354*(6318), 1403–1405. https://doi.org/10.1126/science.aal1303

Smith, E. M., Shirey, S. B., Richardson, S. H., Nestola, F., Bullock, E. S., Wang, J., & Wang, W. (2018). Blue boron-bearing diamonds from Earth's lower mantle. *Nature*, *560*(7716), 84–87. https://doi.org/10.1038/s41586-018-0334-5

Smith, N. J. P., Shepherd, T. J., Styles, M. T., & Williams, G. M. (2005). Hydrogen exploration: A review of global hydrogen accumulations and implications for prospective areas in NW Europe. *Geological Society, London, Petroleum Geology Conference Series*, *6*(1), 349–358. https://doi.org/10.1144/0060349

Song, H., Ou, X., Han, B., Deng, H., Zhang, W., Tian, C., Cai, C., Lu, A., Lin, Z., & Chai, L. (2021). An Overlooked Natural Hydrogen Evolution Pathway: Ni^{2+} Boosting H_2O Reduction by $Fe(OH)_2$ Oxidation during Low-Temperature Serpentinization. *Angewandte Chemie International Edition*, *60*(45), 24054–24058. https://doi.org/10.1002/anie.202110653

Sossi, P. A., Eggins, S. M., Nesbitt, R. W., Nebel, O., Hergt, J. M., Campbell, I. H., O'Neill, H. St. C., Van Kranendonk, M., & Davies, D. R. (2016). Petrogenesis and Geochemistry of Archean Komatiites. *Journal of Petrology*, *57*(1), 147–184. https://doi.org/10.1093/petrology/egw004

Soule, S. A., Fornari, D. J., Perfit, M. R., Ridley, W. I., Reed, M. H., & Cann, J. R. (2006). Incorporation of seawater into mid-ocean ridge lava flows during emplacement. *Earth and Planetary Science Letters*, *252*(3), 289–307. https://doi.org/10.1016/j.epsl.2006.09.043

Stevens, T. O., & McKinley, J. P. (1995). Lithoautotrophic Microbial Ecosystems in Deep Basalt Aquifers. *Science*, *270*(5235), 450–455. https://doi.org/10.1126/science.270.5235.450

Stevens, T. O., & McKinley, J. P. (2000). Abiotic Controls on H_2 Production from Basalt−Water Reactions and Implications for Aquifer Biogeochemistry. *Environmental Science & Technology*, *34*(5), 826–831. https://doi.org/10.1021/es990583g

Stolper, D. A., Higgins, J. A., & Derry, L. A. (2021). The role of the solid earth in regulating atmospheric O_2 levels. *American Journal of Science*, *321*(10), 1381–1444. https://doi.org/10.2475/10.2021.01

Sugisaki, R., Ido, M., Takeda, H., Isobe, Y., Hayashi, Y., Nakamura, N., Satake, H., & Mizutani, Y. (1983). Origin of Hydrogen and Carbon Dioxide in Fault Gases and Its Relation to Fault

Activity. *The Journal of Geology*, *91*(3), 239–258. https://doi.org/10.1086/628769

Suzuki, N., Koike, K., Kameda, J., & Kimura, G. (2024). Thermogenic methane and hydrogen generation in subducted sediments of the Nankai Trough. *Communications Earth & Environment*, *5*(1), Article 1. https://doi.org/10.1038/s43247-024-01252-7

Suzuki, N., Saito, H., & Hoshino, T. (2017). Hydrogen gas of organic origin in shales and metapelites. *International Journal of Coal Geology*, *173*, 227–236. https://doi.org/10.1016/j.coal.2017.02.014

Svensen, H. H., Jones, M. T., & Mather, T. A. (2023). Large Igneous Provinces and the Release of Thermogenic Volatiles from Sedimentary Basins. *Elements*, *19*(5), 282–288. https://doi.org/10.2138/gselements.19.5.282

Svensen, H. H., Planke, S., Malthe-Sørenssen, A., Jamtveit, B., Myklebust, R., Rasmussen Eidem, T., & Rey, S. S. (2004). Release of methane from a volcanic basin as a mechanism for initial Eocene global warming. *Nature*, *429*(6991), 542–545. https://doi.org/10.1038/nature02566

Sverjensky, D., Daniel, I., & Vitale Brovarone, A. (2020). The Changing Character of Carbon in Fluids with Pressure: Organic Geochemistry of Earth's Upper Mantle Fluids. In C. E. Manning, J. Lin, & W. L. Mao (Eds.), *Carbon in Earth's Interior* (1st ed., pp. 259–269). Wiley. https://doi.org/10.1002/9781119508229.ch22

Swanson-Hysell, N. L., Hoaglund, S. A., Crowley, J. L., Schmitz, M. D., Zhang, Y., & Miller, J. D. (2021). Rapid emplacement of massive Duluth Complex intrusions within the North American Midcontinent Rift. *Geology*, *49*(2), 185–189. https://doi.org/10.1130/G47873.1

Symonds, R. B., Gerlach, T. M., & Reed, M. H. (2001). Magmatic gas scrubbing: Implications for volcano monitoring. *Journal of Volcanology and Geothermal Research*, *108*(1), 303–341. https://doi.org/10.1016/S0377-0273(00)00292-4

Symonds, R. B., Rose, W. I., Bluth, G. J. S., & Gerlach, T. M. (1994). Volcanic-gas studies: Methods, results, and applications. In M. R. Carroll & J. R. Holloway (Eds.), *Volatiles in Magmas* (Vol. 30, pp. 1–66). De Gruyter. https://doi.org/10.1515/9781501509674-007

Tagawa, S., Sakamoto, N., Hirose, K., Yokoo, S., Hernlund, J., Ohishi, Y., & Yurimoto, H. (2021). Experimental evidence for hydrogen incorporation into Earth's core. *Nature Communications*, *12*(1), 2588. https://doi.org/10.1038/s41467-021-22035-0

Takai, K., Gamo, T., Tsunogai, U., Nakayama, N., Hirayama, H., Nealson, K. H., & Horikoshi, K. (2004). Geochemical and microbiological evidence for a hydrogen-based, hyperthermophilic subsurface lithoautotrophic microbial ecosystem (HyperSLiME) beneath an active deep-sea hydrothermal field. *Extremophiles*, *8*(4), 269–282.

https://doi.org/10.1007/s00792-004-0386-3

Tamblyn, R., & Hermann, J. (2023). Geological evidence for high H_2 production from komatiites in the Archaean. *Nature Geoscience*, *16*(12), 1194–1199. https://doi.org/10.1038/s41561-023-01316-x

Tao, R., Zhang, L., Tian, M., Zhu, J., Liu, X., Liu, J., Höfer, H. E., Stagno, V., & Fei, Y. (2018). Formation of abiotic hydrocarbon from reduction of carbonate in subduction zones: Constraints from petrological observation and experimental simulation. *Geochimica et Cosmochimica Acta*, *239*, 390–408. https://doi.org/10.1016/j.gca.2018.08.008

Tarnas, J. D., Mustard, J. F., Sherwood Lollar, B., Bramble, M. S., Cannon, K. M., Palumbo, A. M., & Plesa, A.-C. (2018). Radiolytic H_2 production on Noachian Mars: Implications for habitability and atmospheric warming. *Earth and Planetary Science Letters*, *502*, 133–145. https://doi.org/10.1016/j.epsl.2018.09.001

Tarnas, J. D., Mustard, J. F., Sherwood Lollar, B., Stamenković, V., Cannon, K. M., Lorand, J.-P., Onstott, T. C., Michalski, J. R., Warr, O., Palumbo, A. M., & Plesa, A.-C. (2021). Earth-like Habitable Environments in the Subsurface of Mars. *Astrobiology*, *21*(6), 741–756. https://doi.org/10.1089/ast.2020.2386

Teknik, V., Artemieva, I. M., & Thybo, H. (2024). Limited arc magmatism and seismicity due to extensive mantle wedge serpentinization in the Makran subduction zone. *Earth and Planetary Science Letters*, *645*, 118950. https://doi.org/10.1016/j.epsl.2024.118950

Telling, J., Boyd, E. S., Bone, N., Jones, E. L., Tranter, M., MacFarlane, J. W., Martin, P. G., Wadham, J. L., Lamarche-Gagnon, G., Skidmore, M. L., Hamilton, T. L., Hill, E., Jackson, M., & Hodgson, D. A. (2015). Rock comminution as a source of hydrogen for subglacial ecosystems. *Nature Geoscience*, *8*(11), Article 11. https://doi.org/10.1038/ngeo2533

Telling, J., Voglesonger, K., Sutcliffe, C. N., Lacrampe-Couloume, G., Edwards, E., & Sherwood Lollar, B. (2018). Bioenergetic Constraints on Microbial Hydrogen Utilization in Precambrian Deep Crustal Fracture Fluids. *Geomicrobiology Journal*, *35*(2), 108–119. https://doi.org/10.1080/01490451.2017.1333176

Templeton, A. S., & Caro, T. A. (2023). The Rock-Hosted Biosphere. *Annual Review of Earth and Planetary Sciences*, *51*(1), 493–519. https://doi.org/10.1146/annurev-earth-031920-081957

Templeton, A. S., & Ellison, E. T. (2020). Formation and loss of metastable brucite: Does Fe(II)-bearing brucite support microbial activity in serpentinizing ecosystems? *Philosophical Transactions of the Royal Society A: Mathematical, Physical and Engineering Sciences*, *378*(2165), 20180423. https://doi.org/10.1098/rsta.2018.0423

Thayer, T. P. (1966). Serpentinization considered as a constant-volume metasomatic process. *American Mineralogist*, *51*(5–6), 685–710.

Thaysen, E. M., McMahon, S., Strobel, G. J., Butler, I. B., Ngwenya, B. T., Heinemann, N., Wilkinson, M., Hassanpouryouzband, A., McDermott, C. I., & Edlmann, K. (2021). Estimating microbial growth and hydrogen consumption in hydrogen storage in porous media. *Renewable and Sustainable Energy Reviews*, *151*, 111481. https://doi.org/10.1016/j.rser.2021.111481

The Matplotlib Development Team. (2024). *Matplotlib: Visualization with Python* (Version v3.9.1) [Computer software]. Zenodo. https://doi.org/10.5281/zenodo.12652732

Tian, F., Toon, O. B., Pavlov, A. A., & De Sterck, H. (2005). A Hydrogen-Rich Early Earth Atmosphere. *Science*, *308*(5724), 1014–1017. https://doi.org/10.1126/science.1106983

Tichadou, C., Godard, M., Muñoz, M., Labaume, P., Vauchez, A., Gaucher, E. C., & Calassou, S. (2021). Mineralogical and geochemical study of serpentinized peridotites from the North-Western Pyrenees: New insights on serpentinization along magma-poor continental passive margins. *Lithos*, *406–407*, 106521. https://doi.org/10.1016/j.lithos.2021.106521

Tissot, B., Califet-Debyser, Y., Deroo, G., & Oudin, J. L. (1971). Origin and Evolution of Hydrocarbons in Early Toarcian Shales, Paris Basin, France. *AAPG Bulletin*, *55*. https://doi.org/10.1306/819A3E2E-16C5-11D7-8645000102C1865D

Tollan, P., & Hermann, J. (2019). Arc magmas oxidized by water dissociation and hydrogen incorporation in orthopyroxene. *Nature Geoscience*, *12*(8), 667–671. https://doi.org/10.1038/s41561-019-0411-x

Toulhoat, H., & Zgonnik, V. (2022). Chemical Differentiation of Planets: A Core Issue. *The Astrophysical Journal*, *924*(2), 83. https://doi.org/10.3847/1538-4357/ac300b

Truche, L., Bourdelle, F., Salvi, S., Lefeuvre, N., Zug, A., & Lloret, E. (2021). Hydrogen generation during hydrothermal alteration of peralkaline granite. *Geochimica et Cosmochimica Acta*, *308*, 42–59. https://doi.org/10.1016/j.gca.2021.05.048

Truche, L., Donzé, F.-V., Goskolli, E., Muceku, B., Loisy, C., Monnin, C., Dutoit, H., & Cerepi, A. (2024). A deep reservoir for hydrogen drives intense degassing in the Bulqizë ophiolite. *Science*, *383*(6683), 618–621. https://doi.org/10.1126/science.adk9099

Truche, L., Jodin-Caumon, M.-C., Lerouge, C., Berger, G., Mosser-Ruck, R., Giffaut, E., & Michau, N. (2013). Sulphide mineral reactions in clay-rich rock induced by high hydrogen pressure. Application to disturbed or natural settings up to 250 °C and 30 bar. *Chemical Geology*, *351*, 217–228. https://doi.org/10.1016/j.chemgeo.2013.05.025

Truche, L., Joubert, G., Dargent, M., Martz, P., Cathelineau, M., Rigaudier, T., & Quirt, D. (2018).

Clay minerals trap hydrogen in the Earth's crust: Evidence from the Cigar Lake uranium deposit, Athabasca. *Earth and Planetary Science Letters*, *493*, 186–197. https://doi.org/10.1016/j.epsl.2018.04.038

Turcotte, D. L., & Morgan, J. P. (1992). The Physics of Magma Migration and Mantle Flow Beneath a Mid-Ocean Ridge. In *Mantle Flow and Melt Generation at Mid-Ocean Ridges* (pp. 155–182). American Geophysical Union (AGU). https://doi.org/10.1029/GM071p0155

Türke, A., Nakamura, K., & Bach, W. (2015). Palagonitization of Basalt Glass in the Flanks of Mid-Ocean Ridges: Implications for the Bioenergetics of Oceanic Intracrustal Ecosystems. *Astrobiology*, *15*(10), 793–803. https://doi.org/10.1089/ast.2014.1255

Turner, A. C., Korol, R., Eldridge, D. L., Bill, M., Conrad, M. E., Miller, T. F., & Stolper, D. A. (2021). Experimental and theoretical determinations of hydrogen isotopic equilibrium in the system CH_4–H_2–H_2O from 3 to 200 °C. *Geochimica et Cosmochimica Acta*, *314*, 223–269. https://doi.org/10.1016/j.gca.2021.04.026

Tutolo, B. M., Seyfried, W. E., & Tosca, N. J. (2020). A seawater throttle on H_2 production in Precambrian serpentinizing systems. *Proceedings of the National Academy of Sciences*, *117*(26), 14756–14763. https://doi.org/10.1073/pnas.1921042117

Tutolo, B. M., & Tosca, N. J. (2023). Observational constraints on the process and products of Martian serpentinization. *Science Advances*, *9*(5), eadd8472. https://doi.org/10.1126/sciadv.add8472

Ueda, H., Shibuya, T., Sawaki, Y., Shozugawa, K., Makabe, A., & Takai, K. (2021). Chemical Nature of Hydrothermal Fluids Generated by Serpentinization and Carbonation of Komatiite: Implications for H_2-Rich Hydrothermal System and Ocean Chemistry in the Early Earth. *Geochemistry, Geophysics, Geosystems*, *22*(12), e2021GC009827. https://doi.org/10.1029/2021GC009827

Ulmer, P., & Trommsdorff, V. (1995). Serpentine Stability to Mantle Depths and Subduction-Related Magmatism. *Science*, *268*(5212), 858–861. https://doi.org/10.1126/science.268.5212.858

Vacquand, C., Deville, E., Beaumont, V., Guyot, F., Sissmann, O., Pillot, D., Arcilla, C., & Prinzhofer, A. (2018). Reduced gas seepages in ophiolitic complexes: Evidences for multiple origins of the H_2-CH_4-N_2 gas mixtures. *Geochimica et Cosmochimica Acta*, *223*, 437–461. https://doi.org/10.1016/j.gca.2017.12.018

van Avendonk, H. J. A., Holbrook, W. S., Lizarralde, D., & Denyer, P. (2011). Structure and serpentinization of the subducting Cocos plate offshore Nicaragua and Costa Rica. *Geochemistry, Geophysics, Geosystems*, *12*(6). https://doi.org/10.1029/2011GC003592

van Keken, P. E., Hacker, B. R., Syracuse, E. M., & Abers, G. A. (2011). Subduction factory: 4. Depth-dependent flux of H_2O from subducting slabs worldwide. *Journal of Geophysical Research: Solid Earth*, *116*(B1). https://doi.org/10.1029/2010JB007922

van Keken, P. E., & Wilson, C. R. (2023). An introductory review of the thermal structure of subduction zones: III—Comparison between models and observations. *Progress in Earth and Planetary Science*, *10*(1), 57. https://doi.org/10.1186/s40645-023-00589-5

Vandieken, V., Finke, N., & Thamdrup, B. (2014). Hydrogen, acetate, and lactate as electron donors for microbial manganese reduction in a manganese-rich coastal marine sediment. *FEMS Microbiology Ecology*, *87*(3), 733–745. https://doi.org/10.1111/1574-6941.12259

Vitale Brovarone, A., Martinez, I., Elmaleh, A., Compagnoni, R., Chaduteau, C., Ferraris, C., & Esteve, I. (2017). Massive production of abiotic methane during subduction evidenced in metamorphosed ophicarbonates from the Italian Alps. *Nature Communications*, *8*(1), 14134. https://doi.org/10.1038/ncomms14134

Vitale Brovarone, A., Piccoli, F., Frasca, G., & Giuntoli, F. (2021). Fresh, pseudotachylyte-bearing mantle peridotites from the lawsonite eclogite-facies San Petrone Unit, Alpine Corsica. *Ofioliti*, *46*(2), Article 2. https://doi.org/10.4454/ofioliti.v46i2.545

Vitale Brovarone, A., Sverjensky, D. A., Piccoli, F., Ressico, F., Giovannelli, D., & Daniel, I. (2020). Subduction hides high-pressure sources of energy that may feed the deep subsurface biosphere. *Nature Communications*, *11*(1), Article 1. https://doi.org/10.1038/s41467-020-17342-x

Vlasov, K., Audétat, A., & Keppler, H. (2023). H_2-H_2O immiscibility in Earth's upper mantle. *Contributions to Mineralogy and Petrology*, *178*(7), 36. https://doi.org/10.1007/s00410-023-02019-7

Wada, I., Behn, M. D., & Shaw, A. M. (2012). Effects of heterogeneous hydration in the incoming plate, slab rehydration, and mantle wedge hydration on slab-derived H_2O flux in subduction zones. *Earth and Planetary Science Letters*, *353–354*, 60–71. https://doi.org/10.1016/j.epsl.2012.07.025

Wakita, H., Nakamura, Y., Kita, I., Fujii, N., & Notsu, K. (1980). Hydrogen Release: New Indicator of Fault Activity. *Science*, *210*(4466), 188–190. https://www.jstor.org/stable/1685017

Walter, S., Kock, A., Steinhoff, T., Fiedler, B., Fietzek, P., Kaiser, J., Krol, M., Popa, M. E., Chen, Q., Tanhua, T., & Röckmann, T. (2016). Isotopic evidence for biogenic molecular hydrogen production in the Atlantic Ocean. *Biogeosciences*, *13*(1), 323–340. https://doi.org/10.5194/bg-13-323-2016

Walter, S., Laukenmann, S., Stams, A. J. M., Vollmer, M. K., Gleixner, G., & Röckmann, T. (2012).

The stable isotopic signature of biologically produced molecular hydrogen (H_2). *Biogeosciences*, *9*(10), 4115–4123. https://doi.org/10.5194/bg-9-4115-2012

Wang, W., Li, Y., Brodholt, J. P., Vočadlo, L., Walter, M. J., & Wu, Z. (2021). Strong shear softening induced by superionic hydrogen in Earth's inner core. *Earth and Planetary Science Letters*, *568*, 117014. https://doi.org/10.1016/j.epsl.2021.117014

Wang, W., Liu, C., Liu, W., Wang, X., Guo, P., Wang, J., Wang, Z., Li, Z., & Zhang, D. (2022). Dominant products and reactions during organic matter radiolysis: Implications for hydrocarbon generation of uranium-rich shales. *Marine and Petroleum Geology*, *137*, 105497. https://doi.org/10.1016/j.marpetgeo.2021.105497

Wang, W., Liu, C., Liu, W., & Zhang, D. (2018). Factors influencing hydrogen yield in water radiolysis and implications for hydrocarbon generation: A review. *Arabian Journal of Geosciences*, *11*(18), 542. https://doi.org/10.1007/s12517-018-3903-x

Wang, W., Walter, M. J., Brodholt, J. P., Huang, S., & Petaev, M. I. (2023). Chalcogen isotopes reveal limited volatile contribution from late veneer to Earth. *Science Advances*, *9*(49), eadh0670. https://doi.org/10.1126/sciadv.adh0670

Wang, Y., Wu, J., Xue, S., Wang, J., Zhang, Y., & Tang, Y. (2017). Hydrogen production by low-temperature oxidation of coal: Exploration of the relationship between aliphatic CH conversion and molecular hydrogen release. *International Journal of Hydrogen Energy*, *42*(39), 25063–25073. https://doi.org/10.1016/j.ijhydene.2017.08.040

Wankel, S. D., Germanovich, L. N., Lilley, M. D., Genc, G., DiPerna, C. J., Bradley, A. S., Olson, E. J., & Girguis, P. R. (2011). Influence of subsurface biosphere on geochemical fluxes from diffuse hydrothermal fluids. *Nature Geoscience*, *4*(7), 461–468. https://doi.org/10.1038/ngeo1183

Ware, R. H., Roecken, C., & Wyss, M. (1984). The detection and interpretation of hydrogen in fault gases. *Pure and Applied Geophysics*, *122*(2), 392–402. https://doi.org/10.1007/BF00874607

Warr, O., Giunta, T., Ballentine, C. J., & Sherwood Lollar, B. (2019). Mechanisms and rates of ^{4}He, ^{40}Ar, and H_2 production and accumulation in fracture fluids in Precambrian Shield environments. *Chemical Geology*, *530*, 119322. https://doi.org/10.1016/j.chemgeo.2019.119322

Warr, O., Song, M., & Sherwood Lollar, B. (2023). The application of Monte Carlo modelling to quantify in situ hydrogen and associated element production in the deep subsurface. *Frontiers in Earth Science*, *11*. https://www.frontiersin.org/articles/10.3389/feart.2023.1150740

Welhan, J. A., & Craig, H. (1979). Methane and hydrogen in East Pacific Rise hydrothermal fluids. *Geophysical Research Letters*, *6*(11), 829–831. https://doi.org/10.1029/GL006i011p00829

Werner, C., Fischer, T. P., Aiuppa, A., Edmonds, M., Cardellini, C., Carn, S., Chiodini, G., Cottrell, E., Burton, M. R., Shinohara, H., & Allard, P. (2019). Carbon Dioxide Emissions from Subaerial Volcanic Regions: Two decades in review. In B. Orcutt, R. Dasgupta, & I. Daniel (Eds.), *Deep Carbon: Past to Present*. Cambridge University Press.

Williams, Q., & Hemley, R. J. (2001). Hydrogen in the Deep Earth. *Annual Review of Earth and Planetary Sciences*, *29*(1), 365–418. https://doi.org/10.1146/annurev.earth.29.1.365

Williams, S. E., & Gubbins, D. (2019). Origin of Long-Wavelength Magnetic Anomalies at Subduction Zones. *Journal of Geophysical Research: Solid Earth*, *124*(9), 9457–9473. https://doi.org/10.1029/2019JB017479

Wilson, C. R., Spiegelman, M., van Keken, P. E., & Hacker, B. R. (2014). Fluid flow in subduction zones: The role of solid rheology and compaction pressure. *Earth and Planetary Science Letters*, *401*, 261–274. https://doi.org/10.1016/j.epsl.2014.05.052

Wilson, D. S., Teagle, D. A. H., Alt, J. C., Banerjee, N. R., Umino, S., Miyashita, S., Acton, G. D., Anma, R., Barr, S. R., Belghoul, A., Carlut, J., Christie, D. M., Coggon, R. M., Cooper, K. M., Cordier, C., Crispini, L., Durand, S. R., Einaudi, F., Galli, L., … Ziegler, C. (2006). Drilling to Gabbro in Intact Ocean Crust. *Science*, *312*(5776), 1016–1020. https://doi.org/10.1126/science.1126090

Wordsworth, R. (2012). Transient conditions for biogenesis on low-mass exoplanets with escaping hydrogen atmospheres. *Icarus*, *219*(1), 267–273. https://doi.org/10.1016/j.icarus.2012.02.035

Worman, S. L., Pratson, L. F., Karson, J. A., & Klein, E. M. (2016). Global rate and distribution of H_2 gas produced by serpentinization within oceanic lithosphere. *Geophysical Research Letters*, *43*(12), 6435–6443. https://doi.org/10.1002/2016GL069066

Worman, S. L., Pratson, L. F., Karson, J. A., & Schlesinger, W. H. (2020). Abiotic hydrogen (H_2) sources and sinks near the Mid-Ocean Ridge (MOR) with implications for the subseafloor biosphere. *Proceedings of the National Academy of Sciences*, *117*(24), 13283–13293. https://doi.org/10.1073/pnas.2002619117

Wright, V., Morzfeld, M., & Manga, M. (2024). Liquid water in the Martian mid-crust. *Proceedings of the National Academy of Sciences*, *121*(35), e2409983121. https://doi.org/10.1073/pnas.2409983121

Yang, H., Gandhi, H., Cornish, A. J., Moran, J. J., Kreuzer, H. W., Ostrom, N. E., & Hegg, E. L.

(2016). Isotopic fractionation associated with [NiFe]- and [FeFe]-hydrogenases. *Rapid Communications in Mass Spectrometry: RCM*, *30*(2), 285–292. https://doi.org/10.1002/rcm.7432

Yang, X., Gaillard, F., & Scaillet, B. (2014). A relatively reduced Hadean continental crust and implications for the early atmosphere and crustal rheology. *Earth and Planetary Science Letters*, *393*, 210–219. https://doi.org/10.1016/j.epsl.2014.02.056

Yang, X., Keppler, H., & Li, Y. (2016). Molecular hydrogen in mantle minerals. *Geochemical Perspectives Letters*, 160–168. https://doi.org/10.7185/geochemlet.1616

Yang, Y., Zandanel, A., Liu, S., W. Neil, C., C. Germann, T., & R. Gross, M. (2024). Temperature dependence of hydrogen diffusion in reservoir rocks: Implications for hydrogen geologic storage. *Energy Advances*, *3*(8), 2051–2065. https://doi.org/10.1039/D4YA00233D

Yoshida, K., Okamoto, A., Shimizu, H., Oyanagi, R., Tsuchiya, N., & Party, O. D. P. P. 2 S. (2020). Fluid Infiltration Through Oceanic Lower Crust in Response to Reaction-Induced Fracturing: Insights From Serpentinized Troctolite and Numerical Models. *Journal of Geophysical Research: Solid Earth*, *125*(11), e2020JB020268. https://doi.org/10.1029/2020JB020268

Yoshizaki, M., Shibuya, T., Suzuki, K., Shimizu, K., Nakamura, K., Takai, K., Omori, S., & Maruyama, S. (2009). H_2 generation by experimental hydrothermal alteration of komatiitic glass at 300°C and 500 bars: A preliminary result from on-going experiment. *Geochemical Journal*, *43*(5), e17–e22. https://doi.org/10.2343/geochemj.1.0058

Young, E. D., Shahar, A., & Schlichting, H. E. (2023). Earth shaped by primordial H_2 atmospheres. *Nature*, *616*(7956), Article 7956. https://doi.org/10.1038/s41586-023-05823-0

Zgonnik, V. (2020). The occurrence and geoscience of natural hydrogen: A comprehensive review. *Earth-Science Reviews*, *203*, 103140. https://doi.org/10.1016/j.earscirev.2020.103140

Zgonnik, V., Beaumont, V., Larin, N., Pillot, D., & Deville, E. (2019). Diffused flow of molecular hydrogen through the Western Hajar mountains, Northern Oman. *Arabian Journal of Geosciences*, *12*(3), 71. https://doi.org/10.1007/s12517-019-4242-2

Zhang, L., Nasika, C., Donzé, F.-V., Zheng, X., Renard, F., & Scholtès, L. (2019). Modeling Porosity Evolution Throughout Reaction-Induced Fracturing in Rocks With Implications for Serpentinization. *Journal of Geophysical Research: Solid Earth*, *124*(6), 5708–5733. https://doi.org/10.1029/2018JB016872

Zhang, L., Qi, N., Li, Y., Wang, X., & Zhang, L. (2024). Immiscible metamorphic water and methane fluids preserved in carbonated eclogite. *Communications Chemistry*, *7*(1), 1–10.

https://doi.org/10.1038/s42004-024-01355-4
Zhang, L., Zhang, L., Tang, M., Wang, X., Tao, R., Xu, C., & Bader, T. (2023). Massive abiotic methane production in eclogite during cold subduction. *National Science Review*, *10*(1), nwac207. https://doi.org/10.1093/nsr/nwac207
Zhang, Y., & Ni, H. (2010). Diffusion of H, C, and O Components in Silicate Melts. *Reviews in Mineralogy and Geochemistry*, *72*(1), 171–225. https://doi.org/10.2138/rmg.2010.72.5
Zivar, D., Kumar, S., & Foroozesh, J. (2021). Underground hydrogen storage: A comprehensive review. *International Journal of Hydrogen Energy*, *46*(45), 23436–23462. https://doi.org/10.1016/j.ijhydene.2020.08.138
Zwaan, F., Brune, S., Glerum, A., Vasey, D. A., Naliboff, J. B., Manatschal, G., & Gaucher, E. C. (2023). *Rift-inversion orogens are potential hotspots for natural H_2 generation* [Preprint]. In Review. https://doi.org/10.21203/rs.3.rs-3367317/v1